Jefferson Lab PAC19
Proposal Cover Sheet

This document must be received by close of business Thursday,

December 14, 2000 at:

Jefferson Lab
User Liaison,
Mail Stop 12B
12000 Jefferson Ave.
Newport News, VA
23606

Experimental Hall: Hall C

Days Requested for Approval: 40

❒ **Proposal Title:**
Spectroscopic study of Lambda hypernuclei up to the medium-heavy mass region using the (e,e'K+) reaction

Proposal Physics Goals
Indicate any experiments that have physics goals similar to those in your proposal.

Approved, Conditionally Approved, and/or Deferred Experiment(s) or proposals:

1. update to the previous conditionally approved E97-008
2. Completed Hall C E89-009 (1p shell only)
3. Hall A E94-107 (1p shell only)

Contact Person

Name: Osamu Hashimoto/L. Tang/J. Reinhold
Institution: Tohoku University
Address: Department of Physics
Address: Tohoku University
City, State, ZIP/Country: Sendai, 980-8578, Japan
Phone: 81-22-217-6452 **Fax:** 81-22-217-6455
E-Mail: hashimot@lambda.phys.tohoku.ac.jp

Jefferson Lab Use Only

Receipt Date:_____

By:_____

LAB RESOURCES LIST

JLab Proposal No.: _____ Date 12/14/00

(For JLab ULO use only.)

List below significant resources — both equipment and human — that you are requesting from Jefferson Lab in support of mounting and executing the proposed experiment. Do not include items that will be routinely supplied to all running experiments such as the base equipment for the hall and technical support for routine operation, installation, and maintenance.

Major Installations *(either your equip. or new equip. requested from JLab)*

HKS spectrometer(QQD)
HKS detector/frame
Enge split-pole/support
Enge detectors/support
Splitter magnet
Dump line/bending magnets

New Support Structures:

HKS support/shielding house
Enge Shielding house
Splitter magnet support
Supports for dump lines and bending magnets

Data Acquisition/Reduction

Computing Resources:

All standard and routinely supported

New Software:

none

Major Equipment

Magnets: HKS Q1, Q2, D, Enge split-pole, Splitter

Power Supplies: 1 new PS for D puchased by Tohoku university
Others used for E89-09

Targets: CH2, C, Si, V, Y(all solid)
ladder(water cooled)/control

Detectors: WCs, Scintillation Hodos, Aerogel, Lucite, Gas Cerenkov or Shower counter

Electronics: All standard and routinely supported.

Computer Hardware: Standard

Other:

Other:

Vacuum connections, LCW, magnet and detector survey.

BEAM REQUIREMENTS LIST

JLab Proposal No.: _____ Date: 12/14/00

Hall: Hall C Anticipated Run Date: _____ PAC Approved Days: _____

Spokesperson: Osamu Hashimoto/L. Tang/J. Reinhold Hall Liaison: H. Fenker
Phone: 81-22-217-6452
E-mail: hashimot@lambda.phys.tohoku.ac.jp

List all combinations of anticipated targets and beam conditions required to execute the experiment. (This list will form the primary basis for the Radiation Safety Assesment Document (RSAD) calculations that must be performed for each experiment.)

Condition No.	Beam Energy (MeV)	Mean Beam Current (μA)	Polarization and Other Special Requirements (e.g., time structure)	Target Material (use multiple rows for complex targets — e.g., w/windows)	Material Thickness (mg/cm^2)	Est. Beam-On Time for Cond. No. (hours)
1	1800	5	2.5x2.5 mm2 rastered	CH2	200	144
2	1800	30	unrastered	C12	50	168
3	1800	30	unrastered	C12	100	96
4	1800	30	unrastered	Si28	100	192
5	1800	30	unrastered	V51	100	336
6	1800	30	unrastered	Y89	100	96
7	900	15	unrastered	C12	50	24

The beam energies, E_{Beam}, available are: $E_{Beam} = N \times E_{Linac}$ where N = 1, 2, 3, 4, or 5. E_{Linac} = 800 MeV, i.e., available E_{Beam} are 800, 1600, 2400, 3200, and 4000 MeV. Other energies should be arranged with the Hall Leader before listing.

HAZARD IDENTIFICATION CHECKLIST

JLab Proposal No.: _____ Date: 12/14/00

(For CEBAF User Liaison Office use only.)

Check all items for which there is an anticipated need.

Cryogenics

- [ ] beamline magnets
- [ ] analysis magnets
- [ ] target

type: _____
flow rate: _____
capacity: _____

Electrical Equipment

- [ ] cryo/electrical devices
- [ ] capacitor banks
- [x] high voltage
- [ ] exposed equipment

Radioactive/Hazardous Materials

List any radioactive or hazadorous/ toxic materials planned for use:

Pressure Vessels

_____ inside diameter
_____ operating pressure
_____ window material
_____ window thickness

Flammable Gas or Liquids

type: _____
flow rate: _____
capacity: _____

Drift Chambers

type: 50/50 Argon/Ethane
flow rate: 0.15/0.15
capacity: 0.015m3 total

Other Target Materials

- [ ] Beryllium (Be)
- [ ] Lithium (Li)
- [ ] Mercury (Hg)
- [ ] Lead (Pb)
- [ ] Tungsten (W)
- [ ] Uranium (U)
- [x] Other (list below)

Boron

Vacuum Vessels

1.2x0.2m inside diameter
10**-5 operating pressure
Mylar/Ke window material
0.005"/0. window thickness

Radioactive Sources

- [ ] permanent installation
- [ ] temporary use

type: _____
strength: _____

Large Mech. Structure/System

- [ ] lifting devices
- [ ] motion controllers
- [ ] scaffolding or
- [x] elevated platforms

Lasers

type: _____
wattage: _____
class: _____

Installation:

- [ ] permanent
- [ ] temporary

Use:

- [ ] calibration
- [ ] alignment

Hazardous Materials

- [ ] cyanide plating materials
- [ ] scintillation oil (from)
- [ ] PCBs
- [ ] methane
- [ ] TMAE
- [ ] TEA
- [ ] photographic developers
- [ ] other (list below)

General:

Experiment Class:

- [ ] Base Equipment
- [ ] Temp. Mod. to Base Equip.
- [ ] Permanent Mod. to Base Equipment
- [x] Major New Apparatus

Other:

Computing Requirements List

Proposal Title: Spectroscopic study of Lambda hypernuclei up to the medium-heavy mass region using the (e,e'K+) reaction

Spokesperson: Osamu Hashimoto/L. Tang/J. Reinhold **Experimental Hall:** Hall C

Raw Data Expected

Total: 3 TB **Per Year (long duration experiments only):** _____

Simulation Compute Power (SPECint95 hours) Required: None

On-Line Disk Storage Required: Standard Hall C storage

Imported Data Amount from Outside Institutions: None

Exported Data Amount to Outside Institutions:w 1 TB

Expected Mechanism for Imported/Exported Data: DVD

Special Requirements

For example, special configuration of data acquisition systems) that may require resources and/or coordination with JLab's Computer Center. Please indicate, if possible, what fraction of these resources will be provided by collaborating institutions and how much is expected to be provided by JLab.

None

Submit

Spectroscopic study of Λ hypernuclei up to medium-heavy mass region through the (e,e'K^+) reaction

(Update to the conditionally approved E97-008)

O. Hashimoto (Spokesperson)*, S.N. Nakamura, Y. Fujii, H. Tamura, T. Takahashi, K. Maeda, H. Kanda, T. Miyoshi, H. Yamaguti, Y. Okayasu, K. Tsukada

Department of Physics, Tohoku University, Sendai, 980-8578, Japan

S. Kato

Department of Physics, Yamagata University, Yamagata, 990-8560, Japan

H. Noumi

Institute for Particle and Nuclear Physics, KEK, Tsukuba, 305-0801, Japan

T. Motoba

Laboratory of Physics, Osaka Electro-Communication University, Neyagawa, 572-8530, Japan

L. Tang (Spokesperson), O.K. Baker, L. Cole, M. Christy, L. Gan, A. Gasparian, P. Gueye, B. Hu, C. Jackson, C. Keppel, Y. Sato, A. Uzzle, L. Yuan, X.F. Zhu

Department of Physics, Hampton University, Hampton, VA 23668, USA

J. Reinhold (Spokesperson), P. Markowiz

Department of Physics, Florida International University, Miami, FL 27411 USA

Ed. V. Hungerford, K. Lan, G.H. Xu

Department of Physics, University of Houston, Houston, TX 77204 USA

R. Carlini, R. Ent, H. Fenker, K. Garrow, D. Mack, G. Smith, W. Vulcan, S. Wood, C. Yan

Thomas Jefferson National Accelerator Facility, Newport News, VA 23606 USA

A. Ahmidouch, S. Danagoulian

Department of Physics, North Carolina A& T State University, Greensboro, NC 27411 USA

D. Dehnhard, H. Jungust, J. Liu

Department of Physics, University of Minnesota, Minnesota, USA

N. Simicevic, S. Wells

Department of Physics, Louisiana Tech University, Ruston, LA USA

M. Elaasar

Department of Physics, Southern University at New Orleans, New Orleans, Louisiana, USA

R. Asaturyan, H. Mkrtchyan, A. Margaryan, S. Stepanyan, V. Tadevosyan

Yerevan Physics Institute, Armenia

D. Androic, M. Planinic, M. Furic

Department of Physics, University of Zagreb, Croatia

T. Angelescu

Department of Physics, University of Bucharest, Bucharest, Romania

V. P. Likhachev

Department of Physics, University of Sao Paulo, Sao Paulo, Brasil

December 14, 2000

* Contact person

Osamu Hashimoto

Department of Physics, Tohoku University, Sendai, 980-8578, Japan
hashimot@lambda.phys.tohoku.ac.jp
Telephone 81-22-217-6452
Fax 81-22-217-6455

Proposal to JLAB PAC-19

Abstract

We propose to perform a spectroscopic study of Λ hypernuclei for wide mass region using the (e,e'K^+) reaction. The expected results will provide Λ hypernuclear spectra with the best energy resolution ($\sim$ 300 keV) ever achieved. An energy resolution of a few hundred keV and high statistical accuracy of the level structure will yield knowledge on the single-particle behavior of a Λ hyperon in a medium mass nuclear system, and allow precise studies of the effective Λ-N interaction. The experiment will take full advantage of high quality electron beam at Jlab by introducing a new experimental geometry and a high resolution kaon spectrometer system now under construction.

The (e,e'K^+) reaction has unique characteristics as outlined below.

- A proton is converted to a Λ hyperon.
- Spin-stretched states are populated with both spin-flip and spin-non-flip amplitude.
- Reaction spectroscopy with resolution as good as 300 keV (FWHM) can be realized.

The proposed experiment has two goals,

1. Excitation spectra of medium-heavy Λ hypernuclei will be studied using the ^{28}Si(e,e'K^+)$^{28}_{\Lambda}$Al and ^{51}V(e,e'K^+)$^{51}_{\Lambda}$Ti reactions. This will provide precision binding energies and widths for the Λ hyperon in its various states in nuclear mass up to A=50. The new structures and/or spin-orbit splittings suggested by the recent (π^+,K^+) reaction spectrum in the medium-heavy hypernuclei can be fully investigated with unprecedented energy resolution.
2. Precision measurement of ^{12}C(e,e'K^+)$^{12}_{\Lambda}$B will be used in order to study the detailed structure of a typical *p*-shell Λ hypernucleus in a qualitative way. In particular, the precision spectrum of $^{12}_{\Lambda}$B can be compared to its the mirror symmetric hypernuclei, $^{12}_{\Lambda}$C, which was studied with high statistics but limited resolution by the (π^+,K^+) reaction.

This experiment can now be undertaken with some confidence due to the pioneering and successful E89-009 experiment, completed in the spring of 2000. We have made a through examination of this experiment, and propose a new experimental geometry for the (e,e'K^+) reaction. This geometry will reduce the bremsstrahlung count-rate in the electron spectrometer, which limited the production rate in the experiment, while preserving the resolution and increasing the signal rate. To increase the coincidence rate and improve the resolution a new high-resolution, large-acceptance kaon spectrometer (HKS) is under construction to replace the SOS spectrometer which was used in E89-009.

This proposed experiment will be the first of the series of studies we would intend to undertake using the new kaon spectrometer.

1 Physics Motivation and Experimental Objectives

1.1 Significance of hypernuclear investigation

A hypernucleus contains a hyperon implanted as an "impurity" within the nuclear medium. This introduces a new quantum number, strangeness, into the nucleus, and if the hyperon maintains its identity it will not experience Pauli-blocking, easily interacting with deeply bound nucleons. In this sense, it has been proposed that the hyperon is a good probe of the interior of a nucleus, where information is difficult to obtain.

In the proposed experiment, we intend to extract the characteristics of a Λ hyperon embedded in a nucleus by observing the spectroscopy of its states. It is a unique characteristic of Λ hypernuclei that deeply bound states, even the ground $s-shell$ states, have very small widths and can be measured as individual peaks in the excitation spectra. These properties have, to some extent, been shown experimentally in recent hypernuclear spectroscopy by the (π^+, K^+) reaction[1, 2, 3].

In hypernuclear production, most of the states are excited as nucleon-hole Λ-particle states, $(\mathrm{N}^{-1},\Lambda)$. The spreading widths of these states were calculated to be less than a few 100 keV [4, 5]. This occurs because: 1) The Λ isospin is 0 and only isoscaler particle-hole modes of the core nucleus are excited; 2) the ΛN interaction is much weaker than the nucleon-nucleon interaction; 3) the ΛN spin-spin interaction is weak and therefore the spin vector p_N-h_N excitation is suppressed; and 4) There is no exchange term.

As a result, particle-hole Λ-hypernuclear states are much narrower than nucleon-nuclear states of the same excitation energy. In the case of Ca for example, it was predicted that $\Gamma_\Lambda(1\mathrm{s} \text{ or } 0\mathrm{d})/\Gamma_N(0\mathrm{s}) = 0.03\text{-}0.07$, resulting in a spreading width narrower than a few hundred keV even for the excited states above the particle emission threshold. This shows that spectroscopic studies of deeply bound Λ-hypernuclear states can be successfully undertaken. Thus through the widths and excitation energies of the single particle levels, the validity of the mean field description of hypernuclear potentials can be examined.

There is also the fundamental question, "to what extent does a Λ hyperon keep its identity as a baryon inside a nucleus?" [6]. Spectroscopic data in heavier hypernuclei can help answer this question. Indeed, the relevance of the mean-field approximation in nuclear physics is one of the prime questions related to role that the sub-structure of nucleons plays in the nucleus. It was, for example, suggested that the mass dependence of the binding energy difference between s and d orbitals may provide information on the "distinguishability" of a Λ hyperon as a baryon in nuclear medium [7].

The effective Λ-Nucleus interaction can be derived from a Λ-nucleon interaction such as the YNG or Njimegen potential forms [8]. The Njimegen potentials are obtained from phenomenological OBE fits to the baryon-baryon data using SU(3) with broken symmetry. The fit well represents the N-N and limited Y-N data. The YNG analytical form of the Λ-N effective interaction [9] is particularly useful in calculating hypernuclear binding energies, level structure, and reaction cross sections and polarizations. Because the Y-N interactions are weaker than N-N, and the Pauli exclusion principle is absent for the Λ hyperons in nucleus, hypernuclear properties can be reliably calculated. Therefore, experimental observables can be connected in

a straightforward way to YN interactions, and precision spectroscopic data can constrain the elementary Λ-N interaction. Indeed, because hyperon-nucleon scattering data cannot be easily obtained, the interaction is mainly constrained by hypernuclear structure.

1.2 Recent hypernuclear investigation

Although the spectra of many light Λ hypernuclei have been studied, there are only a few experiments on hypernuclear systems beyond the *p*-shell. Most of these later data were obtained using the (π^+, K^+) reaction, which strongly populates deeply-bound, high-spin states due to the large momentum transfer in this reaction. The BNL-AGS experiments surveyed the single particle nature of Λ hypernuclei up to ${}^{89}_{\Lambda}\mathrm{Y}$, and observed peaks corresponding to the major Λ shell structure [1]. The KEK E140a experiment made an intensive spectroscopic study using the SKS spectrometer, and observed the major shell structure of the single particle Λ orbits up to ${}^{208}_{\Lambda}\mathrm{Pb}$ [2, 10]. These spectra, shown in Fig. 1 were interpreted in terms of a Λ bound in a Woods-Saxon, density-dependent potential. However, the spectra are of poor quality as seen in the spectra, and the peak positions of the various shell structures were not well determined. Resolutions varied from 1.5 to 4 MeV FWHM from the light to heavy systems.

The best hypernuclear spectrum in the medium-heavy mass region was taken for the ${}^{89}_{\Lambda}\mathrm{Y}$ by the (π^+, K^+) reaction having an energy resolution of 1.7 MeV (FWHM). This spectrum is shown in Fig. 2 [11]. In addition to the major shell structure, the figure clearly shows the splitting of the higher shell orbitals, e.g. the *f* orbit. The origin of this splitting is under intensive discussion, and may be related to the hypernuclear *ls* splitting.

The progress (π^+, K^+) reaction spectroscopy has largely been driven by the superconducting kaon spectrometer (SKS), which has momentum resolution of 0.1 %, and a large solid angle of 100 msr. [12, 13] Using this spectrometer as a microscope, an intensive spectroscopic study of Λ hypernuclei has been undertaken at KEK. Binding energies of a Λ within nuclei as heavy as Pb have been extracted from the spectra, and the central part of the Λ hyperon potential has been experimentally investigated .

For *p*-shell Λ hypernuclei, high quality hypernuclear spectra have been derived again by the (π^+, K^+) reaction at KEK PS and the structure information on light Λ hypernuclei were obtained.[3] The spectra yielded information on the hypernuclear structure such as core excited states and also on spin-dependent ΛN interaction. A sample spectrum for the ${}^{12}\mathrm{C}(\pi^+,\mathrm{K}^+)$ reaction is shown in Fig. 3.

Other recent progress in hypernuclear spectroscopy involves the observation of γ transitions between hypernuclear states which are excited by pion or kaon production reactions. The γ rays are observed by Germanium and NaI detectors in coincidence with the production of bound hypernuclear levels. Because the splitting of the hypernuclear states by spin-dependent interactions (spin-spin and spin-orbit) is small, high precision γ ray spectroscopy is the only technique available which can directly measure these splittings. Of course identifying hypernuclear as opposed to nuclear gammas is difficulty and is presently limited to states in light Λ hypernuclei in the low excitation region. Previously observation of the ${}^{7}_{\Lambda}\mathrm{Li}$ E2 and M1 transition gave crucial information on the spin-spin interaction, and the structure change of the nucleus when a Λ is added to the system.[15] The observation of the E1 gamma

transition between the $p_{3/2}$ excited and the $s_{1/2}$ ground states of ${}^{13}_{\Lambda}$C[17] and the determination of the splitting between $5/2^+$ and $3/2^+$ spin-orbit partners in ${}^{9}_{\Lambda}$Be[16] confirmed the smallness of the ΛN spin-orbit splitting.

Both reaction and the γ ray spectroscopy have greatly advanced in the past few years, but spin splittings are too small to be observed by reaction spectroscopy. The best energy resolution achievable by the (π^+, K^+) reaction spectroscopy is 1.5 MeV (FWHM), and is mainly dependent on beam quality and target thickness. Thus until improved kaon and pion beams of much higher intensity become available, this resolution cannot be improved.

In summary, the present issues in hypernuclear spectroscopy are as follows.

- One would like to know the extent to which the single-particle properties of a baryon remain unchanged in deeply bound states. This can be explored by placing a Λ hyperon deeply within the nucleus.
- One would like to determination the spin dependent interaction strengths, of the effective Λ-Nucleus and thus extract the form of the Λ-N potential.

Although the spin-dependent interaction is best intensively studied in the *p*-shell by the γ-ray spectroscopy, complementary information from higher mass nuclei and higher excitation energies will be important. However the single particle nature of the Λ hyperon embedded in nuclear matter must be studied by the spectroscopy of heavy hypernuclei, and this is the key motivation of this proposal.

1.3 Experimental objectives

The proposed experiment is intended to establish high-precision spectroscopy of Λ hypernuclei for wide mass range by the (e,e'K^+) reaction. Such experimental investigation is possible only by utilizing the high precision and power of the Jlab electron beam, and a new high resolution, large solid-angle spectrometer system under construction.

The experimental objectives of the proposal are summarized below.

1. We propose to obtain high-precision binding energies of Λ single particle states from the excitation spectra of Λ hypernuclei up to A=50 region.

   The limited resolution of the (π^+, K^+) reaction makes it difficult to extract precise Λ binding energies, except for the light Λ hypernuclei. Energy resolutions of a few 100 keV are needed to extract these binding energies. This information provides the depth of the central potential and possible spin-orbit splittings over a wide mass region. The mass dependence of the single particle levels can be directly compared to calculations using single particle potentials and mean-field theory. Since *p*-shell orbitals are barely bound in *p*-shell hypernuclei, it is essential to extend this measurement to heavier systems. The proposed experiment also provides information on the widths of these single particle orbitals.

   As the effective mass of a Λ hyperon appears to be close to that of the free Λ hyperon, the potential seems to be local in contrast to ordinary nuclei. Thus the proposed precision measurement of the single particle levels can address the degree of non-locality of the effective Λ-Nucleus potential. This can be related

to the nature of the ΛN and ΛNN interactions, and to the ΛN short range interactions.[18]

In a more exotic way, the binding energies can be discussed in terms of the distinguishability of a Λ hyperon in nuclear medium, which will result in different A dependence of the binding energy as suggested by Dover.[7]

2. We propose to study the spin-orbit splitting of the Λ single particle states in heavier hypernuclei. As previously discussed, the ^{89}Y spectra taken by the (π^+, K^+) reaction show that the higher l states are split by about 1 MeV. These splittings are suggested to be due to the ΛN ls interaction, although the magnitude of the splitting is much larger than expected from previous measurements in the p-shell, and in particular from the recent γ ray data of $^{9}_{\Lambda}$Be and $^{13}_{\Lambda}$C.[16, 17] However the splitting could also be due to an interplay of different neutron hole states. With a resolution of about 300 keV, we will be able to entangle closely degenerate hypernuclear states, and clarify the situation. If the origin of the splitting is due to ls interaction it will give us the magnitude of the interaction, and introduce a deeper puzzle about the changes in the ls strength between the p and deeper shell structure. If the splitting is due to hypernuclear structure, it will give us information on the characteristics of medium-heavy hypernuclei. In either case, new information is required to address this issue.

3. We propose to study the ^{12}C(e,e'K$^+$)$^{12}_{\Lambda}$B reaction as a reference reaction in order to tune the new spectrometer system. As a byproduct of this calibration we will accumulate a high statistics $^{12}_{\Lambda}$B spectrum with a resolution of a few 100 keV. This should clearly separate the controversial core excited states. These states were observed in the ^{12}C(π^+,K$^+$) reaction, and a high precision - high statistics study will provide information on inter-shell mixing and perhaps on the splitting of the ground state doublet.[14, 24, 25]

2 The (e,e'K$^+$) reaction for the hypernuclear spectroscopy

2.1 Hypernuclear production reactions

The (e,e'K$^+$) reaction has a unique characteristics for the hypernuclear spectroscopy among a wide variety of reactions which can be used to produce a strangeness -1 hyperon as listed in Table 1. Each reaction has its own characteristics and will plays its role for hypernuclear spectroscopy. However, only the (K^-, π^-) and (π^+, K^+) reactions have been intensively used for the spectroscopic investigation in these reactions, so far. These reactions supposed to convert a neutron in the target nucleus to a Λ hyperon. Although the (π^+, K^+) reaction is relatively new compared to the (K^-, π^-) reaction, it is now considered as one of the best reactions for hypernuclear spectroscopy because it favorably populates deeply bound hypernuclear states.[1, 14, 2] The smaller cross sections of the (π^+,K$^+$) reaction compared to that of the (K$^-$,π^-) reaction is easily compensated by intensity of pion beams, which is much higher than that of kaon beams. The (π^+,K$^+$) reaction selectively populates angular momentum stretched states because of the large momentum transfer to the recoil hypernuclei.[19, 20, 18] This is in contrast to the (K^-, π^-) reaction, which transfers small momentum and thus preferentially excites

Table 1: Comparison of Λ Hypernuclear production reactions

$\Delta Z = 0$ *neutron to* Λ	ΔZ = -1 *proton to* Λ	comment
(π^+, K^+)	(π^-, K^0)	stretched,high spin
in-flight (K^-, π^-) stopped (K^-, π^-)	in-flight (K^-, π^0) stopped (K^-, π^0)	substitutional
$(e, e'K^0)$ (γ, K^0)	$(e, e'K^+)$ (γ, K^+)	spin-flip,unnatural parity

substitutional states. By high quality (π^+, K^+) spectra with resolution better than 2 MeV (FWHM), it becomes possible to qualitatively study the unique structure of Λ hypernuclei and characteristics of the Λ-nucleon interaction.

2.2 The (e,e'K$^+$) reaction

Since the momentum transfer of the (e,e'K$^+$) reaction is almost the same as that of the (π^+, K^+) reaction, it is expected to preferentially populate high-spin bound hypernuclear states. However, in contrast to reactions with meson beams, the electromagnetic reaction will populate spin-flip hypernuclear states as well as non-spin-flip states, since the transition operator has spin-independent (f) and spin-dependent (g) terms.[21, 22] Although the spin independent term is significantly smaller than the spin-dependent term, the spin-flip and non-spin-flip components in the spin-dependent term have comparable amplitudes.

Also the (e,e'K$^+$), in contrast to the (π^+, K^+) and (K^-, π^-) reactions, converts a proton to a Λ hyperon. This results in proton-hole-Λ-particle states in the configuration $[(lj)_N^{-1}(lk)^\Lambda]_J$. When the proton hole state is $j_> = l + 1/2$, the highest spin states of $J = J_{max} = j_> + j_>^\Lambda = l_N + l_\Lambda + 1$ are favorably excited. These hypernuclear states are of unnatural parity when the original proton orbit is $J_>$. On the other hand, if the hole state has spin $j = j_< = l - 1/2$, the highest spin states of the multiplet $J'_{max} = j_< + j_>^\Lambda = l_N + l_\Lambda$ with natural parity are strongly populated. This selectivity is particularly important as it allows us to directly study the spin-dependent structure of Λ hypernuclei.

Experimentally, the most important characteristics of the (e,e'K$^+$) reaction is that it can provide significantly better energy resolution because the reaction is initiated with a primary electron beam of extremely good beam emittance, in contrast to secondary meson beams. With a high performance spectrometer, energy resolution of a few 100 keV can be achieved.

The unique characteristics of the (e,e'K$^+$) reaction are summarized below.

- Extremely good energy resolution when coupled with the high resolution kaon spectrometer (HKS) under construction in Japan.
- The production of natural and non-natural parity states.

- The production of neutron rich hypernuclei as the reaction replaces a proton by a Λ.
- calibration of the (e,e'K^+) reaction can be performed by the elementary p(e,e'K^+)Λ reaction on a CH_2 target which provides an exact energy scale.

Although the (e,e'K^+) reaction has many advantages for hypernuclear spectroscopy, it has disadvantage that the cross section is much smaller than reactions using hadronic beams. For example, the calculated cross section for the ^{12}C(e,e'K^+)$^{12}_{\Lambda}$B$_{gr}$ is two orders of magnitude smaller than that of the corresponding ^{12}C(π^+,K^+)$^{12}_{\Lambda}$C$_{gr}$ reaction. With the E89-009 setup, hypernuclear yields of the ground state of $^{12}_{\Lambda}$B are smaller by almost two order of magnitude compared with that of $^{12}_{\Lambda}$C by the SKS experiment. However, this disadvantage can be overcome by employing a new geometry which we propose for this experiment. The new geometry uses a new Kaon spectrometer, HKS, which is described in the next section.

2.3 Previous E89-009 experiment

The first hypernuclear electro-production experiment has been successfully completed in Hall C at Jlab in the spring of 2000. This experiment used the ^{12}C(e,e'K^+)$^{12}_{\Lambda}$B reaction, and observed the ground state peak of $^{12}_{\Lambda}$B hypernucleus. The experiment demonstrated that Λ hypernuclear spectroscopy can be performed by the (e,e'K^+) reaction and that sub-MeV energy resolution can be obtained as shown in Fig. 4. The resolution obtained in the experiment, $\sim$ 650 keV, is better by a factor of 3 than that previously obtained.

The E89-009 experiment was designed to take advantage of the peak in the virtual photon flux at very forward angles. Thus it had low luminosity since a maximum number of photons/incident electron were available for reactions. The experimental setup is schematically shown in Fig. 5. Zero degree electrons and positive kaons were bent into their respective spectrometers on opposite sides of the beam by a splitter magnet. The electron momentum was analyzed by a small Split-Pole spectrometer positioned to detect zero degree electrons. Positive kaons were detected also at around 0 degrees using the SOS spectrometer. Typical count rates of each particle in the Enge and SOS spectrometers were summarized in section 14.4 of Appendix B. The experiment utilized a low beam current of 0.66 μA with a ^{12}C target 20 mg/cm^2 thick.

Although the experiment was successful, the yields were limited due to the background flux of bremsstrahlung in the electron spectrometer. We had recognized that further improvement of experimental configuration would be required to extend these studies to heavier systems. However E89-009 was needed to provide valuable information on rates and cross sections in order to design a geometry which could be successfully be extended.

3 Proposed experiment

3.1 Experimental goals

Based on the experience obtained in the E89-009 experiment, we plan to take into account the following two key points for the proposed experimental configuration.

- A new high resolution kaon spectrometer (HKS) which is under construction will have 20 msr solid angle with the splitter and simultaneously achieve around a few 100 keV resolution.
- A new experimental configuration will maximize hypernuclear production rates by avoiding the 0-degree bremsstrahlung electrons but still measure scattered electrons at a sufficiently forward angle. "Tilt method" in which the Enge electron spectrometer is tilted by 2-3 degrees vertically will allow us to accept a beam current as high as a few tens μA.

It is emphasized that hypernuclear yield/nb/sr is approximately inversely proportional to hypernuclear mass number with the proposed "Tilt method", while the beam intensity was limited by brems electron rates since it is governed by inverse of $Z^{2+\delta}$ when the 0 degree tagging method is employed. Therefore, the "Tilt method" is much advantageous for the spectroscopy of heavier Λ hypernuclei than the "0 degree tagging method". The new "Tilt method" inherits advantageous aspects of the 0-degree tagging method, but allows us to accept much higher beam currents because the high rate brems electrons are not allowed to enter the Enge spectrometer.

3.2 Proposed experimental condition

In the proposed experiment, the followings were taken into account to optimize experimental conditions for high-resolution and high efficiency hypernuclear spectroscopy.

1. As shown in Fig. 6 and Fig. 7, angular distributions of virtual photons and kaons in the (e,e'K^+) reaction is forward peaked and thus both the electron and the kaon spectrometer should be positioned at as forward angles as possible.
2. The virtual photons at 0 degrees have the energy, E_γ, is given as,

$$E_\gamma = E_e - E_{e'} \tag{1}$$

   where E_e and $E_{e'}$ are beam and scattered electron energies. The elementary cross section of the (γ,K^+) reaction has relatively weak E_γ dependence above the threshold.
3. Once the energy of virtual photon is fixed, outcoming K^+ momentum is given assuming hypernuclear mass. P_{K^+} is about 1 GeV/c for E_γ = 1.8 - 0.3 = 1.5 GeV where the scattered electron energy is assumed to be 0.3 GeV as an example. Photon energy effective for the production of kaons will have a range that corresponds to the energy acceptance of the electron spectrometer. Thus, the momentum acceptance of the kaon spectrometer and the electron spectrometer should match each other.
4. Maximum kaon momentum to be detected should be optimized considering
   (a) Yield of hypernuclei
   (b) Energy resolution and acceptance of the spectrometer. Naturally, the energy resolution becomes worse with higher momentum.
   (c) Particle identification, particularly between pions and kaons.

(d) Size of the kaon spectrometer and consequently construction cost.

5. For the yield of Λ hypernuclei, three factors contribute,

   (a) The elementary cross section of n(γ,K^+)Λ is almost constant for the energy range of real γ from 1.1 - 2.0 GeV. Corresponding kaon momentum is from $\sim$ 0.7-1.6 GeV/c. However, the hypernuclear cross sections get greater with the higher γ energy because the recoil momentum becomes smaller.

   (b) With higher kaon momentum, the survival rate of the kaon becomes higher for the given flight path of the spectrometer.

   (c) With higher kaon momentum, the cone of scattered kaons becomes narrower. Thus, larger fraction of the hypernuclei produced in the reaction will be captured for the same solid angle if the spectrometer is positioned at or close to 0 degrees.

   The figure of merit as a function of electron energy assuming the scattered electron energy is 0.285 GeV is shown in Fig. 8. It is shown the higher the energy of the electron beam, the larger the yield of the hypernuclear ground states for a given spectrometer configuration.

6. Although the hypernuclear yield is expected to increase with beam energy, reaction channels strangeness production other than a Λ hyperon open at higher energy and will become sources of background, because that bremsstrahlung photons up to the beam energy are produced in the targets. The electron beam energy is better kept as low as possible from the points of background and particle identification.

7. Taking into account above conditions, the optimum kaon momentum is set at 1.2 GeV/c aiming 2×10^{-4} momentum resolution. The momentum resolution corresponds to about 100 keV energy resolution in hypernuclear excitation spectra.

8. The electron spectrometer also should have momentum resolution of $\leq 3 \times 10^{-4}$, matching that of the kaon spectrometer. Since the momentum of scattered electron is low compared to that of kaons, better momentum resolution can be achieved.

3.3 Proposed experimental geometry

The E89-009 experimental setup accepted reaction electrons and kaons at angles down to zero degrees. The singles rates in each arm of electrons, positrons, pions and protons were analyzed and compared with theoretical calculations. However the calculated rates were renormalized to the experimental rates when used for the various estimates to be described below. It was found that the 0-degree electron-tagging method was limited by the accidental rate from bremsstrahlung electrons. We therefore propose to tilt the electron spectrometer by a small angle sufficient to exclude electrons from the bremsstrahlung process. This technique is described in detail in Appendix A.

A plan view of the proposed geometry, splitter+Enge spectrometer +high resolution kaon spectrometer (HKS), is shown in Fig. 9. Both the HKS spectrometer and the Enge spectrometer are positioned as far forward in angle as possible,

without accepting 0-degree electrons or positrons. The HKS spectrometer, having a QQD configuration, was designed for the kaon arm. Details are found in the Appendix B. It has a momentum resolution of 2×10^{-4} at 1.2 GeV/c, and a large solid angle of 20 msr, including the splitter. This is summarized in Table 2.

In designing the proposed experiment, data taken in E89-009 experiment were analyzed and singles rates of electrons, positrons, pions and protons in each arm were extracted. These are compared with the EPC code calculations and the normalization factors were derived. Assuming the obtained normalization factor for the hadron production rate at the forward angles, singles rates of the counters in the proposed setup were evaluated.

For the scattered electrons, the Enge split-pole spectrometer used for the E89-009 experiment will be adopted. However, the spectrometer is to be vertically tilted by 2.25 degrees so that the Bremsstrahlung electrons will not enter the spectrometer acceptance. The components of the focal plane detector system are redesigned and are explained later.

The splitter magnet has the same geometry used in E89-009 but the gap will be widened so that it matches the HKS geometrical acceptance.

The configuration and specification of the proposed hypernuclear spectrometer system is summarized in Table 2 and is shown in Fig. 9.

Table 2: Experimental condition and specification of the proposed hypernuclear spectrometer system

Beam condition	
Beam energy	1.8 GeV
Beam momentum stability	1×10^{-4}
General configuration	Splitter+Kaon spectrometer+Enge spectrometer
Kaon spectrometer	
Configuration	QQD and horizontal bend
Central momentum	1.2 GeV/c
Momentum acceptance	$\pm$ 10 %
Momentum resolution ($\Delta p/p$)	2×10^{-4}
	(beam spot size 0.1mm assumed)
Solid angle	20 msr with a splitter
	(30 msr without splitter)
Kaon detection angle	Horizontal : 7 degrees
Enge split-pole spectrometer	
Central momentum	0.3 GeV/c
Momentum acceptance	$\pm$ 20 %
Momentum resolution ($\delta p/p$)	2×10^{-4}
Electron detection angle	Horizontal : 0 degrees
	Vertical : 2.25 degrees

3.4 Proposed reactions

1. **$p(e,eK^+)\Lambda$ reaction**

   The reaction is used to calibrate the spectrometer system with a CH_2 target for

the absolute missing mass scale. The procedure has been established in the E89-009 experiment. By the known Λ mass, the absolute scale of the binding energy can be determined reliably. Since we aim to determine absolute binding energies of a Λ hyperon in the mass region where no emulsion experiments can be applied, the reaction is important for the present experiment. It is in contrast to the (π^+, K^+) reaction in which we have to rely on other in direct reactions since a neutron target is not available.

2. **^{12}C(e,e'K$^+$)$^{12}_{\Lambda}$B reaction**

   The reaction is used as a reference reaction for examining overall performance of the spectrometer. Since the excitation function of $^{12}_{\Lambda}$B is expected relatively simple and high statics data can be obtained in relatively short data taking hours, the reaction will allow us to optimize the optics of the entire system thus the overall missing mass resolution. Also, short runs before any beam period will allow us to correct any possible shifts in the system settings.

   In addition, the reaction will provide us with significant physics information. As already mentioned in the preceding section, the $^{12}_{\Lambda}$C hypernucleus studied by the (π^+, K^+) reaction revealed hypernuclear core excited states for the first time. Since then, the excitation energies of the 1^-_2 and 1^-_3 states which supposed to be generated by coupling of a Λ hyperon in the s orbital and the core excited ^{11}C have been under intensive discussion. Role of intershell mixing of positive-parity states and the relation with the ΛN spin-spin interaction have been suggested.[24, 25] Precision spectrum of the mirror symmetric Λ hypernucleus, $^{12}_{\Lambda}$B, with much better resolution will resolve these states unambiguously as demonstrated in Fig. 10 and the excitation energies and cross sections of the states will be determined reliably. We also intend to determine or set the limit of spin-spin splitting of the ground state since the (e,e'K$^+$) reaction populates both states in comparable strengths. Due to the high yield of the new geometry and statistics needed for calibration of system optics, the angular distributions are automatically measured for the major shell states because of the large HKS angular acceptance.

3. **^{28}Si(e,e'K$^+$)$^{28}_{\Lambda}$Al reaction**

   The ^{28}Si(π^+,K$^+$)$^{28}_{\Lambda}$Si reaction was studied using the SKS spectrometer, a spectrum of which is shown in Fig. 11.[2] In the spectrum, major shell structure corresponding to the s and p orbitals with 2 MeV (FWHM) resolution was seen. At the same time unexpected peak structure was observed between the two peaks, although the origin is not known. Since the mass dependence of Λ spin-orbit splitting of the p orbital is expected to be almost maximum at $^{28}_{\Lambda}$Si, it was also aimed to resolve the splitting.

   The excitation spectrum of the ^{28}Si(γ,K$^+$)$^{28}_{\Lambda}$Al reaction has been calculated at E_γ = 1.30 GeV and θ = 3 degrees. A simulated spectrum assuming the spin-orbit strength (V_{so} = 2 MeV) with 300 keV (FWHM) resolution and with expected statistics for the proposed running time is shown in Fig. 12. Peaks corresponding to each major shell orbitals will be distinctively identified and their binding energies will be derived reliably. For a Λ hyperon in the p orbital, $[\pi d^{-1}_{5/2} \otimes \Lambda p_{3/2}]4^-$ and $[\pi d^{-1}_{5/2} \otimes \Lambda p_{1/2}]3^-$ states are dominantly populated, providing a good opportunity to directly observe the ls splitting. Figure 12 clearly demonstrates possibility of observing the splitting.

4. **^{51}V(e,e'K$^+$)$^{51}_{\Lambda}$Ti reaction**

   In the ^{51}V target, the neutron $f_{7/2}$ shell is well closed and stable because N=28. The reaction is supposed to convert one of the three protons in the f-shell to a Λ hyperon. In this hypernuclear mass region, a hyperon is bound up to the d-orbital, providing us an opportunity to determine the binding energies up to higher l. The hypernucleus, $^{51}_{\Lambda}$V, was studied by the (π^+, K^+) reaction at BNL with resolution around 3 MeV (FWHM) and it is shown in Fig.13.[1] The quality of the spectrum is poor but the major shell structure is seen. For the (γ,K$^+$) reaction, a model calculation has been carried out similarly as ^{28}Si(γ,K$^+$)$^{28}_{\Lambda}$Al.[26, 22] In Fig.14, the calculated excitation spectrum is shown. The $[\pi f_{7/2}^{-1} \otimes \Lambda d_{5/2}]6^-$ and $[\pi f_{7/2}^{-1} \otimes \Lambda d_{3/2}]5^-$ states, which are spin-orbit partners, are expected to be split by more than 1 MeV if $V_{so} = 2$ MeV. The calculated spectrum suggests that these states will be simultaneously populated and can be observed in the (e,e'K$^+$) reaction.

   Since nuclei in this mass region are rather well described by shell-model wave functions, it is expected that comparison between experimental data and theoretical calculations will have less ambiguities. We will therefore have a good chance to investigate the single-particle nature of a Λ hyperon and also investigate the splitting of the single particle states not only in the s and p orbitals but also in the d orbital.

5. **^{89}Y(e,e'K$^+$)$^{89}_{\Lambda}$Sr reaction**

   As mentioned already, $^{89}_{\Lambda}$Y is the Λ hypernucleus studied with the best statistics in medium-heavy mass region by the (π^+, K^+) reaction. As seen in Fig. 2, in addition to the major shell peak structure, splitting of these peaks were observed. If the (e,e'K$^+$) reaction can be applied to this heavier mass region, we will better investigate Λ hyperon single-particle nature and also splitting of these states by ΛN interaction. Therefore, we also propose to conduct an exploratory R&D run with the ^{89}Y target to examine feasibility of extending the (e,e'K$^+$) hypernuclear spectroscopy to the heavier mass region.

4 Experimental setup and expected performance

In this section, we describe the proposed experimental setup and also the expected performance of the spectrometer system which is evaluated based on the experience of E89-009. Further detail of the HKS spectrometer design and construction plan will be given in Appendix B.

4.1 General configuration

The present spectrometer system consists of 1) the HKS spectrometer for the kaons, 2) Enge spectrometer for the scattered electron and 3) the splitter. In Fig. 15, plan view of the spectrometer system installed in Hall C is shown. It would fit in the space between the HMS-SOS pivot and the G0 detector system. Our intension is to install the spectrometer system as upstream us possible so that the interference with the G0 experimental setup is minimum. It is required that the beam swingers are installed downstream of the splitter magnet and the beam is directed to the beam dump of Hall C. It is necessary since the high intensity beam of 30 μA are required

in the proposed experiment, contrasting E89-009 which used low beam current of about 1 μA.

4.2 High resolution Kaon spectrometer (HKS)

General specifications of the HKS spectrometer are given in Table. 2. The HKS is designed to achieve simultaneously 2×10^{-4} momentum resolution and 20 msr solid angle acceptance with the splitter. Figure 16 shows the angular and momentum acceptance of the HKS spectrometer with the splitter calculated with a GEANT simulation code. The HKS is placed rotated horizontally by 7 degrees with respect to the beam to avoid zero degree positive particles, mostly positrons. The solid angle is more than 20 msr over the momentum region of 1.2 GeV/c $\pm$ 10%, as designed. Figure 17 shows the momentum resolution obtained with the code as a function of momentum for three different positions of the tracking chambers with respect to the focal plane. In the simulation, realistic matter distributions such as a vacuum window and chamber windows, and drift chamber position resolutions were taken into account. Even with a modest chamber resolution of 200 μm, momentum resolution of 2×10^{-4} will be achieved.

The detector system for the HKS and Enge is summarized in Table 3. The HKS detector system has similar configuration to the one in SOS. However, as seen in Table 4, HKS singles rate is dominated by pions, whose rate will be up to a few MHz. In order to achieve efficient pion rejection rate as high as 10^{-4}, two layers of aerogel Cerenkov counter with refractive index of 1.055 will be installed. For the proton rejection, Lucite Cerenkov counter with wavelength shifter in it will be employed, so that the Cerenkov counter has good efficiency for the wide range of incident angles. Time resolution of as good as 80 ps is a goal for the time-of-flight scintillators. By having the good time resolution, we plan to minimize the distance between the two time-of-flight wall and achieve large solid angle. A Gas Cerenkov counter will also be installed as a trigger counter so that positrons can be tagged for calibration purposes. The tracking chambers of HKS should have high rate capability and accept the rate up to a few MHz.

4.3 Enge spectrometer

The Enge spectrometer which was used in E89-009 will be installed as a spectrometer to analyzes scattered electron momentum. However, as already mentioned, the spectrometer will be tilted vertically by 2.25 degrees, which was not the case in the previous E89-009 experiment.

The detectors required at the Enge are also summarized in Table 3. For the Enge spectrometer, tracking of the electrons are required to achieve good momentum resolution since it is tilted and the focal plane is no more the one originally designed. The expected rate is only a few MHz and is 2 order of magnitude smaller than the case of E89-009, in which the beam intensity as limited by this Brems electron rate.

The optics of the combined system of Splitter plus the tilted Enge spectrometer shows the same general features about focal plane geometry and momentum dispersion as the original untilted geometry used in E89-009. However, with the introduced tilted angle with respect to the horizontal plane, the momentum correlates to all the focal plane parameters, x, x', y, and y', where the x' and y' are the in-plane and out-of-plane angles, respectively. Thus, a full tracking including

both position and angular measurements is needed. The momentum resolution is studied as a function of position and angular errors as shown in Fig.18. The dominant contributions are from x and x', which means that the measurements in y and y' are less crucial. The results showed that using a 4th-order optical matrix and the momentum resolution can be better than 3×10^{-4} (FWHM), if the position error is about 0.15 mm (r.m.s.) and the angular error is about 1 mr (RMS). Such precision can be easily reached by the conventional wire chamber technique and the multiple scattering contributions from the light vacuum window material used in the HNSS experiment and wire chambers is small, if the first tracking plane is located along the focal plane. With a central momentum about 300 MeV/c, the resolution contribution is about 90 keV (FWHM) or less, thus small compare to other contributions. Similarly segmented scintillation hodoscope array as used in the HNSS experiment will be used. The thickness will be increased to improve the time resolution of 250 ps achieved in the HNSS experiment for better signal /accidental separation. An on-line coincidence between the e' and K^+ will be used for this proposed experiment to reduce the data size.

Table 3: Detectors for the proposed experiment

Nomenclature	Size	Comments
HKS spectrometer		
Drift chamber		
HDC1	$30^H \times 90^W \times 2^T cm$	xx'uu'(+30deg)vv'(-30 deg) 5 mm drift distance
HDC2	$30^H \times 105^W \times 2^T cm$	xx'uu'(+30deg)vv'(-30 deg) 5 mm drift distance
Time of flight wall		
TOF1	$30^H \times 110^W \times 2^T cm$	7.5^W cm × 15-segments, H1949
TOF2X	$30^H \times 130^W \times 2^T cm$	7.5^W cm × 17-segments, H1949
TOF2Y	$30^H \times 130^W \times 1^T cm$	4^W cm × 8-segments, H1161
Cerenkov counter		
AC1	$40^H \times 135^W \times 30^T cm$	n = 1.055 water-proof aerogel 16 × 5" PMT
AC2	$40^H \times 135^W \times 30^T cm$	n = 1.055 water-proof aerogel 16 × 5" PMT
LC	$40^H \times 135^W \times 2^T cm$	7.5^W cm × 18-segments, H1161 Lucite with wavelength shifter
GC	$40^H \times 200^W \times 100^T cm$	10 × 5" PMT
Enge spectrometer		
Drift chamber		
EDC1	$10^H \times 72^W \times 10^T cm$	VDC
EDC2	$10^H \times 72^W \times 10^T cm$	VDC
Hodoscope		
EHODO	$10^H \times 80^W \times 1^T cm$	80 segmentation

4.4 Singles rates

Count rates in HKS and Enge spectrometers were estimated as follows:

1. π^+ and proton rates in HKS were calculated based on the EPC code, and were normalized by the experimental values measured in E89-009 for a carbon target at 2.2 degrees. The data obtained in E89-009 are summarized in section 14.4 of Appendix B.
2. Quasifree kaon production cross section was assumed to scale as $A^{0.8}$.
3. Electron rate in Enge was evaluated by two methods, one by EGS code and the other by Light body code, which agreed more or less to each other.
4. Pion rate in Enge was calculated based on the EPC code, and normalized by the same factor used for hadron rates in HKS.

As seen in Table 4, singles rate of HKS is dominated by positive pions. while that for Enge is by electrons. It is noted that we expect the positron rate in HKS is low since we setup HKS at an angle off 0 degrees. The singles rate of the ENGE hodoscope is expected almost two orders of magnitude less than that of E89-009. With this rate, the hardware coincidence between electron arm and kaon arm can form good triggers.

Table 4: Singles rates

Target	Beam Intensity (μA)	HKS e^+ rate (MHz)	HKS π^+ rate (kHz)	HKS K^+ rate (Hz)	HKS p rate (kHz)	Enge e^- rate (MHz)	Enge π^- rate (kHz)
^{12}C	30	-	800	340	280	2.6	2.8
^{28}Si	30	-	800	290	240	2.6	2.8
^{51}V	30	-	770	260	230	2.6	3.0

4.5 Resolution of excitation energy spectra

The following factors contribute to the total resolution of the experiment:

1. HKS momentum resolution
   With a Monte Carlo simulation, the momentum resolution of the HKS was estimated to be 75 keV/c (RMS) for a spatial resolution of 200μm of the chambers.
2. Beam momentum resolution
   Assuming 1×10^{-4}, it will be 180 keV/c (FWHM) for 1.8 GeV/c beam.
3. Enge momentum resolution
   For vertical and horizontal resolutions of the chamber as 150μm, the momentum resolution of the Enge spectrometer is estimated to be 93 keV (FWHM).
4. Kinematical broadening due to uncertainty of the K^+ scattering angle
   The uncertainty of the K^+ emission angle is dominated by the multiple scattering through the materials between the target and the chambers

(uncertainty due to the spatial resolution of the chambers are less than 0.2 mrad). Contribution of the following materials are taken into account: the target (100 mg/cm^2), vacuum windows (kevlar 0.008", mylar 0.005"), helium bag (100 cm) and chambers (mylar 0.0045", argon 5.08 cm @ STP).

Total uncertainty of the K^+ angle was estimated to be 3.3 mrad (r.m.s.) for the carbon target. This angular uncertainty corresponds to 152 keV (FWHM) ambiguity to the ${}^{12}_{\Lambda}$B mass. Similarly, this effect to ${}^{28}_{\Lambda}$Al (Si target) will be 64 keV (FWHM).

5. Momentum loss in the target
The momentum loss in the target was calculated for 1.2 GeV/c K^+ assuming Vavilov distribution. The whole momentum loss in the target will contribute the mass resolution without any correction. The average momentum loss of 1.2 GeV/c K^+ in the carbon 100 mg/cm^2 was 195 keV/c which corresponds to the energy resolution of 180 keV(FWHM).

The results are summarized in Table 5. Present proposed experimental setup will achieve the resolution around 300 keV (FWHM).

Table 5: The energy resolution of the HKS system

Item	Contribution to the resolution (keV, FWHM)			
Target	C	Si	V	Y
HKS momentum			190	
Beam momentum			$\leq$ 180	
Enge momentum			93	
K^+ angle	152	64	36	20
Target (100 mg/cm^2)	$\leq$ 180	$\leq$ 171	$\leq$ 148	$\leq$ 138
Overall	$\leq$ **360**	$\leq$ **330**	$\leq$ **320**	$\leq$ **310**

4.6 Background and signal/noise ratios

One of the major sources of background in the proposed setting that facilitates detection of very forward particles is electrons associated with Bremsstrahlung process. During the E89-009 experiment, a data was taken with Pb sheet blocking 0 degree Brems electrons just at the entrance of the Enge spectrometer. Although it was tricky to place a thin material at 0 degrees, it was learned that blocking 0 degree Brems electrons helps improve signal to noise ratio considerably by this 0-degree blocking technique. The Tilt method, which offers us 2 order of magnitude more hypernuclear yield and a factor of 10 better signal to noise ratio compared to the E89-009 setup.

Electron and positron rates were estimated as given in Table 4 for the beam current of 30 μA and the target thickness of 100 mg/cm^2. It shows that 2.6 MHz of the electron background in the Enge spectrometer which placed with 2.25 degrees to the beam axis (electron beam, 100 mg/cm^2 carbon target). Kaon single rate for the HKS spectrometer was estimated to be 340 Hz as shown in Table 4. With a coincidence window of 2 ns, we have accidental coincidence rate as:

$$N_{ACC} = (2.6 \times 10^6 \text{Hz}) \cdot (2 \times 10^{-9} \text{sec}) \cdot (340 \text{Hz}) \sim 1.8/\text{sec}.$$

Assuming that the accidental coincidence events spread uniformly over the energy matrix (Enge 149 MeV × HKS 240 MeV), the largest background per bin (100 keV) projected on the hypernuclear mass spectrum will be 8 × 10^{-4} /sec. A typical hypernuclear (^{12}C target) event rate will be 48.4 / (100 nb/Sr) / h = 1.3 ×10^{-2} / (100 nb/Sr) / sec as shown in Table 6.

Table 6: Expected hypernuclear production rates in the (e,e'K^+) reaction

Target	beam Intensity (μA)	Counts per 100nb/sr · hour	Qfree K^+ in HKS(Hz)
^{12}**C**	30	48.4	340
^{28}**Si**	30	20.7	288
^{51}**V**	30	11.4	228

5 Yield estimate and requested beam time

The expected yield of the hypernuclear states are evaluated based on the E89-009 result for $^{12}_{\Lambda}$B ground state in the ^{12}C(e,e'K^+)$^{12}_{\Lambda}$B reaction. As described in Appendix B, the proposed "Tilt method" is expected to realize more than factor of 50 yield gain. It is partly because we can use higher intensity beams and thick targets and partly because the kaon spectrometer has a larger solid angle acceptance.

The cross sections of the hypernuclear states for the targets, ^{12}C,^{28}Si,^{51}V have been calculated by Motoba and Sotona.[26, 22] They are listed in Table 7.

It is noted, however, the calculated cross sections vary by a factor of 2-5 depending on the choice of model parameters for the elementary reaction, hypernuclear potentials and configuration of the states etc. In the present yield estimate, the cross sections were normalized assuming the cross section of the ^{12}C(e,e'K^+)$^{12}_{\Lambda}$B reaction for the ground state doublet is 100 nb/sr.

For the beam time, we request commissioning beam time for the HKS itself as the spectrometer is newly installed. The performance of the HKS spectrometer, particularly momentum resolution, will be examined using the requested beam time for the commissioning.

It is our request that the commissioning beam time is allocated a few months before the tuning and data taking beam time so that we can analyze the data and understand the performance of the spectrometer in advance.

Tuning the spectrometer system coupled with the tilted Enge spectrometer will be carried out with a CH_2 target using the Λ peak and with the ^{12}C target.

The requested data taking hours for C, Si and V targets were calculated so that 3000 counts for ground states of $^{12}_{\Lambda}$B, 1000 counts for $^{28}_{\Lambda}$Al and 400 counts for $^{51}_{\Lambda}$Ti can be accumulated, assuming 50 % efficiency for data taking and data analysis. For $^{89}_{\Lambda}$Sr, the requested beam time is only for an exploratory run. The requested beam times are summarized in Table 8. Requested beam conditions are listed in Table 9.

Table 7: Cross sections of ${}^{12}_{\Lambda}$B, ${}^{28}_{\Lambda}$Al and ${}^{51}_{\Lambda}$Ti calculated by DWIA [26]

Target	Hypernucleus	Hypernuclear configuration	Cross section (nb/sr)
^{12}C	${}^{12}_{\Lambda}$B	$s_{1/2}$	112
		$p_{3/2}$	79
		$p_{1/2}$	45
^{28}Si	${}^{28}_{\Lambda}$Al	$s_{1/2}$	56
		$p_{3/2}$	95
		$p_{3/2}$	57
		$d_{5/2}$	131
		$d_{3/2}$	111
^{51}V	${}^{51}_{\Lambda}$Ti	$s_{1/2}$	18
		$p_{3/2}$	41
		$p_{3/2}$	26
		$d_{5/2}$	52
		$d_{3/2}$	48
		$1s_{1/2}$	16
		$f_{7/2}$	32
		$f_{5/2}$	38

6 Schedule of the spectrometer construction and requested support

The construction of the HKS spectrometer and the new hypernuclear spectrometer system has already started in 2000. The present schedule for the construction is shown in Table 10. It is the present plan to ship the HKS spectrometer system from Japan to Jlab by the end of 2002. Detectors are under construction by the collaboration groups and will also be prepared by then.

It is planned that the spectrometer system will be assembled in the Test Lab. prior to the installation in Hall C. The collaboration sets the due date ready to accept a beam March 2003.

7 Summary

High-resolution (e,e'K$^+$) spectroscopy for the four targets, ^{12}C, ^{28}Si, ^{51}V and ^{89}Y has been proposed. By the proposed spectroscopy, we plan to reveal 1) Single-particle nature of a Λ hyperon by deriving single particle binding energies and widths and/or splitting of the single-particle states in wide mass range; 2) Splitting of higher-l single particle states in view of ΛN ls interaction and also structural origin; and 3) Characteristic structure of ${}^{12}_{\Lambda}$B, ${}^{28}_{\Lambda}$Al, ${}^{51}_{\Lambda}$Ti and ${}^{89}_{\Lambda}$Sr. Puzzling core excited states in ${}^{12}_{\Lambda}$B(${}^{12}_{\Lambda}$C) will be intensively studied with high quality spectrum.

An exploratory spectrum will be also taken for the ^{89}Y target, in order to examine the possibility to extend hypernuclear spectroscopy to the heavier targets.

The present proposal assumes the high resolution kaon spectrometer (HKS) under construction by the Tohoku group with the Monbusho budget. The proposal

Table 8: Requested beam time

	Target	Hypernucleus	Number of days	Number of hours
HKS commissioning			7	168
Tuning and calibration			7	168
Data taking				
	^{12}C	$^{12}_{\Lambda}$B	4	96
	^{28}Si	$^{28}_{\Lambda}$Al	8	192
	^{51}V	$^{51}_{\Lambda}$Ti	14	336
	^{89}Y	$^{89}_{\Lambda}$Sr	4	96
Total			40	**960**

Table 9: Requested beam conditions

Typical beam energy	1.8 GeV
Typical beam current	30 μA
Beam energy stability	$\leq 1 \times 10^{-4}$

is fully based on the success of the E89-009 experiment carried out in the spring of 2000. Once the proposed experiment is successfully carried out, we envision that the hypernuclear physics program by the (e,e'K$^+$) reaction will be fully explored as 1) Λ hypernuclear spectroscopy for targets as heavy as Pb; 2) Intensive high quality spectroscopy of light Λ hypernuclei; and also 3) Open a path way toward weak decay experiments taking advantage of high-quality high-power electron beam at Jefferson Laboratory.

Table 10: Present expected time line of the project

April, 2000 - March, 2001	
	Design of the spectrometer system
	Contract with a magnet manufacture
	Construction of Q1 and Q1
	Design of detectors
April, 2001 - March, 2002	
	Construction of the dipole magnet
	R&D test of detectors (TOF, AC etc.)
	Design and construction of the drift chambers
	Design and construction of TOF, LC
April, 2002 - March, 2003	
	Field mapping of the dipole magnet
	Transportation of the dipole to Jlab
	Assembly and test of the spectrometer magnet at Jlab
	Completion of the detector construction
	Assembly of the detector system at Jlab
	Installation of the spectrometer system in the Hall

References

[1] C. Milner *et. al.*, Phys. Rev. Lett. **54** (1985) 1237;
P. H. Pile *et al.*, Phys.Rev.Lett.**66** (1991) 2585.

[2] T. Hasegawa *et al.*, Phys. Rev. **C53** (1996) 1210.

[3] O. Hashimoto, Proc. Int. Workshop on Strangeness Nuclear Physics, Seoul (World Scientific 1999), p. 116.

[4] H. Bandō, T. Motoba and Y. Yamamoto, Phys. Rev. **C31** 265 (1985).

[5] A. Likar, M. Rosina and B. Povh, Z. Phys. **A324** 35 (1986).

[6] T. Yamazaki
Proc. KEK Int. Workshop on Nuclear Physics in the GeV region, KEK Report 84-20(1984) p.3.

[7] C.B. Dover
Proc. Int. Symp. on medium energy physics, Beijing, World Scientific 1987) p.257.

[8] Th.A. Rijken *et al.*, Nucl. Phys.**547** (1992) 245c.

[9] Y. Yamamoto and H. Bando, Prog. Theor. Phys. Suppl.**81** (1985) 9.

[10] O. Hashimoto, Hyperfine Interactions **103** (1996) 245.

[11] T. Nagae, Nucl. Phys. **A670** (2000) 269c-272c.

[12] O. Hashimoto *et al.* Il Nuovo Cimento **102** 679 (1989).

[13] T. Fukuda *et al.*, Nucl. Instr. Meth. **A361** (1995) 485.

[14] T. Hasegawa *et al.*, Phys. Rev. Lett. **74** (1995) 224.

[15] T. Tamura *et al.*, Phys. Rev. Lett. **84** (2000) 5963.

[16] H. Tamura, Talk at HYP2000, October 21-26, 2000, Torino, Italy.

[17] T. Kishimoto, Talk at HYPJLAB99, December 5-7, 2000, Hampton, Virginia, USA.

[18] T. Motoba, H. Bandō, R. Wünsch and J. Zofka, Phys. Rev. **C38** 1322 (1988).

[19] C.B. Dover, L. Ludeking and G.E. Walker, Phys. Rev. **C22** 2073 (1980).

[20] H. Bandō and T. Motoba, Prog. Theor. Phys. **76** 1321 (1986).

[21] T. Motoba, M. Sotona and K. Itonaga, Prog. Thor. Phys. Suppl. No. 117 (1994) 123.

[22] M. Sotona *et. al.*, Proceedings of Mesons and Light Nuclei '98, p. 207. 1998.

[23] E. Hungerford, Talk at HYP2000, October 21-26, 2000, Torino, Italy.

[24] A. Gal, Proc. 23rd INS symp., p.23, Eds. S. Sugimoto and O. Hashimoto (University Academy 1995)

[25] T. Motoba *et. al.* Nucl. Phys. **A639** (1998) 135c.

[26] T. Motoba, Private communication, 1997.

Figures

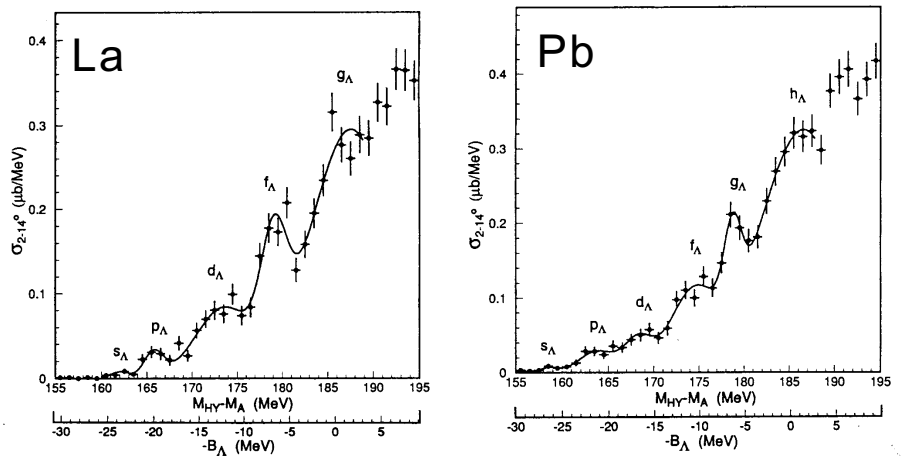

Figure 1: Excitation energy spectrum of ${}^{139}_{\Lambda}$La and ${}^{208}_{\Lambda}$Pb measured with the SKS spectrometer of KEK-PS by the (π^+, K^+) reaction.

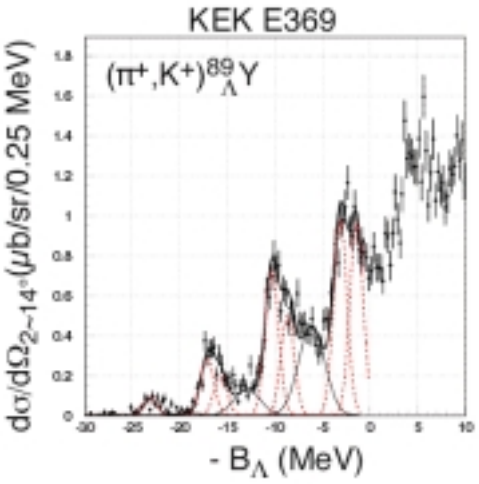

Figure 2: Excitation energy spectrum of ${}^{89}_{\Lambda}$Y measured with the SKS spectrometer of KEK-PS by the (π^+, K^+) reaction.

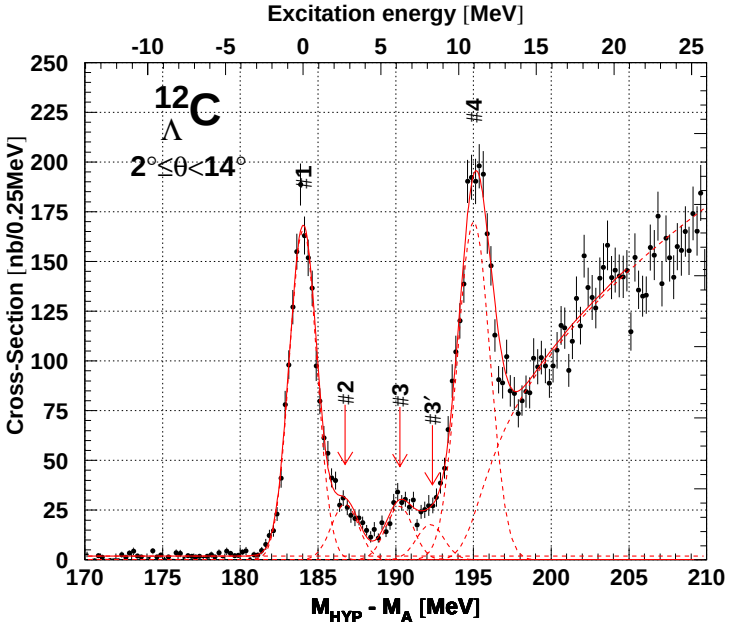

Figure 3: Excitation energy spectrum of ${}^{12}_{\Lambda}$C measured with the SKS spectrometer of KEK-PS by the (π^+, K^+) reaction.

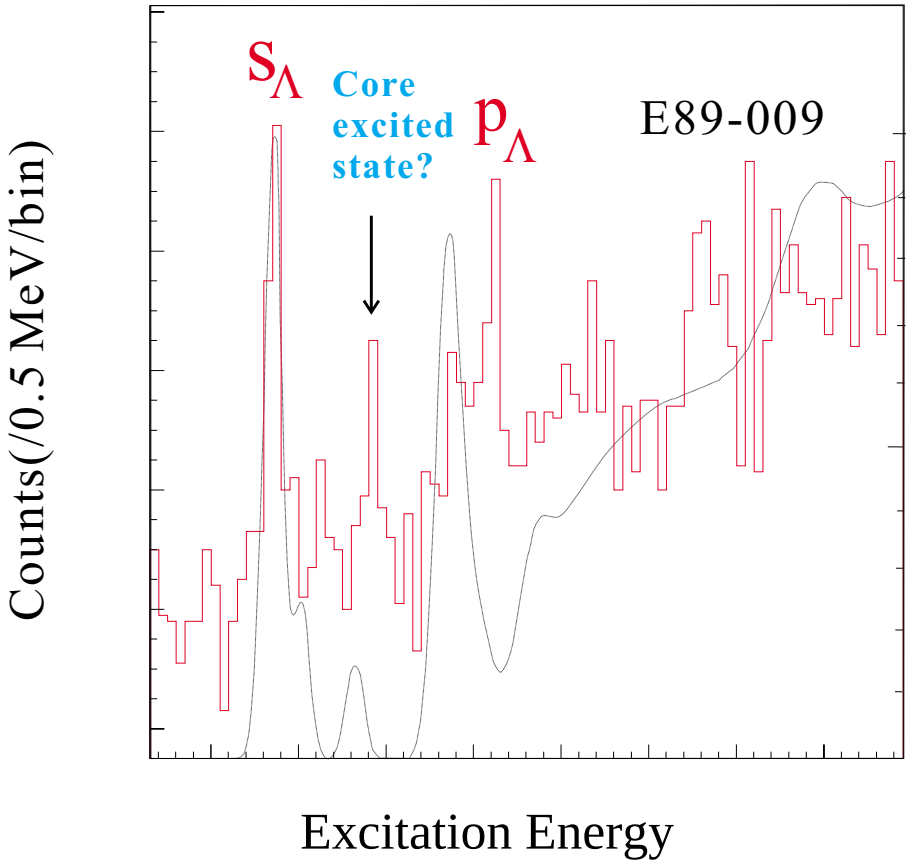

Figure 4: Excitation energy spectrum measured in the E89-009 experiment. Solid line shows the result of Motoba's calculation.

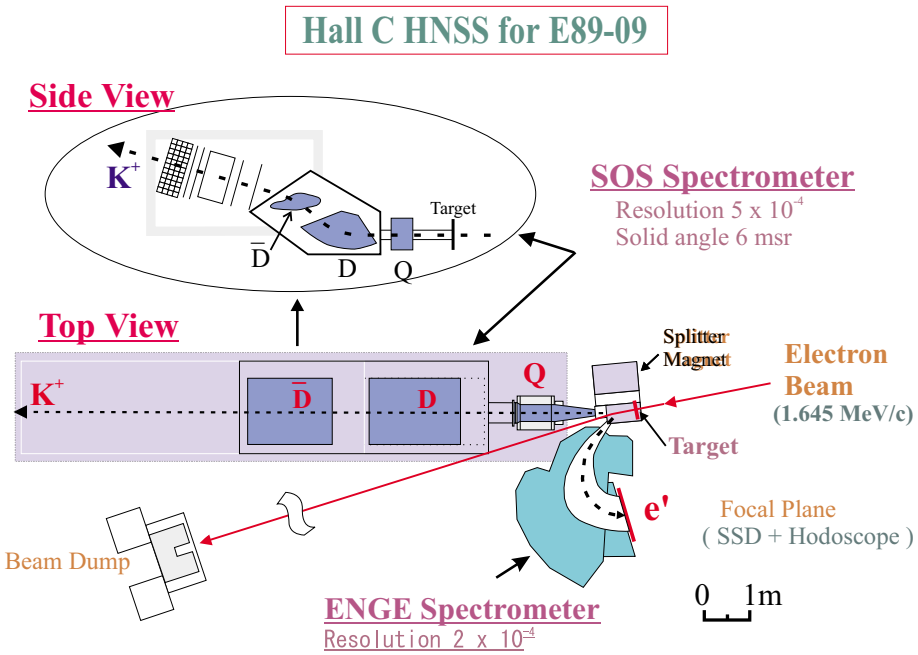

Figure 5: A schematic view of the E89-009 setup.

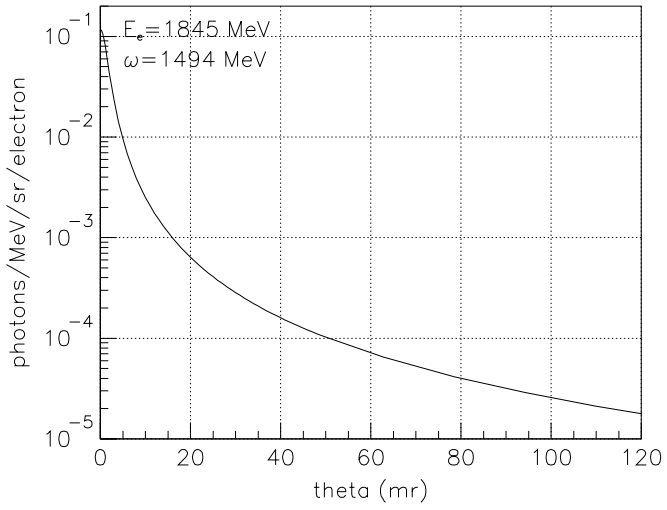

Figure 6: Angular distribution of virtual photons with the ^{12}C target

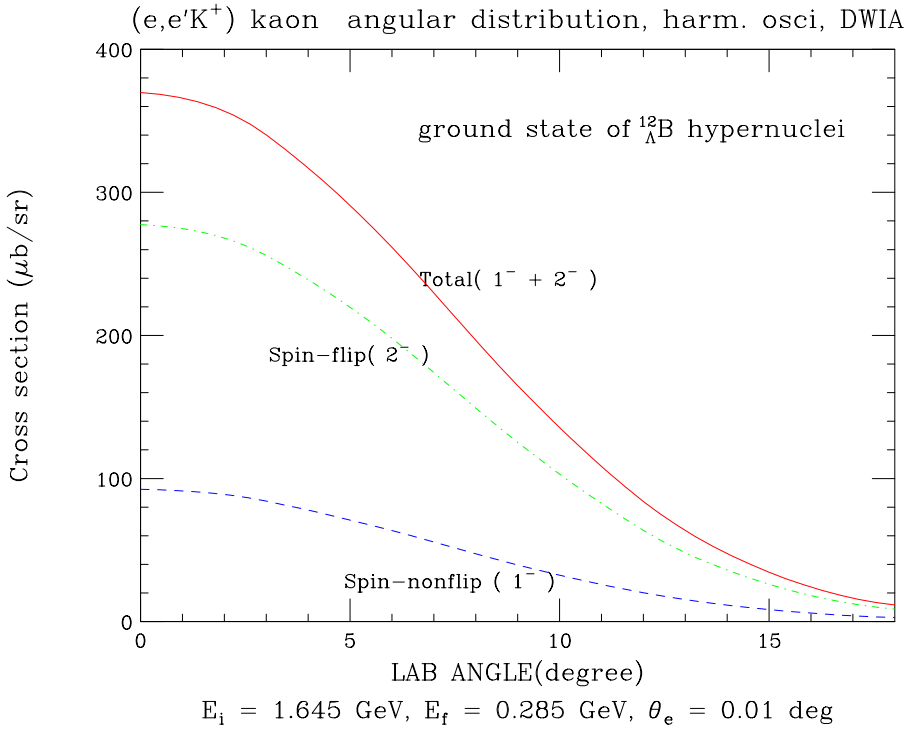

Figure 7: Angular distribution of kaon in the ^{12}C(e,e'K$^+$)$^{12}_{\Lambda}$B reaction.

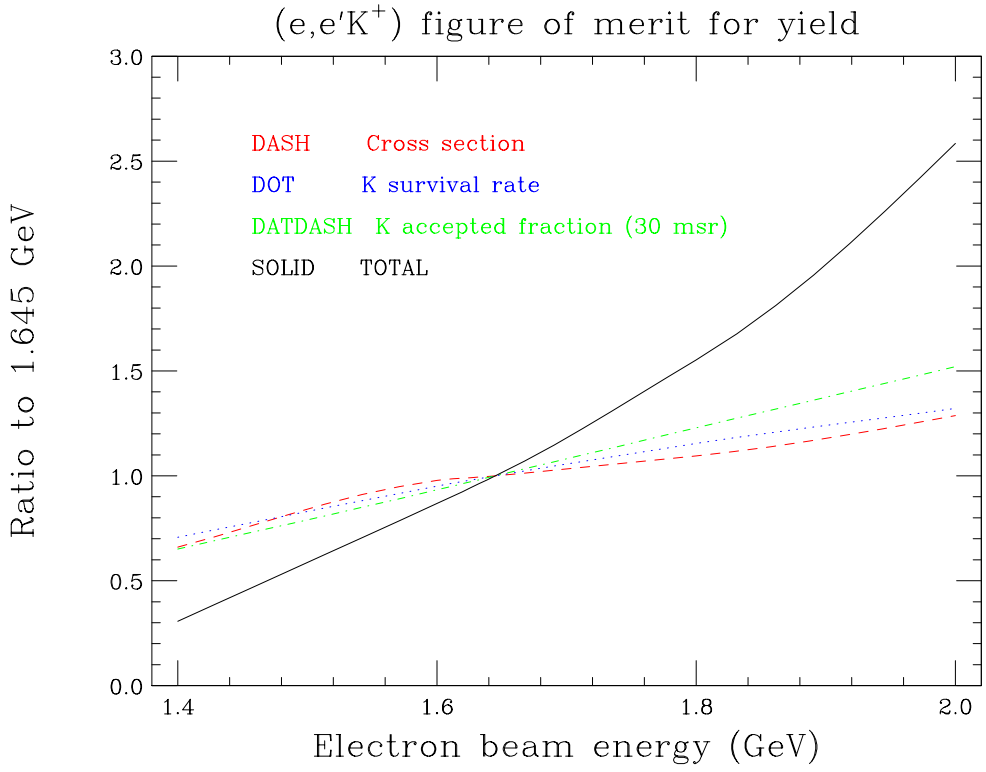

Figure 8: Hypernuclear yield of $^{12}_{\Lambda}B_{gr}$ as a function of the beam energy assuming scattered electrons are measured at E_e = 0.285 GeV.

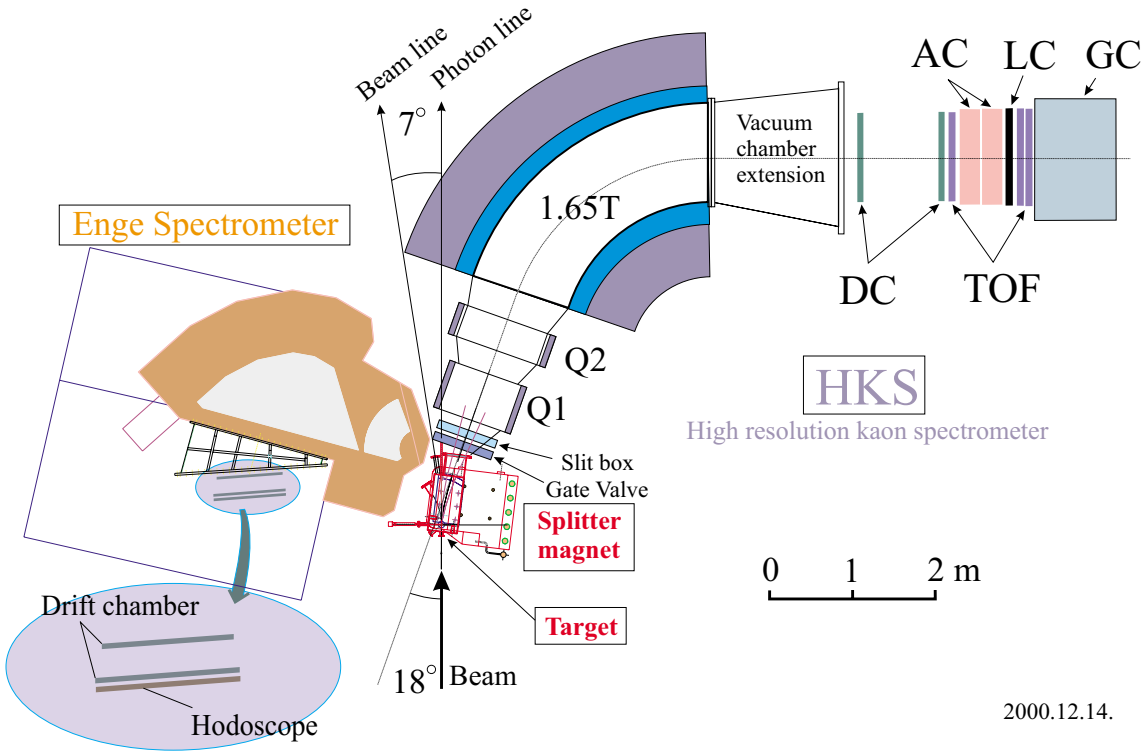

Figure 9: Plan view of the high-resolution kaon spectrometer (HKS) and Enge spectrometer for the proposed experiment.

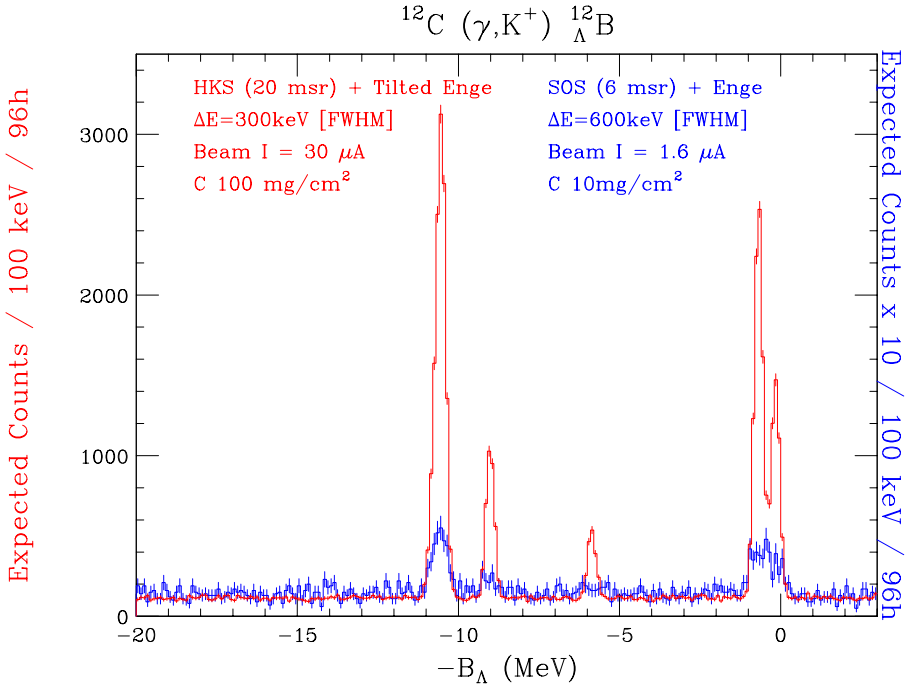

Figure 10: Simulated spectrum of the ^{12}C(e,e'K$^+$)$^{12}_{\Lambda}$B reaction to be observed by the HKS in the proposed beam hours.

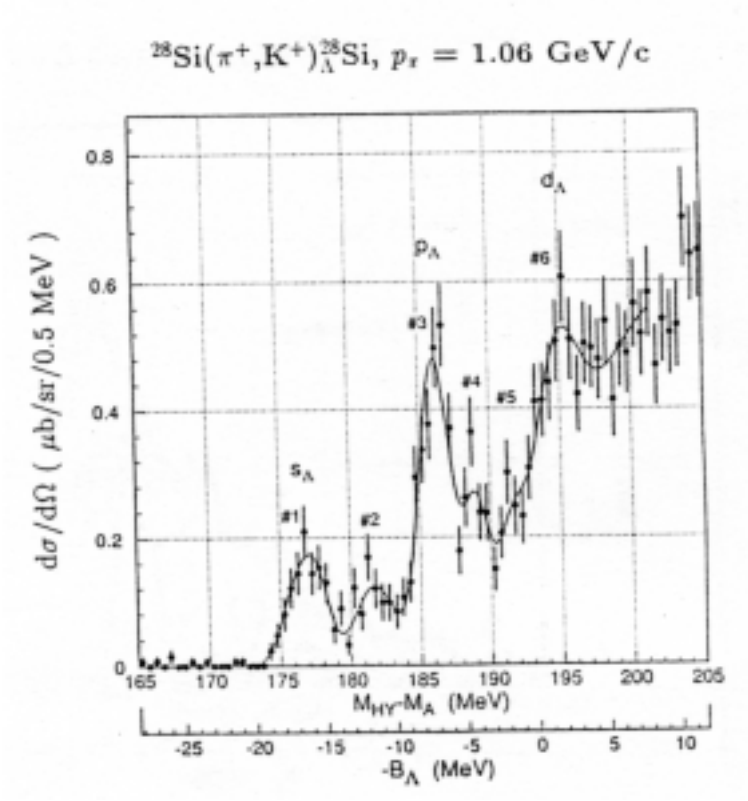

Figure 11: Excitation energy spectrum of $^{28}_{\Lambda}$Si measured with the SKS spectrometer of KEK-PS by the (π^+, K^+) reaction.

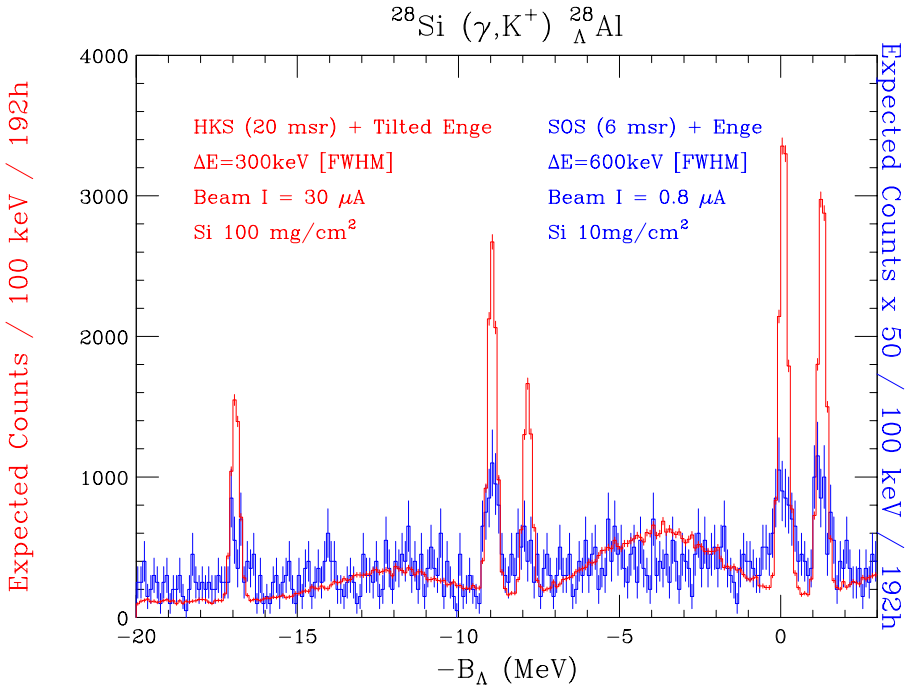

Figure 12: Simulated spectrum of the ^{28}Si(e,e'K$^+$)$^{28}_{\Lambda}$Al reaction to be observed by the HKS in the proposed beam hours.

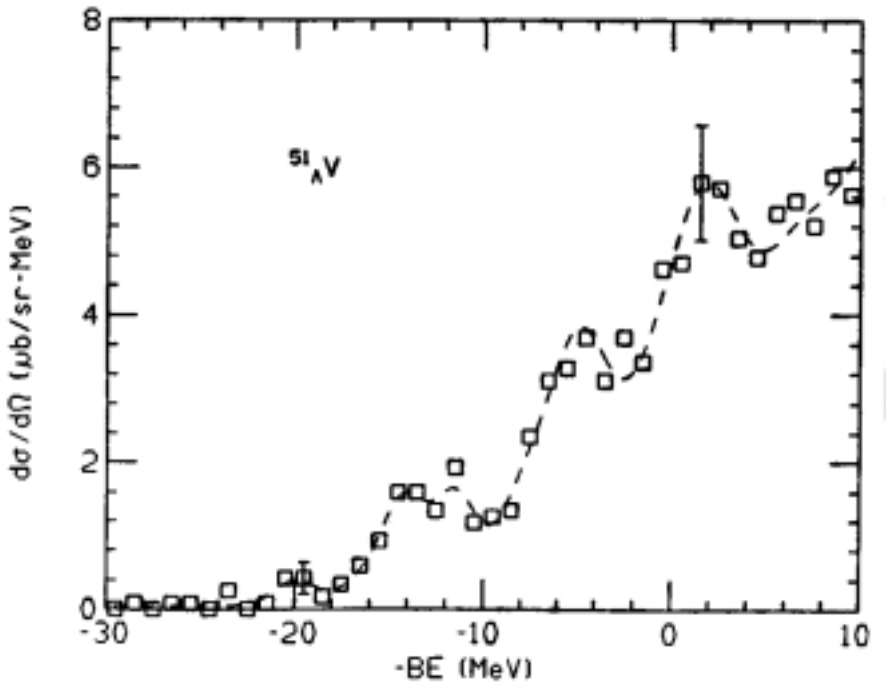

Figure 13: Excitation spectrum of the ^{51}V(π^+,K$^+$)$^{51}_{\Lambda}$V reaction measured at BNL.[1]

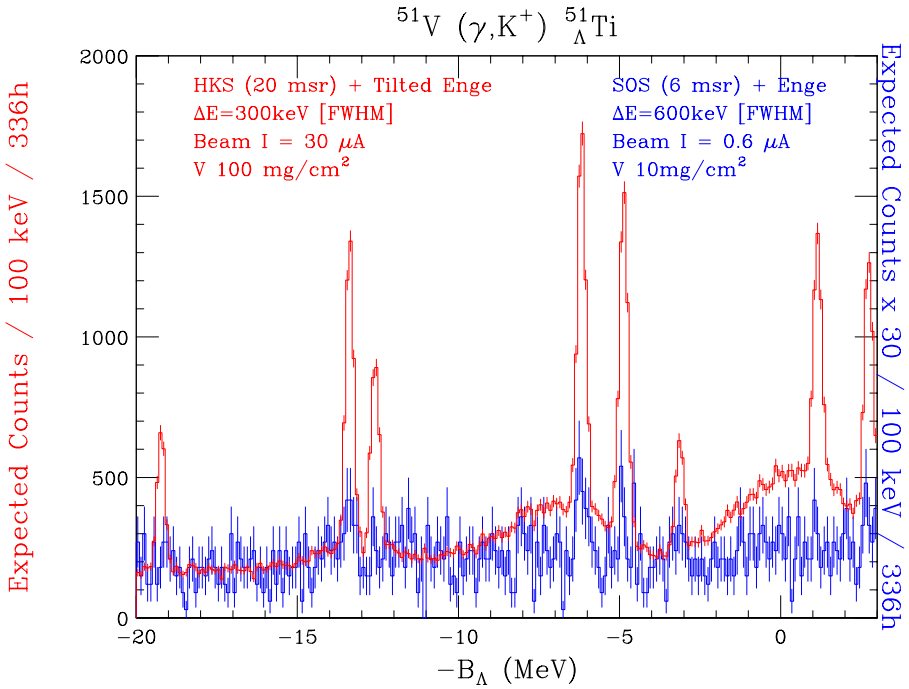

Figure 14: Simulated spectrum of the ^{51}V(e,e'K$^+$)$^{51}_{\Lambda}$Ti reaction to be observed by the HKS in the proposed beam hours.

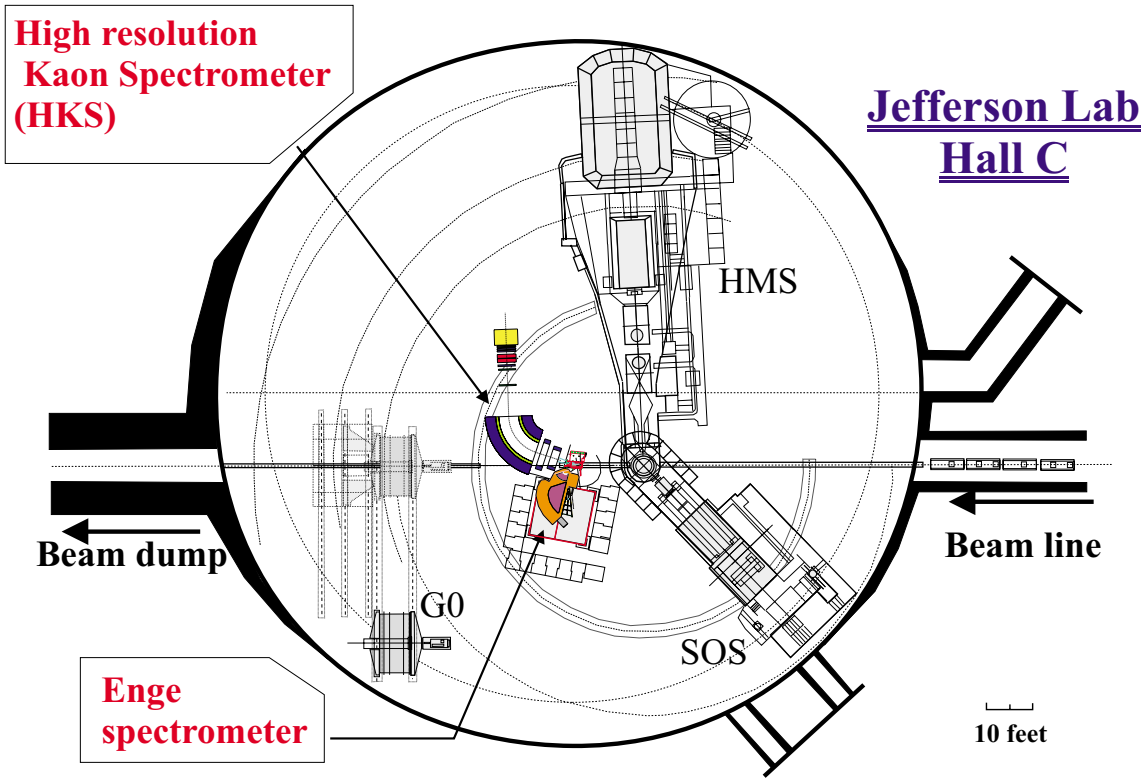

Figure 15: Expected Hall C setup of the HKS and Enge spectrometer. The installation can be compatible with the G0 setup.

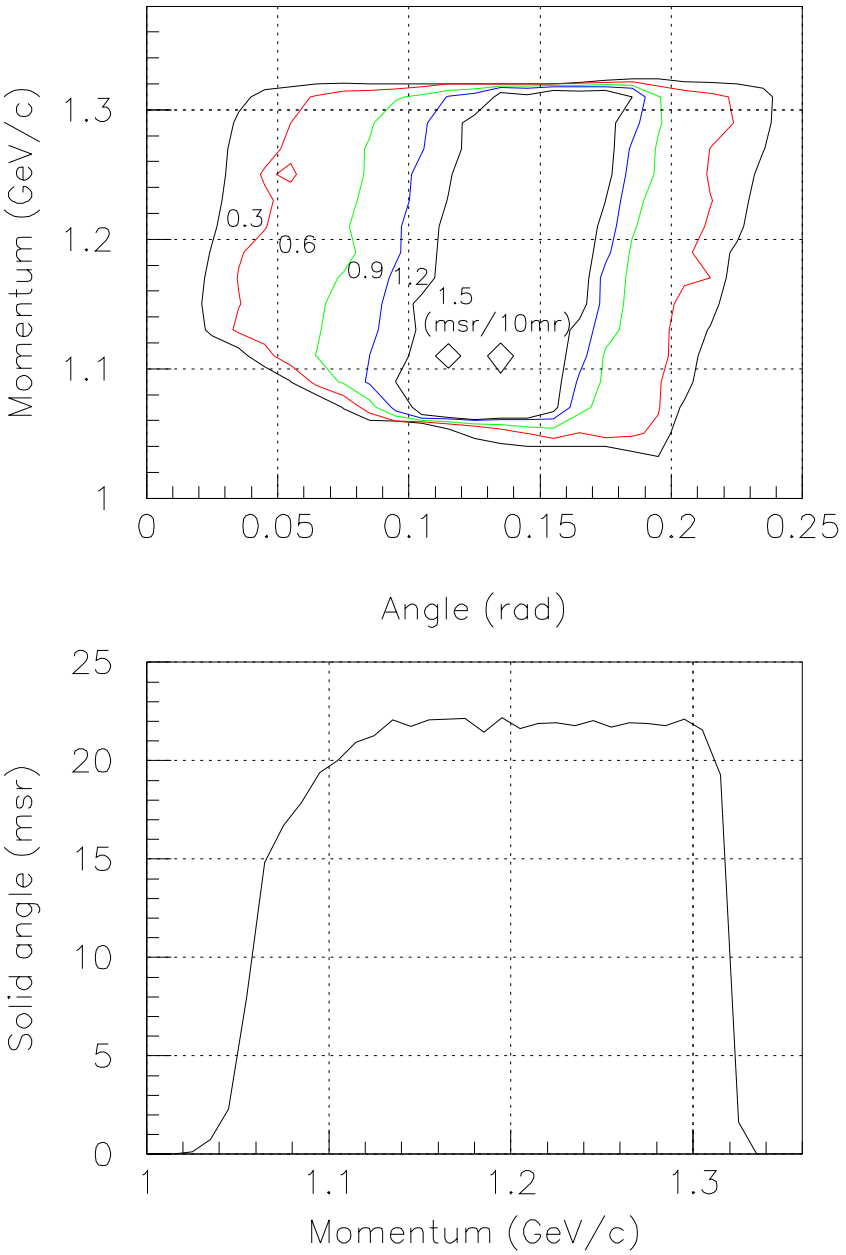

Figure 16: Acceptance of the HKS spectrometer with the splitter installed.

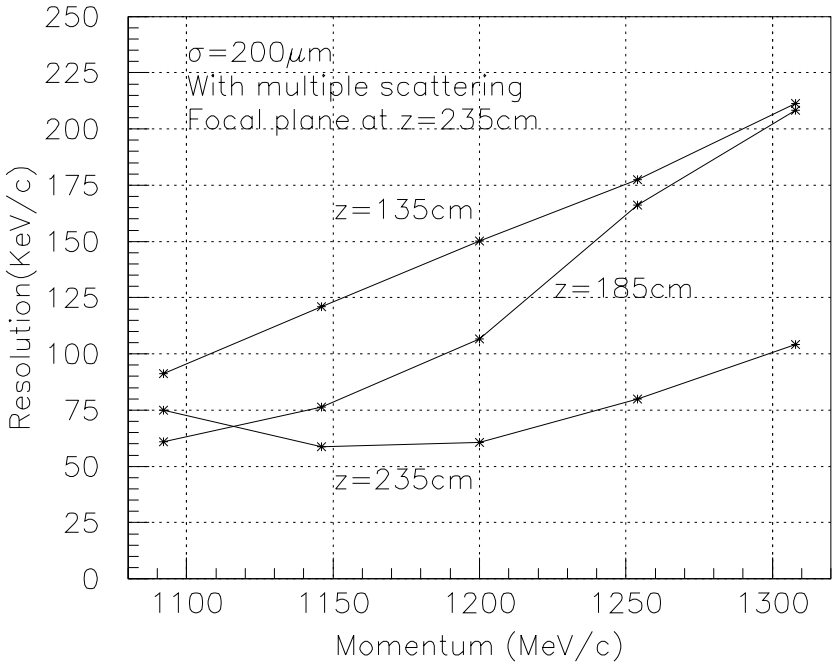

Figure 17: Resolution of the HKS spectrometer.

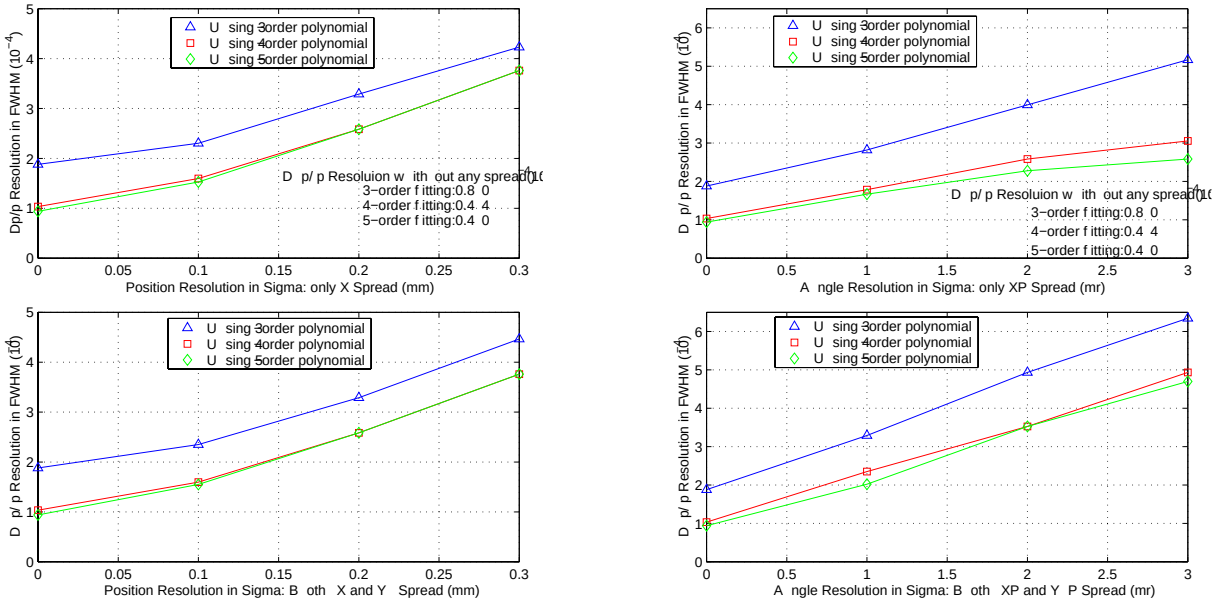

Figure 18: Energy resolution of the Enge spectrometer for electrons.

Appendix A

Optimization of the Experimental Geometry for High Precision Hypernuclear Spectroscopy Experiments Using the (e,e'K^+) Reaction

Liguang Tang
Department of Physics
Hampton University and The Thomas Jefferson Lab
Newport News, VA
and
Osamu Hashimoto
Department of Physics
Tohoku University
Tohoku, Japan

November 30, 2000

Abstract

The first high resolution experiment, E89-009 (HNSS), which uses electrons to produce Λ hypernuclei, has demonstrated that electron machines can be used as precision tools in the study of strange nuclear physics. Although this experiment is still under analysis, it has measured yields and backgrounds, and has demonstrated excellent resolution in the hypernuclear reaction, ^{12}C(e,e'K$^+$)$^{12}_{\Lambda}$B. These measurements now provide the information needed to optimize the geometry of future experiments, fully utilizing the quality of the CEBAF beam. In this report, we study 6 possible geometries for future experiments, including that of E89-009. In particular we study the feasibility of using a high resolution kaon spectrometer, HKS, which was proposed and will be constructed in Japan for use at Jlab. We believe that a hypernuclear program at Jlab will provide exceptional resolution for production experiments, and can have a significant impact on this field of physics.

1 Introduction

A recently completed Hall C experiment, E89-009, is the first high precision study of Λ hypernuclear spectroscopy produced by electron beams. This experiment proves the feasibility and potential of the (e,e'K^+) reaction foe hypernuclear studies. More importantly it provides the information necessary to optimize future programs with some confidence.
Professor Hashimoto of Tohoku University has developed a proposal, approved by the Japanese government, to construct a high-resolution kaon spectrometer (HKS) which will be dedicated to kaon programs at Jlab. This spectrometer, which features high resolution and large solid angle acceptance, is incorporated into the future plans discussed below.
In the next section, 6 different experimental geometries will be compared. However we initially summarize several general design considerations here.

1. In any geometry, acceptance of the virtual photon flux should be maximized while the bremsstrahlung acceptance should be minimized or

eliminated. This allows the full use of the power and quality available in the CEBAF beam, and provides the ability to better balance the single rates in each spectrometer arm.

2. The scattered electrons and kaons must be measured in coincidence, so the mismatch of the momentum acceptances in each spectrometer should be minimized. Obviously, any mismatch increases the coincidence background and reduces the signal to noise ratio, S/A.

3. The maximum possible photon energy, w=E-E', should be kept as low as possible. If this is not done the virtual photon spectrum which remains untagged by the electron spectrometer can produce kaons which are not associated with Λ production, reducing the S/N.

These points are discussed in more detail in the next section.

2 Comparison of Six Experimental Geometries

The various experimental geometries considered in this study are listed below and comparisons between them detailed in Table 1. Since all kaon production angles are close to zero, differences in the photo-production cross sections are ignored.

1. Geometry 1: This geometry consists of the original Hall C HNSS (Zero degree splitting magnet coupled with the Enge Split-Pole spectrometer and set for zero degree scattering). It will be the standard by which the other geometries are compared as it provides measured performance parameters.

2. Geometry 2: This geometry consists of the HNSS, as defined above, but with a thin plate inserted in the HNSS transport line to remove electrons produced by bremsstrahlung in the target. The technique was tested during E89-09, and the rates and S/N measured. Presently we are attempting to calculate these yields, which requires precise handling of the angular distribution of the bremsstrahlung electrons. The calculation is very sensitive to atomic screening and multiple scattering, and it changes with beam energy, target, and target thickness. In addition the electrons scatter out of the blocking material, and may contribute to background in the missing mass spectrum. This geometry, then is rather delicate, and our test examined only one C target. However we did consider S/N as the beam intensity changed.

3. Geometry 3: This geometry assumes bremsstrahlung blocking as described in 2 but replaces the Split-Pole with the SOS spectrometer and uses the new high resolution kaon spectrometer, HKS, to detect the kaons. It features better solid angle and momentum acceptances. However, the current SOS detector system can only handle rates of 1-2 MHz.

4. Geometry 4: This geometry is designed to use the spectrometers in Hall A. The electrons are detected in the HRS and the kaons in HKS. It requires two septum magnets (an additional one must be constructed). The scattering angles for both electron and kaon are small but not zero. It is simply an upgrade of the Hall A hypernuclear experiment, E94-107, by increasing the kaon solid angle acceptance and survival. Additional equipment and utilities will be required.

5. Geometry 5: This is the original geometry for the Hall A experiment, E94-107. It utilizes the existing high resolution HRS spectrometers with the new septum magnets built by the Italian group. The HRS spectrometer has sufficient resolution but not is optimized for kaons due to its long path length (23 meters), and the solid angle acceptance is small.

6. Geometry 6: This geometry uses the HKS and the HNSS, but the Split-Pole is tilted by 2.25 degrees so that bremsstrahlung electrons are excluded from the focal plane. This option is a compromise between the zero degree scattering geometry of E89-009 and the finite angle geometry of the Hall A experiment.

In the following subsections we discuss each geometry as they are compared in Table 1.

2.1 Line 1 to 4

Lines 1-4 contain the beam energy, E, the scattered electron energy, E', the virtual photon energy, ω=E-E', and the electron scattering angle. For the geometric options 1, 2, 3, and 6 the forward electrons and kaons are bent into their respective spectrometers by a zero degree dipole magnet. Options 4 and 5 require two septum magnets which bend, the electrons and kaons into their respective spectrometers. A zero degree dipole was used in the successful Hall C HNSS experiment, option 1, but in these experiments the momentum and spectrometer angles of the scattered particles are correlated. Thus in order for the splitter to bend the kaons into their spectrometer at a given angle, the electron momenta and bend angle is fixed. The use of two septum magnets provides much more flexibility in the choice of momenta and angles.
Because options 1, 2, and 3 accept electrons at zero degrees, they are subject to high electron rates from bremsstrahlung electrons. These are partially removed in options 2, and 3 by blocking a small portion of the forward scattering angle which contains the significant fraction of the bremsstrahlung electrons. Although option 6 views small scattering angles, the bremsstrahlung electrons are removed by bounding the minimum scattering angle away from zero degrees. The remaining options are constrained by geometry to view the scattering angles at about 6°, symmetric with respect to the incident beam. These septum magnets must have a sufficiently large gap to match the solid angle of the respective spectrometers. In particular the kaon septum magnet in option 4 must match the large acceptance of the HKS.
The energies of the beam and scattered electrons in options 1, 2, 3, and 6 can be chosen to keep E - ω small so that the production of kaons through unwanted channels is minimized. In general E - $\omega \approx$ 360 MeV for options 2 and 6 and 560 MeV for option 3. These values are 3-5 times higher for options 4 and 5.

2.2 Line 5

Options 1, 2, and 6 use the existing Enge Split-Pole combined with the existing Splitter magnet, HNSS. The the solid angle acceptance is only about 0.6 msr, but at very forward angles, $\approx 0°$, it accepts a higher percentage of the virtual photon flux than the other options. In options 2 and 6, the Split-Pole is moved 5 cm closer to the Splitter magnet to increase the acceptance. A comparison of the various virtual photon flux acceptance after averaging over the corresponding E' momentum bite is given in Table 2.

The reduction of the acceptance in options 2 and 3 as compared to 1 is due to the angle blocking to remove the bremsstrahlung electrons. The tabulated acceptances are obtained from Monte Carlo simulation, effectively integrating over the actual acceptances of the combined Splitter and Split-Pole system. For the options 4 and 5 the incident and scattered electron energies produce a much more forward peaked electron distribution, and in any event the virtual photon flux, as a function of scattered electron angle, is small and flat over the solid angle acceptance (variation less than a few %). Option 6 has a larger acceptance than 4 and 5 due to the fact that for these energies the scattered electron angular distribution is wider and the spectrometer is set at a smaller scattering angle. Figure 1 shows comparisons of the virtual photon flux factor as a function of scattering angle for four different energy settings in the geometry of option 1. In Fig.1 c and d the scattering angle range is 0-6° in order which shows the distribution in an angular region which is applicable for options 4 and 5. The acceptance of option 6 is obtained by Monte Carlo integration with the Split Pole set at a tilt angle of 2.25°.
However, even though options 1, 2, and 3 have significantly larger acceptance than options 4, 5, and 6, bremsstrahlung electrons dominant the scattered electron angular distribution at these angles.

2.3 Line 6

Line 6 compares the total virtual photon flux that contributes to the coincidence rate. This is the effective flux integrated over scattering angle and momentum acceptance. Options 2 - 6 have larger momentum acceptance than 1, and this increased acceptance compensates for the smaller angular acceptance. The scattered electron rate is also effected by the this factor and thus must be properly included in the design.

2.4 Line 7

This line gives the vertical angle used for bremsstrahlung blocking. The vertical blocking angle is optimized by choosing the maximum ratio of electrons producing virtual photons to those producing bremsstrahlung. Figure 2 illustrates the principle of this technique for option 2. Obviously the optimum blocking angle depends on the shape of the virtual and bremsstrahlung angular distributions. Since the luminosity is set by the electron rate, the beam current can be increased to not only recover the loss of virtual flux from the original yield, but but to produce a larger number of virtual photons. Thus a gain in S/N is obtained.

2.5 Line 8

In option 6 the Split Pole is tilted so that the minimum scattering angle is bounded away from zero degrees. This tilt angle is optimized by considering the surviving virtual photon flux, the number of remaining bremsstrahlung electrons, and the optical properties of the combined Splitter and Split-Pole system. The major advantages of this option are that removal of the Bremsstrahlung electrons can be more complete than blocking, and re-scattered electron backgrounds can be small provided the tilt angle is sufficiently large that the bremsstrahlung electrons remain outside the Split-Pole acceptance. Fig.3a shows the percentage of virtual photon acceptance and image size at the focal plane of the Split Pole as a function of tilt angle. At a tilt angle of 2.25 degrees, only about 9% of the virtual flux

remains but the bremsstrahlung is completely removed. On the other hand the image size has increased so that the resolution is significantly worse. Fig.3b. shows the comparison of resolution with and without tracking in the x' plane. Therefore one must implement tracking in the electron arm to preserve the resolution, and the scattered electron rate rate must be kept at a level where tracking is possible.

2.6 Line 9

Line 9 compares the change in the scattered electron rate due to the change in momentum acceptance. When the blocking technique is applied, not all of the bremsstrahlung electrons are removed, thus the increase in momentum acceptance must be applied before the allowed increase in current is determined. For other options the scattered electron rate is no longer dominated by the bremsstrahlung electrons, and S/N ratio is evaluated differently.

2.7 Line 10 and 11

Lines 10 and 11 summarize the previous vitural flux factors. Line 10 gives the total integrated flux per beam electron,and line 11 gives the gain factor for a particular geometry. For options using the Split Pole, the integration over the system acceptance was carried out by a realistic Monte Carlo simulation including beam-defining collimators and blocked angles. For options 4 and 5 the average flux factor was multiplied by the solid angle and momentum acceptances because the virtual photon flux distribution is essentially uniform over the acceptances for these options.
For options 2 and 3, the ratio of the integrated flux to the integrated flux in option 1, divided by the survival ratio of the Bremsstrahlung electrons is the gain factor listed in Line 11. For options 4, 5, and 6, the ratio of the integrated flux to that in 1 is the reduction factor for the gain of the S/N ratio. This is because the coincidence rate is reduced from the measured rate in option 1 by this factor. The result includes the change in momentum acceptance, the actual change in the flux factor due to different kinematics, and the solid angle acceptance differences.

2.8 Line 12 and 13

The HNSS experiment, E89-009, used option 1. Due to an interference between the SOS and the beam electrons, the kaon scattering angle could either be set at 2.2 degrees or $\sim$ 7 degrees. To maximize the yield, the smaller angle was chosen, but a large flux of positrons from pair production was then accepted by the SOS spectrometer. The reconstructed e^+ data had a scattering angle centered about zero degrees with respect to the beam, and a width which was consistent with the SOS angular resolution. This meant that the positrons are emitted essentially at zero degrees.
Fig. 4 shows the correlation of the momentum and angle in the bend plane of the Splitting magnet for the combined Splitter and SOS system. The tilted correlation is due to the absence of focusing in the SOS magnet. Although zero degree positrons lie within the within the SOS acceptance, they could be removed by increasing the spectrometer angle by only one degree. In the HKS the tilt will be small due to its double focusing design, and since it has smaller momentum acceptance a suitable scattering angle can be found to remove the positrons from the hadron arm.

For the options 2, 3, and 6, the non-zero scattering angle removes positrons from the hadron spectrometer acceptance. Although the optics calculations for the HKS are incomplete, we have assumed that the central scattering angle is set at 4° with the horizontal acceptance slightly less than ±4° degrees. Thus the e^+ rate is assumed small compared to the protons. The scattering angle should then be optimized for yield.

2.9 Line 14 - 16

The kaon central momentum is chosen from the kinematics, and in particular, will be 1.2 GeV/c for options 2, 3, 4 and 6 which use the HKS. This setting allows a detector package similar to that of the present SOS, which is well understood. In addition one can keep the kaon survival rate as high as possible (35%). In case of option 5, only 18% of the kaons remain and the ratio of this over that for the other options becomes a reduction factor for both yield and S/N ratio.
The kaon momentum bite must match with the E' bite with a slight enlargement to keep the missing mass region of interest flat. For a given missing mass, the two bites are correlated, and the ratio of the matched bite over that for option 1 is a factor of gain which effects not only yield but not S/N due to the cancellation.

2.10 Line 17 and 18

The change in the solid angle acceptance effects the yield but not the S/N ratio if the distributions of signal and background are the same. Thus we obtain the the yield increase compared to option 1 as presented in line 18. Since the cross section is peaked in the forward direction, the change in yield is not proportional to the increase in solid angle. The cross section decreases with the momentum transfer due to the nuclear form factor, and integration over the solid angle of the spectrometer still gives a significant increase in yield. With respect to option 4, a new septum magnet is needed to match the solid angle acceptance of the HKS. This will be difficult due to the requirements on the size of the magnet gap and the field quality. We have assumed a a smaller overall kaon solid angle acceptance for this option.

2.11 Line 19

Kaon survival rate effects the yield. All options with the exception of 5 have the same survival, $\sim$ 35%. Option 5 has an 18% survival rate and this reduces the yield by a factor of 0.514 compared to option 1.

2.12 Line 20

The maximum beam current which can be used with each option is determined by the singles rate capability in either the electron or the kaon arms.

1. For option 1, the maximum beam current is limited by the rate in the electron arm, HNSS. In E89-009 this rate and the hypernuclear yield was measured. Thus these values are used as the standard reference for comparison.

2. For option 2 the maximum beam current is determined by assuming a scattered electron flux of 70 MHz in the the existing HNSS detector system while keeping the kaon flux to $\leq$ 5MHz. Since the blocking angle

is very small ($\leq 1^\circ$), the optics of the Splitter and Split-Pole magnet system remains almost identical to option 1 and no tracking in the electron spectrometer is required. The assumed rate is that determined by E89-009 as the limiting condition for stable operation. The kaon rate is discussed below.

3. For option 3, the current is determined by the rate capability of the existing SOS detector package. Currently, this is assumed to be 1 MHz, but we have used a value of 2 MHz here anticipating that some improvements could be made to the package.

4. For option 4, the current is determined by the rate in the detector package which must be constructed for the HKS, because the scattered electron rate is small. The design goal for the singles rates of the new HKS detector package is 5 MHz. We will need to design and build a system optimized for kaon identification under high background rate, so we assume for the moment that the limiting beam current produces ≤ 3 MHz in the HKS.

5. For option 5, the we anticipate that the beam current will be limited by the rates in the hadron spectrometer detector package because the scattered electron rate is small.

6. For option 6, the beam current is determined by the singles rate in the kaon arm. We would like to keep the rate below 5MHz.

2.13 Line 21

Line 21 gives the increase in yield due to the increase in beam current over that of option 1. For the options 2 and 3 the dominant electron scattering rate is still bremsstrahlung electrons even though blocking is used. The yield ratio must include the loss of virtual photon flux due to blocking and the increase due to the larger momentum acceptance. For non-zero scattering angles, the yield ratio is a direct comparison to option 1, and the other reduction factors will be considered separately.

2.14 Line 22 and 23

Lines 22 and 23 compare target thickness for the various options. Options 1, 2, and 3 have the same target thickness. Options 4, 5, and 6 use a thicker target which reduces the required beam current for a given luminosity.

2.15 Line 24

The kaon arm singles rate increases due to the change in the total virtual photon flux. This must be determined for the varying kinematic conditions. The increase multiplied by the cross sections normalized to that in option 1 is used to determine the kaon singles rate.
This increase should include the contribution for the differences in total photon energy through the cross sections as obtained from the EPC code. Therefore, we only use the change of the flux factor due to kinematics, and use a factor obtained from the cross section ratios multiplied by the rates from E89-009. This assumption is unimportant for options 2, 3, 4, and 6, but will make significant difference for the option 5.

2.16 Line 25

Line 25 gives the scattered electron singles rate for the various options. The rates for options 1, 2, and 3 are fixed based on an estimated limit. The beam current required for this rate was then determined from option 1 by accounting for the blocking ratio, the momentum acceptance, and the change in the solid angle.
Option 2 will not require tracking and can handle the 70 MHz rate as demonstrated by E89-009. Option 3 will require tracking since a full reconstruction by the measured quantities (Xf, X'f, Yf, Y'f) is needed in order to determine the momentum. If the existing SOS and its detector system is used as the electron spectrometer in this option, we estimate this rate to be $\leq$ 2 MHz.
In option 5, which will be undertaken in Hall A, we use half the rate from this proposal since it assumed a current of 100 instead of 50 muA.
Options 4 and 5 also use non-zero electron scattering angles. To obtain the rates for these options, we scaled option 4 from option 5 using the change in momentum acceptance and assuming that the cross section change is small. In the same way the rates for option 6 were calculated, but in this case we assumed that the cross section increases by an order of magnitude as the scattered electrons are observed at 2.25 degrees instead of 6 degrees. Option 4 uses the existing Hall A HRS spectrometer for these electrons and the rate is low.
In option 6 the system optics were modified by the Splitting magnet, and tracking to determine the scattering angle in the momentum dispersion plane will be required. This is not true at zero degrees as the forward nature of the scattered electrons confines their entrance angle into the magnet system. However, as shown in Fig.5, only a measurement in the dispersion plane with accuracy of 10 mr is required to reach a resolution of about 180 keV. A single-dimensional, small-spaced, fast wire-chamber, placed 10 cm before the existing SSD detector will be able to provide the needed accuracy and handle an overall rate of few MHz. The particle density (vertical spread of a few mm) should be $\leq 10^4$/sec/mm^2, with an overall rate on the 72 cm focal plane of $\leq$ 3MHz.

2.17 Line 26

All options with the exception of 1, optimize their angular settings so as not to include positrons from Dalitz pairs produced at zero degrees. Options 4 and 5 are, in fact, positioned far away from zero degree.

2.18 Line 27 and 28

Lines 27 and 28 give the pion and proton rates for each option. These rates are obtained from scaling the measured numbers in E89-009, option 1. In order to determine the scaling factors, we used; 1) cross section ratios as obtained from the EPC code; 2) the increase of the total photon flux and the increase of luminosity including beam and target thickness; 3) the change in solid angle acceptance; and 4) the change in momentum acceptance.
We assume that the cross sections are flat within the solid angle and momentum acceptances. For option 1 the momentum acceptance was 480 MeV/c. The acceptances for the options 2, 3, 4, and 6, which use the HKS, are 240 MeV/c. The acceptance of the Hall A experiment, option 5, is 162 MeV/c.

2.19 Line 29

The kaon single rate is scaled as in lines 27 and 28 above, with the exception that the cross section is the same for all options. This assumption is not true, but since the kaon singles rate is low it is not important in determining the total singles rate in the hadron spectrometer.

2.20 Line 30

Line 30 gives the total rate in the hadron arm. The detector package for the new HKS will have a 4×10^{-4} pion rejection (two layer of aerogel counters) and a 2×10^{-2} proton rejection (new Lucite counter similar to the one at KEK). The singles rate for each option which uses the HKS is quite reasonable. The trigger for option 2 must be the identification of a kaon in the hadron arm as the high rate in the electron arm makes a coincidence trigger difficult. Options 3, 4, and 6 use a trigger based on coincidence between the hadron and electron arms. With a 50ns coincidence window, the trigger rate is less than 300 Hz, but data-size per event is less than that of the HNSS experiment.

2.21 Line 31

Line 31 gives the gain in S/N as a result of the reduced electron rate. In options 4, 5, and 6 the bremsstrahlung electrons are essentially removed, and a large enhancement occurs. For options 2 and 3 which use the blocking technique this method for calculating this ratio is discussed later.

2.22 Line 32

The loss of virtual photon flux for the finite angle options reduces the coincidence production. The ratio of the acceptance of the total integrated virtual photon flux (line 10) over that of the option 1 is a reduction factor for the S/N. This flux is integrated over the solid angle and momentum acceptances, which represents the flux which contributes to the coincidence rate. The options which using blocking do are calculated differently as discussed below.

2.23 Line 33

As mentioned previously, we use only kaons produced through the elementary process $\gamma + \mathrm{p} \rightarrow \mathrm{K}^+ + \Lambda$, and we would like to preferentially enhance this channel with respect to all others. One way to do this is to keep the value of the maximum beam energy to the photon energy ω as small as possible. The coincidence rate R_c can be expressed by;
$\mathrm{R}_c = \mathrm{R}_v \times \mathrm{R}_m \times \mathrm{R}_w$;
where the R_v is the ratio of the accepted virtual photon flux to the the total flux emitted (obtained in line 10 and 32 above), R_m is the mismatch in momentum acceptance as discussed earlier, and R_w is the ratio of the wanted kaons over the unwanted kaons from additional channels. As an example, a $\pm$ 15 % SOS momentum cut was used in the HNSS experiment. The kaon momentum acceptances $\sim$ 342 MeV/c, and the scattered electron acceptance is $\sim$ 103 MeV/c. Thus R_m is about 0.3 and R_v is about 0.35 as discussed in line 10. The R_c ratio is measured to be 0.064. This means that R_w is about 0.61, or there are about 39% of the kaons produced in unwanted channels. In E89-009 the beam energy above the photon energy is about 270 MeV/c, but apparently kaons from Λ^* and ϕ production are present in the singles rates.

Line 32 gives the reduction factor for R_c due to the reduction in R_v for each of the options.
The ratio, R_m, is essentially constant for all options when a similar, correlated, missing-mass cut is applied at the offline level. Thus, we do not further consider this variable.
The factor, R_w should be similar in options 1, 2, and 6. For options 3, 4, and 5, we simply give our best estimate as a reliable calculation requires a complicated investigation. This estimate could be much larger, particularly for options 4 and 5.

2.24 Line 34

Better resolution gives a better S/N ratio, and we assume that all options other than 1 will have resolutions improved by a factor of 2. Thus the S/N gain is assumed to be 2 for options 2, 3, 4, 5, and 6.

2.25 Line 35 and 36

Line 35 gives the S/N ratio for kaon production in the coincidence timing spectrum, but not in the hypernuclear missing mass spectrum. Line 36 gives the S/N ratio for the ground state of the missing mass spectrum in the ${}^{12}_{\Lambda}$B hypernucleus. The values given for option 1 are obtained from E89-009, however no correlated cut on missing mass has been applied. Without this cut these data have a S/N ratio of 0.15 when using the maximum beam current.
For options 2, and 3 which use the blocking technique, the initial gain factor is given by the ratio of the virtual photon acceptance over the bremsstrahlung acceptance. This factor will be reduced by the flux loss due to blocking, and the increase in beam current to increase in yield. The result when corrected for increased resolution is the final factor giving the change in S/N with respect to option 1.
For options 4, 5, and 6, the S/A ratio is calculated from the measured value in option 1, multiplied by the gain factors in line 31 and 34, and the reduction factors in line 34 and 35. All calculations are for a Carbon target. A further offline correlation cut in missing mass will improve the S/N.
Options 3, 4, 5, and 6 have a good S/A ratio. From E89-009 we have found that a S/N ≈ 1 will yield a clean spectrum and will provide satisfactory statistical accuracy in a reasonable time to identify some of the more weakly core excited states. Our calculation shows option 3 gives the best S/N ratio but cannot use the HKS, and the overall yield is lower than the other options.

2.26 Line 37

Line 37 gives the yield measured in E89-009. This was 0.9 counts/hour as scaled from the measured yield with a current of 0.22μA to the maximum applied current of 0.66 μA for which the scattered electron rate is measured.

2.27 Line 38

Line 38 gives the yield factor with respect to option 1 for all other options. This factor is obtained for options 2 and 3 from the ratio of the accepted virtual photon flux for the specific geometric configuration to that of option 1. The coincidence rate is assumed linear with the flux as the scattered rate is kept below the unstable rate limit set by E89-009.
For options 4, 5, and 6 the yield factor is obtained by multiplying the ratios of the momentum and solid angle acceptances, and the luminosities.

2.28 Line 39

The yield for each option is then obtained by multiplying the reference yield from option 1 and line 38. Although all options show an increased yield, option 6 clearly provides the best geometry for future experiments. Option 5 is the geometry of the Hall A experiment.
Although the reaction cross section for (e,e'K) is 100 times smaller than (π,K), option 6 provides a higher yield and 4-5 times better resolution. A yield of 60 counts/hour for the A=12 hypernuclear system will allow a precise study of the light Λ hypernuclei, and such studies can extended to heavier systems.

3 Discussion

The geometric option 6 will fully take advantage of the CEBAF beam and the new, large solid angle HKS spectrometer. It also offers more flexibility with respect to mounting the spectrometers and is easier to calibrate than the beam blocking options. Since it operates at lower beam energies and more forward angles that options 4 and 5 it offers better yields and particle identification. We believe this choice will provide a window to an exceptionally rich program in hypernuclear physics.

4 The Requirements for Option 6

The HKS project was approved with a specific timeline. We discuss here our assessment with respect to several issues which will be required to complete the project and mount an experiment using the HKS at Jlab.

4.1 Which Hall to Call Home?

A proposed program using the geometry of option 6 could be run in either Hall A or Hall C. Hall C presently has third arm capability for LCW distribution, power outline capability, signal bus system (cables and patches), and third arm electronics and data acquisition. Hall A would require some time, effort, and commitment to make these available. In general, the existing power supplies in Hall C can power all the magnets which would be required, including the splitter, split-pole, two quadrupoles, and one dipole. However one additional supply may need to be acquired. In contrast, Hall A would need to purchase 5 new power supplies. For these reasons we choose to initially place the system in Hall C. At the same time, all the new supporting structures will be made suitable to install in both halls.

4.2 Hall Layout and Modifications

The new spectrometers will be installed down stream from the hall pivot to minimize the interference with existing equipment. A new section of beam line equipped with two sets of BPMs (x and y), one super harp, and one vacuum gate value will be mounted behind the regular target chamber to extend the line to the location of the Splitter magnet.

4.3 Modification of the Splitting Magnet

The gap of the HNSS Splitting magnet is too small to match the solid angle of the HKS. If the poles are removed the gap can be enlarged to 6 inches, but it must be remapped and an optical study concluded to establish the new

features of the optical system. Obviously this should be done as soon as possible.

4.4 Support and Shielding

Once the optics of splitting magnet are analyzed, the floor layout can be finalized. The Japanese company constructing the HKS will also build a foundation which will mount and align all the magnets to a common reference. A structure needs to be built to support this foundation from the hall floor, and in order to place the spectrometer in either Hall A or C, the support should be adjustable. In addition, a shielding house must be designed. Finally a new support platform for the splitting magnet needs to be designed and constructed.

4.5 Split-Pole Alignment

Option 6 requires the Split-pole spectrometer to be tilted by 2.25° with respect to a fixed point between the Splitter and Split-Pole. An engineering design will be required to provide an effective method to install and align the system. Fiducial marks would simplify survey alignment and verification. The alignment will require precision adjustment and reproducibility.

4.6 New target chamber

As a result of the enlargement of the splitting magnet gap a new target chamber must be constructed. Although the previous chamber worked well, some new features should be added to help installation and alignment.

4.7 New beam dump line

A future experiment using the option 6 geometry will not use the local dump as was used for E89-009. Two small bending magnets would be used for vertical adjustment, but one (or two) larger "BZ" type of magnets will be used to bend the deflected electron beam into the normal Hall C beam dump. This will allow the experiment to utilize higher beam power and provide the bending power required for different kinematic operation conditions. These will be especially useful for calibration purposes. This freedom, had it been available, would have greatly facilitated the setup of E89-009.

4.8 The New Scattered Electron Detection System

A new tracking system must be implemented for the scattered electrons. This system will include; 1) a set of small-spaced wire chambers which will provide only bend-plane information; 2) the existing SSD, remounted in a line and placed about 10 cm behind the wire chamber; and 3) a line of 80 scintillation strips behind the SSD for timing and triggering. The wire chamber should have minimum window thickness and the SSD will have to overlap slightly. A new mounting mechanism for this package should be carefully designed to reduce electronic pickup and enhance alignment. In addition the timing scintillator should be constructed of thicker material to ensure a resolution of $\leq$ 200 ps rms.
The support structure should be referenced to the magnet and the detector-magnet system surveyed as one unit. The angle alignment will then be set for the system as a whole.

4.9 A New Kaon Arm Detection System

A new kaon detector package must be installed in the HKS. It will be designed having excellent kaon identification and timing resolution. This package should include the items listed below.

1. Two sets of wire chamber are needed. These must be able to operate under high singles rate conditions.
2. A two-plane, segmented, scintillation hodoscope is required. This hodoscope will be aligned in the vertical direction only. Time resolution is critical, and must be $\leq$ 150 ps rms.
3. A new Lucite Cerenkov counter for proton rejection is needed. This counter could be made using a material similar to one designed at KEK, and should have a 98% online proton rejection rate.
4. Two new aerogel Cerenkov counters for pion rejection are required. These must provide online pion and positron rejections of 98% each. A further study should determine if an additional cherenkov detector will be required to remove positrons.
5. A common support frame for the package must be constructed.
6. A data acquisition system must be designed and implemented.
7. In order to use the data acquisition system a full set of software analysis and calibration codes must be written. The whole package should be tuned and calibrated well before it is used.

5 Conclusion

Experiment 89-009 provides valuable information on rates and yields in the first electroproduced hypernuclear experiment. Using this information we can now optimize the experimental geometry for future experiments and take advantage of the full quality and power of the CEBAF beam. As one initial approach to obtain better S/N rates, a blocking technique was investigated during E89-009, and these data were analyzed. However, we are now able to predict with confidence that a new experiment using a new, large solid angle kaon spectrometer can increase hypernuclear yields by two orders of magnitude with improved resolution and S/N. This new geometry will place the existing Split-pole spectrometer at a small, non-zero angle so that bremsstrahlung electrons are not accepted, but at a sufficiently forward angle that the photon flux remains reasonable. We are then able to attain high production rates by increasing the beam intensity.
It is now necessary to study in detail backgrounds and yields by Monte Carlo to further test the proposed geometry. We anticipate that if these studies verify our preliminary calculations, a rich program of high resolution hypernuclear spectroscopy will unfold at Jlab.

Table 1: Comparison of the Experimental Geometries Discussed in the Text

Line	Parameter	Geometries					
		1	2	3	4	5	6
1	Beam Energy (GeV)	1.72	1.85	2.06	3.00	4.05	1.85
2	Scattered Energy (GeV)	0.276	0.356	0.561	1.50	2.00	0.356
3	Photon Energy ω	1.45	1.495	1.495	1.50	2.0	1.50
4	Scattering Angle (mr)	0.0	0.0	0.0	105	105	39
5	Solid Angle (msr)	0.6	0.6	9.0	3.0	4.5	0.6
6	Electron Momentum Acceptance(MeV)	100	149	236	135	180	149
7	Blocked Angle (mr)	N/A	9	9	N/A	N/A	N/A
8	Tilt Angle (mr)	N/A	N/A	N/A	N/A	N/A	39
9	Increase in Scattering Rate	1	1.49	2.36	N/A	N/A	N/A
10	Tagged Photon Flux per Incident Electron	4.0	0.727	1.15	0.12	0.17	0.35
11	Yield Increase from Bremsstrahlung Blocking	N/A	16.4	146	N/A	N/A	N/A
12	Kaon Angle (mr)	38.4	78.5	78.5	105	105	78.5
13	Kaon Angle with respect to Photon Angle	38.4	78.5	78.5	0	0	78.5
14	Kaon Central Momentum (GeV/c)	1.14	1.2	1.2	1.2	1.8	1.2
15	Kaon Momentum Acceptance (MeV)	100	149	236	135	162	149
16	Yield Increase from Momentum Acceptance	1	1.49	2.36	1.35	1.62	1.49
17	Kaon Solid Angle	6.0	20	20	12	4.5	20
18	Yield Increase from Solid Angle	1	2.5	2.5	1.5	0.75	2.5
19	Yield Increase from Kaon Survival	1	1	1	1	0.52	1
20	Beam Current (μA)	0.66	19	2.7	50	50	30
21	Yield Increase from Beam Current	1	3.5	0.56	76	76	45
22	Target Thickness (mg/cm^2) C Target	22	22	22	100	100	100
23	Yield Increase from Target Thickness	1	1	1	4.6	4.6	4.6
24	Increase in Virtual Flux	1	1	1	1	.98	1

Table 1. Continued

Line	Parameter	Geometries					
		1	2	3	4	5	6
25	Scattered Electron Singles Rate (10^6/s)	220	70	2	0.18	0.21	2.3
26	Positron Rate (kHz)	131	∼0	∼0	∼0	∼0	∼0
27	Pion Rate (kHz)	0.91	18.2	3.02	1,093	385	1,093
28	Proton Rate (kHz)	0.234	4.67	0.777	144	85.6	144
29	Kaon Rate (Hz) (Λ production only)	0.33	6.6	1.1	171	51	171
30	Total Kaon Rate(kHz)	133	40.0	6.65	2,299	837	2,299
31	Increase in S/N from Lower Electron Rate	N/A	N/A	N/A	1,224	1,048	96
32	Decrease in S/N from Lower Virtual Flux	N/A	N/A	N/A	0.018	0.016	0.064
33	Decrease in S/N from Kaon Electoproduction	0.65	0.65	0.60	0.50	0.30	0.65
34	Increase in S/N from Resolution	1.0	2.0	2.0	2.0	2.0	2.0
35	S/N for Kaons	0.15	0.18	6.21	3.25	1.15	1.2
36	S/N for Hypernuclear Ground State	1.4	3.3	116	30.4	14.1	11.2
37	Measured Yield for $^{12}_{\Lambda}$B(gs) (Counts/hr)	0.9	N/A	N/A	N/A	N/A	N/A
38	Total Increase in Yield	N/A	13.1	3.30	21.4	9.15	67.5
39	Estimated Yield for $^{12}_{\Lambda}$B(gs) (Counts/hr)	0.9	11.8	3.0	19.3	8.2	60.8

Table 2: Comparison of the Accepted Virtual Photon Flux between Experimental Geometries

	Geometries					
	1	2	3	4	5	6
Acceptance Ratio (%)	35	11	11	0.62	0.56	1.8

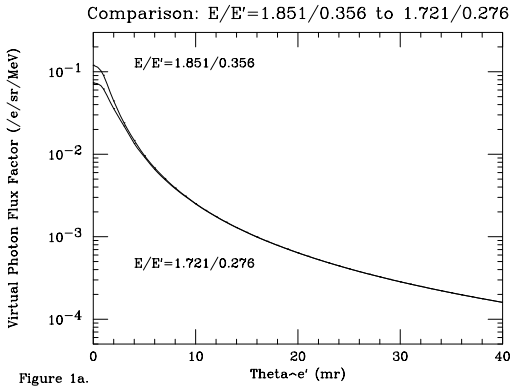

Figure 1a.

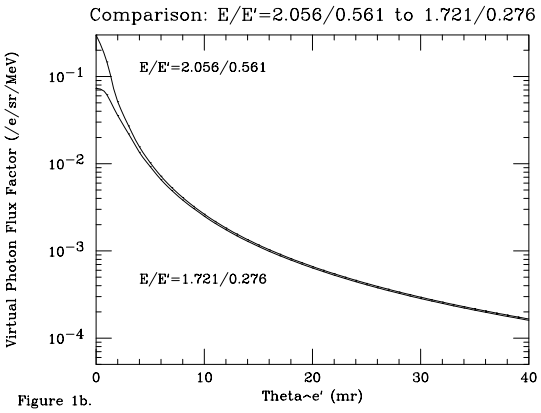

Figure 1b.

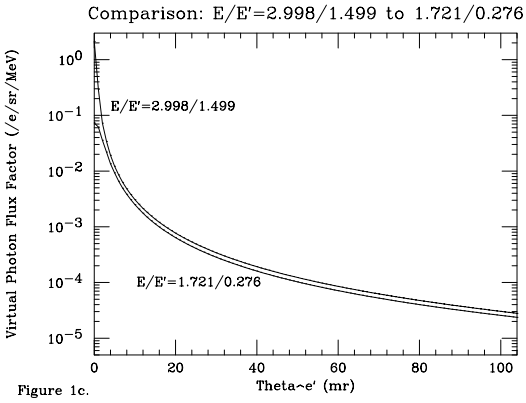

Figure 1c.

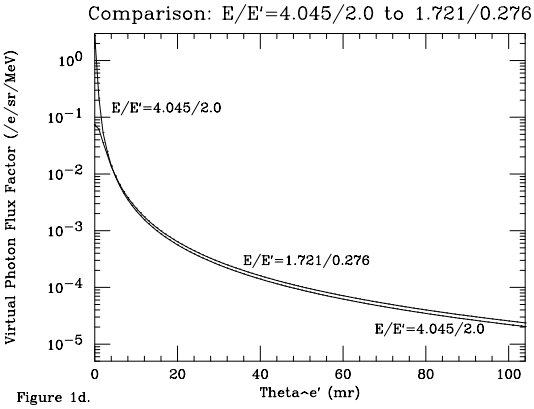

Figure 1d.

Figure 1: Virtual photon flux flux factor as a function of electron scattering angle for different beam energy- scattered electron energy combinations.

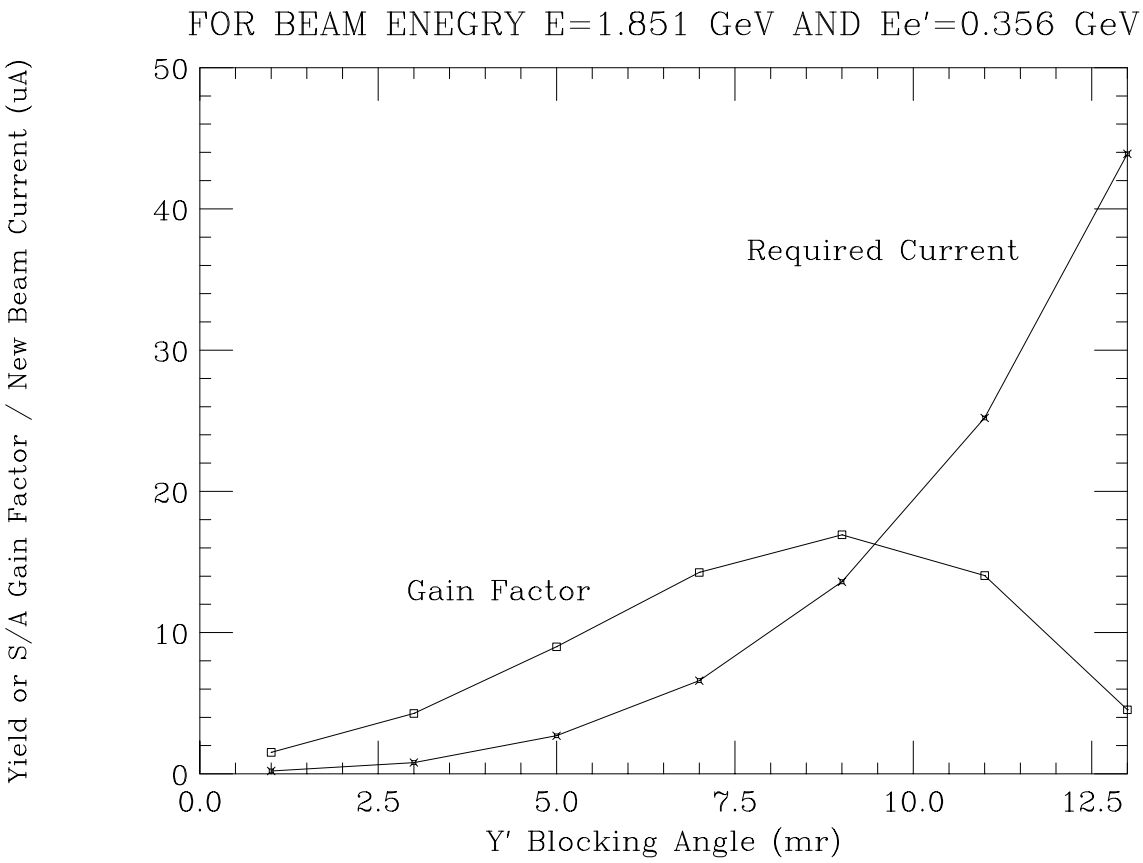

Figure 2: Gain factor and the required beam current as a function of blocking angle.

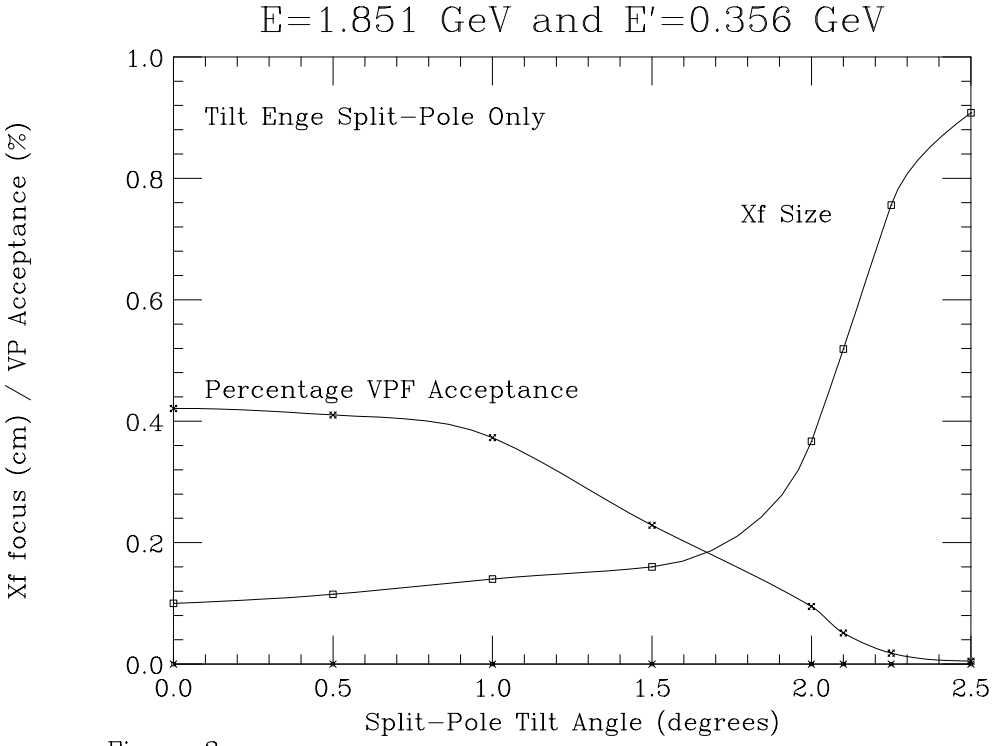

Figure 3a

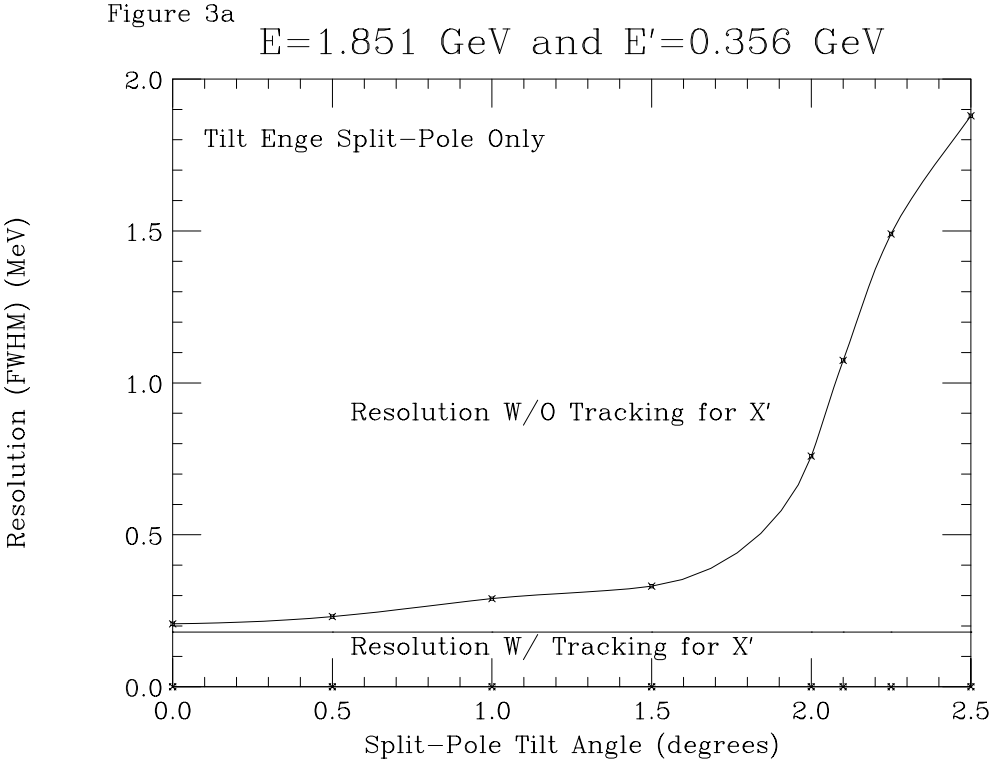

Figure 3b

Figure 3: Split-pole tilt angle dependence of (a) the focusing size and percentage of the virtual photon flux and (b) Expected resolution with and without tracking the incident angle to the focal plane.

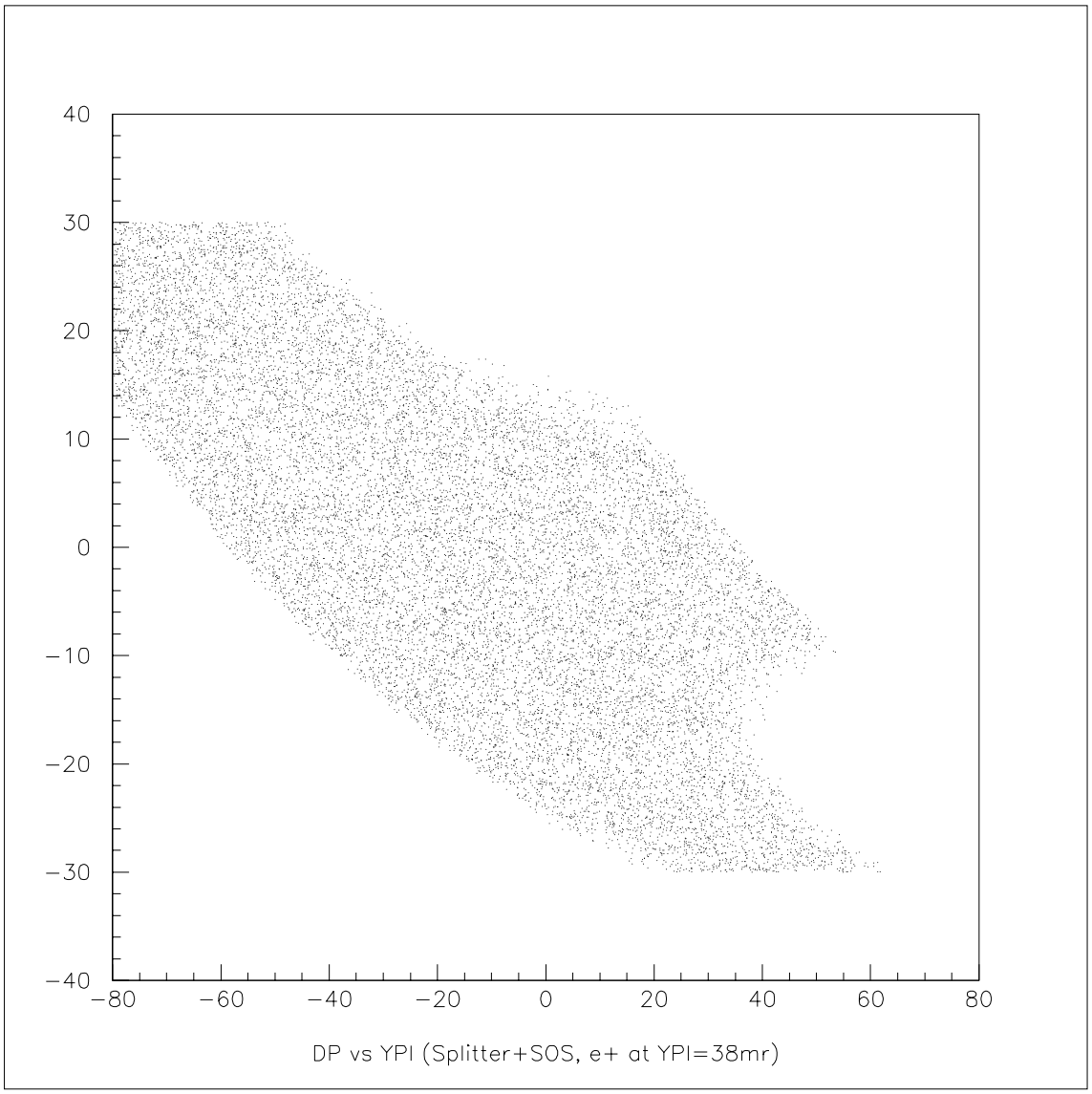

Figure 4: The correlation of the momentum and angle in the bend plane of the Splitting magnet

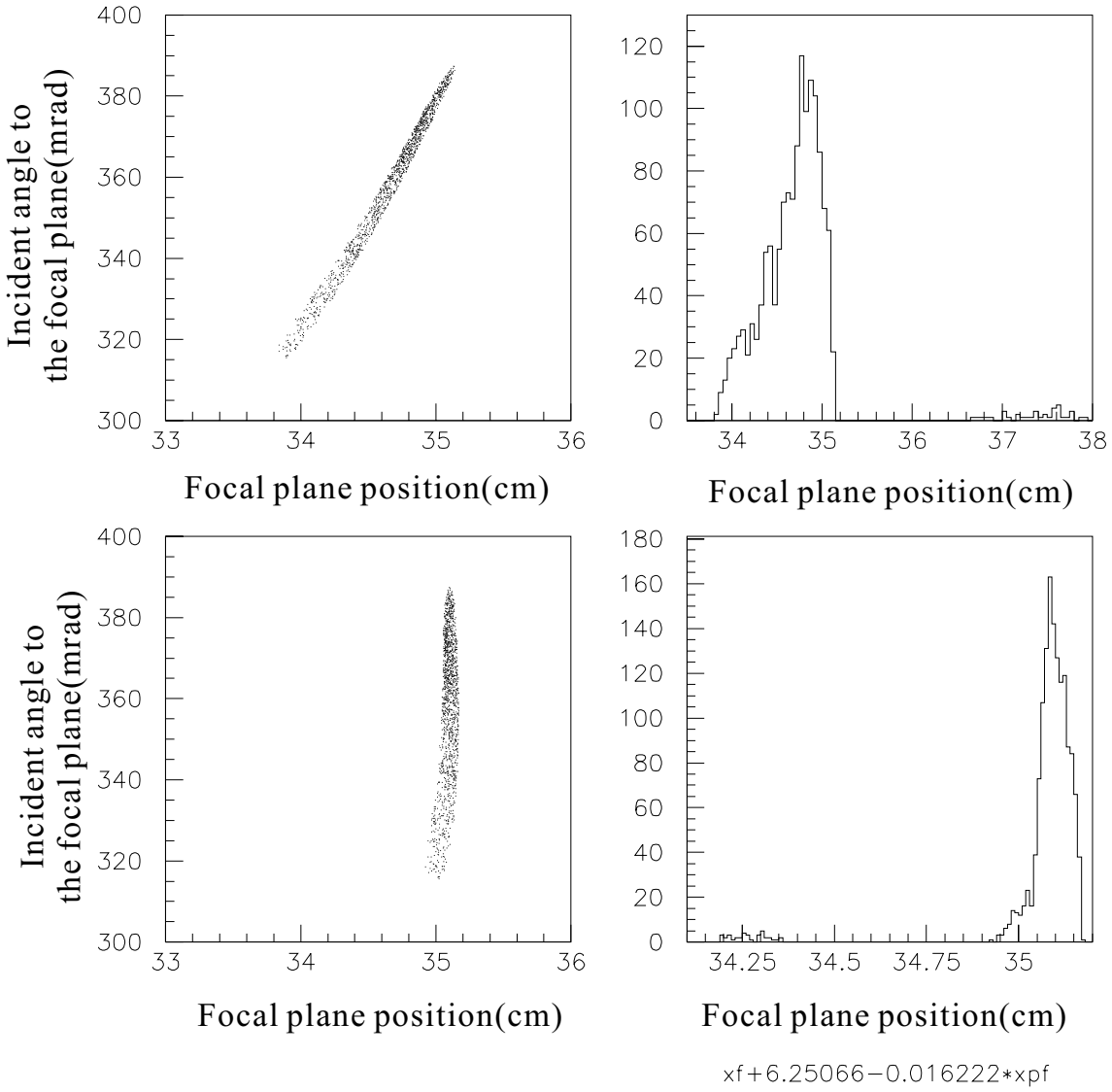

Figure 5: Correlation between focal plane position and the incident angle.

Appendix B

A high-resolution high-efficiency spectrometer system for Λ hypernuclear spectroscopy at Jlab

O. Hashimoto, S. N. Nakamura, Y. Fujii, H. Tamura, T. Takahashi,
T. Miyoshi, H. Yamaguchi, Y. Okayasu, K. Tsukada,
S. Kato[1)], and L. Tang[2)]

Department of physics, Tohoku university, Sendai 980-8578, Japan
Department of Physics, Yamagata University, Yamagata 990-8560
Department of Physics, Hampton University, Newport News, VA 23668, USA

September 14, 2000
Updated December 14, 2000

Abstract

A budget proposal "Investigation of Λ hypernuclei by electromagnetic probes" to the Japanese ministry of education, culture and sports (Monbusho) has been approved in July, 2000 as a 4-year "specially promoted research" after a series of review process. The program starts April 1, 2000 and will be completed by the end of March 31, 2004. Major goal of the proposed program is to pursue efficient high resolution hypernuclear spectroscopy by the (e,e'K^+) reaction at Jlab and open a new era of strangeness nuclear physics in the 21st century through the precision reaction spectroscopy. The outline of the program, present design of the spectrometer system with the high-resolution and large-acceptance kaon spectrometer (HKS) and its construction plan are described. The spectrometer system can be installed either in Hall A or Hall C. The present experimental consideration and optimization of the experimental setup is based on the success of the Hall C HNSS experiment which was carried out from March through May in 2000.

1 Introduction

Recent progress of hypernuclear spectroscopy by meson beams proved its value for the investigation of strangeness nuclear physics. By the greatly improved quality of the spectra which had not been obtained in the previous experiments, the (π^+, K^+) reaction spectroscopy and γ ray spectroscopy provided significant information on the structure of Λ hypernuclei and also on Λ nucleon interaction. Experimentally, it was essential to achieve both high resolution and high statistics simultaneously in order to yield meaningful experimental spectra. It became possible to measure such high quality spectra thanks to the development of high-resolution large-solid angle detector systems such as a magnetic spectrometer and a Ge ball. Value of the Λ hypernuclear spectroscopy by the (e,e'K^+) reaction has long been recognized since it can potentially realize hypernuclear spectroscopy with resolution as good as a few 100 keV. However, the first experiment was conducted only recently using Hypernuclear spectrometer system(HNSS) in Hall C of Jlab. Although the experiment was successful, it was also recognized that HNSS which was configured using the available spectrometers does not fully satisfy the requirement for the hypernuclear spectroscopy. In particular, the kaon spectrometer limits the performance of the hypernuclear spectrometer system at Hall C, both for the momentum

resolution and acceptance. In order to fully explore the possibility of Λ hypernuclear spectroscopy by the (e,e'K^+) reaction, it is necessary to carefully optimize the configuration of the spectrometer system and design the new spectrometer system.
In December 1999, a Jefferson Lab sponsored international workshop on "Hypernuclear physics with electromagnetic probes" was held on the campus of Hampton University, Virginia with an emphasis on the future hypernuclear physics program at Jlab fully utilizing high quality DC electron beam. It was summarized that a new high-efficiency high-resolution kaon spectrometer was deadly needed in the near future.
In September 1999, Hashimoto submitted a proposal to Japanese ministry of education(Monbusho), in which spectroscopic investigation of Λ hypernuclei by the (e,e'K^+) reaction at Jlab plays a key role. It was approved by Monbusho as a "specially promoted research" in July, 2000 as a 4-year project from April 1, 2000 through March 31, 2003.
In the following, we present our present plan for the construction of the high resolution kaon spectrometer that replaces SOS but still coupled with the Enge spectrometer. Since there is room for improving the plan, we solicit any input to the proposed spectrometer and discuss with those who have interest in developing the new spectrometer system for the strangeness nuclear physics at Jlab.

2 Optimization of the (e,e'K^+) hypernuclear spectroscopy

The experimental advantage of the (e,e'K^+) reaction in the hypernuclear spectroscopy is that high resolution spectroscopy can be realized since we can use the high quality low emittance primary beams to excite Λ hypernuclei. It is strongly in contrast to the case of hypernuclear production by secondary beams such as pions and kaons, which have been employed so far for the hypernuclear spectroscopy at KEK and BNL.
However, the hypernuclear cross sections by an electron beam is about 2 order of magnitude smaller compared with those by the meson beams. Although the advantage and significance of the hypernuclear spectroscopy by the (e,e'K^+) reaction is widely known, it has been difficult to conduct such experiments until E89-09 experiment was successfully carried out at Jlab Hall C in spring, 2000.
Upgrade of the hypernuclear spectroscopy experiments has been investigated parallel to E89-09 experiment, aiming to find experimental conditions that can compete the quality and yield rates of the hypernuclear spectroscopy by meson beams.
Points considered in the investigation are summarized below.

1. Yields of hypernuclei can be maximized utilizing the 0-degree tagging method, which requires relatively low current of electron beam, that is, around 1 μA for a 22 mg/cm^2 Carbon target. E89-09 experiment adopted this configuration. However, the 0-degree tagging method has a disadvantage that the electron arm will suffer huge background from bremsstrahlung electrons which have a sharp forward angular distribution as that of electrons associated with the virtual photon. If we move the electron detection angle to 6 degrees for example, then virtual photon flux drops by more than a factor of 10−3 as shown in Fig. 2-1.

2. The kaon should be detected at most forward angles in order to maximize hypernuclear yield as seen in the angular distribution of the kaons shown in Fig. 2-2. In case we accept 0 degree particles, however, we have to suffer from 0 degree positrons as well as hadron backgrounds. An example of positron angular distribution from the targets are also shown in Fig. 2-3.

3. The virtual photons at 0 degrees are almost real and the energy, E_γ, is given as,

$$E_\gamma = E_e - E_{e'} \tag{1}$$

where E_e and $E_{e'}$ are beam and scattered electron energies. The elementary cross section of the (γ,K^+) reaction has relatively weak above the threshold.

4. Once the energy of virtual photon is fixed, outcoming K^+ momentum is given assuming hypernuclear mass. P_{K^+} is about 1 GeV/c for E_γ = 1.645 - 0.285 = 1.36 GeV where the scattered electron energy is assumed to be 0.285 GeV as an example. Photon energy effective for the production of kaons will have a range that corresponds to the energy acceptance of the electron spectrometer. Thus, the momentum acceptance of the kaon spectrometer and the electron spectrometer should match each other. It is important to minimize background events in the trigger.

5. Maximum kaon momentum to be detected can be optimized considering

   (a) Yield of hypernuclei

   (b) Energy resolution and acceptance of the spectrometer. Naturally, the energy resolution becomes worse with the momentum.

   (c) Particle identification, particularly between pions and kaons.

   (d) Size of the kaon spectrometer and consequently construction cost.

6. For the yield of Λ hypernuclei, three factors contribute,

   (a) The elementary cross section of N(γ,K^+)Λ is almost constant for the energy range of real γ from 1.1 - 2.0 GeV. Corresponding kaon momentum is from $\sim$ 0.7-1.6 GeV/c. However, the form factor to hypernuclei gets with the higher γ energy larger because the recoil momentum becomes smaller.

   (b) With higher kaon momentum, the survival rate of the kaon becomes higher for the given flight path of the spectrometer.

   (c) With higher kaon momentum, the cone of scattered kaons becomes narrower. Thus, larger fraction of the hypernuclei produced in the reaction will be detected for the same solid angle if the spectrometer is positioned at or close to 0 degrees.

   The figure of merit as a function of electron energy assuming the scattered electron energy is 0.285 GeV is shown in Fig. 2-4. It is found that the higher the energy of the electron beam, the larger the yield of the hypernuclear ground states for a given spectrometer configuration.

7. Although the hypernuclear yield is expected increase with beam energy, bremsstrahlung photons up to the beam energy are produced in the targets and thus reactions associated with high energy photons contribute to the background. Particularly, K^+ production channels other than $\gamma + p \rightarrow \Lambda + K^+$ open at higher photon energy. These K^+s will be sources of background in the kaon spectrometer. The electron beam energy is better kept as low as possible from the points of background and particle identification.

8. Taking into account above conditions, the optimum kaon momentum to be measured by the kaon spectrometer is around 1.2-1.3 GeV/c as far as 1-2 $\times$ 10^{-4} momentum resolution is aimed. The momentum resolution corresponds to a few 100 keV energy resolution in hypernuclear excitation spectra, assuming the electron spectrometer gives better resolution.

9. The electron spectrometer also should have momentum resolution of 1-2 $\times$ 10^{-4}, matching that of the kaon spectrometer. Since the momentum of scattered electron is low compared to that of kaons, good momentum resolution will be achieved easily.

3 Comparison and optimization of the spectrometer configuration

Tang and Hashimoto investigated 6 possible configurations for the (e,e'K^+) spectrometer system including the new kaon spectrometer which has a large acceptance(20 msr) and high momentum resolution(2×10^{-4}) for the kaon arm.
The considered configurations include,

(1) Splitter+SOS+ENGE in Hall C "Original HNSS"

(2) Splitter+SOS+ENGE in Hall C "0 degree blocking"

(3) Splitter+New Kaon Spectrometer+SOS in Hall C "SOS for electrons"

(4) Septum+HRS+HRS in Hall A "Hall A original"

(5) Septum+HRS+New kaon spectrometer in Hall A "two septum required"

(6) Splitter+New kaon spectrometer+ENGE in Hall C(A) "Tilt method"

Hypernuclear yield, signal to noise ratio, singles rates of the 6 configurations are compared on the same footing.(For the detail see the report by L. Tang and O. Hashimoto) The newly proposed "tilt method"(#6) which takes advantages of both Hall A and Hall C configurations, is found promising for the future hypernuclear spectroscopy in this investigation. By the the "tilt" method, we try to maximize the hypernuclear yield while avoiding the huge background of 0-degree bremsstrahlung electrons. To meet the requirement, the electron spectrometer is tilted vertically by 2.25 degrees.
It was found we can get as much as a few tens events/hour for the $^{12}_{\Lambda}$B ground state with the beam intensity of 30 μA and the target thickness of 100 mg/cm^2. This is considerable improvement of the previous HNSS experiment in which 0.9 events/hour with the beam intensity of 0.66 μA and the target thickness of 10 mg/cm^2 was achieved. The signal to accidental ratio also improves by almost an order of magnitude. The yield will be comparable with the present (π^+,K^+) Λ hypernuclear spectroscopy with the SKS spectrometer at KEK-PS as compared in Table 1.

The present "tilt method" has an advantage for the spectroscopic investigation of heavier Λ hypernuclei. Since singles rate of the scattered electron spectrometer is no more dominated by the bremsstrahlung electrons, it becomes much easier to measure heavier Λ hypernuclear spectra with high Z target. Since the bremsstrahlung electron rate is inversely proportional to Z to the $2+\delta$, the electron beam current is strongly limited in heavier target in the case of the 0-degree tagging. It is not the case in the "Tilt method". The background of the kaon spectrometer positioned off 0 degrees will be of hadronic origin, in particular pions. Thus, the ratio between kaon events and hadronic background is possibly kept constant over the wide mass region and the heavier target experiments become more feasible.

4 Proposed spectrometer system

Since both resolution and acceptance are of vital importance to conduct hypernuclear spectroscopy, the design goal of the spectrometer system was set so that it simultaneously realizes high resolution and high efficiency. The general configuration of the proposed hypernuclear spectrometer system is based on the "Tilt method" and requires a splitter magnet. Both the kaon spectrometer and the scattered electron spectrometer are to be positioned at as forward angles as possible, still avoiding 0-degree bremsstrahlung electrons in the electron spectrometer and positrons in the kaon spectrometer.

Table 1: Yield comparison of the (π^+, K^+) reaction and the (e,e'K$^+$) reaction for the hypernuclear spectroscopy

	(π^+,K^+) SKS	(e,e'K^+) HNSS	(e,e'K^+)^{HNSS}/$(\pi^+,K^+)^{SKS}$ RATIO	HKS/HNSS GAIN factor
Cross sections to ${}^{12}_{\Lambda}\mathrm{C}_{gr}$ or ${}^{12}_{\Lambda}\mathrm{B}_{gr}$ (μb/sr)	10	0.05 (γ,K^+)	5×10^{-3}	1
Target thickness (g/cm^2)	1	0.01	10^{-2}	5
Beam Intensity (particle/sec)	10^6	$10^{9\sim10}$ (virtual photon flux)	$10^{3\sim4}$	10
K^+ momentum (GeV/c)	0.72	1.2		
K^+ solid angle coverage(%)	$\sim$60% (100 msr)	$\sim$15% (6 msr)	0.25	3
K^+ survival rate(%) (Flight path)	$\sim$0.35 (5m)	$\sim$0.4 (8m)	1	1
Overall			$1.25\times10^{-1\sim-2}$	150

For the measurement of kaons in the 1 GeV/c region, a new high resolution kaon spectrometer with QQD configuration has been designed. It has high momentum resolution of 2×10^{-4} at 1.2 GeV/c and a large solid angle of 30 msr when it is used stand alone as summarized in Table 2. The justification for the QQD configuration is explained in Appendix. The kaon spectrometer is located at finite angle(7-8 degrees) to avoid the 0 degree particles, particularly positron.
For the scattered electrons, the Enge split-pole spectrometer of HNSS will be adopted, but the focal plane detector system is to be reconfigured to meet the requirement of the "Tilt method" as described later. The spectrometer is vertically tilted by 2.25 degrees to be free from the Bremsstrahlung electrons.
The splitter magnet will have the same geometry as that of HNSS but will have a larger gap that matched the bore of Q1.
The configuration and specification of the proposed hypernuclear spectrometer system is summarized in Table 2 and is shown in Fig. 4-1.
The blowup CAD drawing near the target region is also given in Fig. 4-2. The first Q of the kaon spectrometer should have narrow width so that the kaon spectrometer should be as close to the splitter as possible. It is presently designed that the first Q is installed at 1.1 m from the target.
It is noted that the large acceptance spectrometer can be used in other experiments, such as those that need to detect two particle correlation within very small relative q and as a backward spectrometer in the forward-backward correlation measurements etc. It may be more desirable to mount HKS on the rotating platform, so that it is easy to change kinematical condition. Such option is open to the future but is not implemented at the first stage of the present program.

Table 2: Configuration and specification of the proposed hypernuclear spectrometer system

General configuration	
	Splitter+Kaon spectrometer+Enge spectrometer
Kaon spectrometer	
Configuration	QQD and horizontal bend
Maximum central momentum	1.2 GeV/c
Momentum resolution($\Delta p/p$)	2×10^{-4}
	(beam spot size 0.1mm assumed)
Momentum acceptance	$\pm$ 10 %
Solid angle	20 msr with a splitter
	(30 msr without splitter)
Kaon detection angle	Horizontal : 7 degrees
ENGE split-pole spectrometer	
Maximum central momentum	0.35 GeV/c
Momentum acceptance	$\pm$ 20 %
Momentum resolution(δ/p)	3×10^{-4}
Electron detection angle	Horizontal : 0 degrees
	Vertical : 2.25 degrees

5 Design of the high resolution kaon spectrometer

The basic parameters of the high resolution kaon spectrometer(HKS) is given in Table 3. As discussed in section 2, the maximum momentum of the kaon is set to 1.2 GeV/c.
An example of particle trajectories in the splitter, Q1, Q2 and dipole is shown for the three momenta(1.08, 1.2, 1.32 GeV/c) in Fig. 5-1. The optical condition was searched requiring point-to-point focus(R_{12}=0) for the dispersive(horizontal) direction, while for the vertical direction either point-to-point(R_{34}=0) or point-to-parallel(R_{44}=0) condition. For those two cases, the envelopes of trajectories are shown in Fig. 5-2.
Acceptance and optical properties were further studied using the TURTLE code as described in the Appendix. About 65 % of 1.2 GeV/c $\pm$ 10% kaons emitted in the angular range of $\pm$ 100 mrad (horizontal) and $\pm$ 75 mrad (vertical) reaches the second TOF wall at 9m from the target, which corresponds to about 20 msr solid angle.
Using the GEANT code, the acceptance map as a function of scattered angle and momentum was also obtained as seen in Fig. 5-3. It shows momentum dependence of the acceptance whose value is consistent with the TURTLE calculation.
The resolution of the kaon spectrometer was studied by the GEANT code with the configuration given in Table 3.
In the calculation, it was assumed (1) The vacuum chamber is extended to the first drift chamber. (2) The exit window of the vacuum chamber is made of 0.008" Kevlar to minimize multiple scattering. (3) A He bag is installed in the space between the two drift chambers.
In Fig. 5-4 is shown the HKS momentum resolution over the momentum acceptance of 1.2 GeV/c $\pm$ 10 % for the three different DC1 distances from the magnet exit boundary. The required resolution can be achieved when the drift chambers are located so that the focal point of the central trajectory is in the middle of the two drift chambers even if the multiple scattering is included.
In order to achieve good energy resolution with light targets, where contribution due to kinematical broadening cannot be neglected, angular resolution of the spectrometer is also required. In Fig. 5-6, vertical(V) and horizontal(U) angular resolutions are shown as a function of chamber resolution studied by GEANT. We expect to achieve angular resolution better than 5

Table 3: Parameters of the proposed high resolution kaon spectrometer(HKS)

Maximum central momentum	1.2 GeV/c	
Momentum resolution($\Delta p/p$)	2×10^{-4}	beam spot size 0.1mm assumed
Magnet configuration	Q-Q-D and splitter	
Momentum acceptance	$\pm$ 10 %	
Solid angle	20 msr	with splitter
	(30 msr)	without splitter
Maximum horizontal angular acceptance	$\pm$ 100 mr	
Maximum vertical angular acceptance	$\pm$ 75 mr	
Bending radius	2.5 m	
Bending angle	70 degrees	
Momentum dispersion	3.6 cm/%	
Focal plane distance from the target	8.35 m	
Flight length to the last TOF	10.0 m	
Focal plane tilt angle	69 degrees	
Dipole gap	0.2 m	
Magnet coil	Normal conductors	

mrad(FWHM) even for the vertical direction, although they should be proved with real data. The kinematical broadening for the light target of ^{6}Li is dipicted as an example in Fig. 5-5. It is shown the kinematical shift of the hypernuclear mass is can be kept better than 200 keV. The contribution is much smaller for the heavier targets.
Although the beam energy fluctuation also contributes to the energy resolution of the hypernuclear mass spectra, we assume the beam energy is well controlled and stabilized within the level of 100 keV as was the case in the previous E89-09 experiment. In addition, energy loss difference of electrons and kaons and energy loss straggling in the target is kept less than the required energy resolution by choosing the proper target thickness.

6 Detectors for High Resolution Kaon Spectrometer

The detector configuration is similar to SOS as listed in Table 5 Basic considerations on the detectors of the kaon spectrometer are listed below,

(1) The singles rates are dominated by pions but not positrons and will amount up to a few MHz.

(2) The rate as high as several MHz should be accepted. Particularly, drift chamber should be operable at that high rate.

(3) Pion veto will be most important to form triggers and therefore two layers of Aerogel cerenkov counters will be required.

The singles rates of particles under the given condition of HKS are summarized in table 4 and are used for the following discussion. The hadronic rates in the kaon spectrometer were evaluated using the data measured during the E89-09 experiment. Bremsstrahlung electron rate was estimated assuming the calculated angular distribution.
A design parameters of the detectors is given in the following table.

Table 4: Singles rates of kaon and electron arms

HKS Spectrometer		
	Positron	~ 0
	Pion	800 kHz
	Kaon	340 Hz
	Proton	280 kHz
ENGE spectrometer		
	Electron	2.6 MHz
	Pion	2.8 kHz

Table 5: Specifications of the detectors. z is measured from dipole exit (z=0 corresponds to 6.0 m from target).

Name	Sensitive area (cm)	z (cm)	Description
HDC1	$90^{\mathrm{W}}\times30^{\mathrm{H}}\times2^{\mathrm{T}}$	185	$xx'uu'(+30deg)vv'(-30deg)$, 5 mm drift distance, $\sigma = 150$ μm
HDC2	$105^{\mathrm{W}}\times30^{\mathrm{H}}\times2^{\mathrm{T}}$	285	$xx'uu'(+30deg)vv'(-30deg)$, 5 mm drift distance, $\sigma = 150$ μm
TOF1	$110^{\mathrm{W}}\times30^{\mathrm{H}}\times2^{\mathrm{T}}$	298	7.5 cm × 15-segments, $\sigma = 80$ ps
AC1	$135^{\mathrm{W}}\times40^{\mathrm{H}}\times25^{\mathrm{T}}$	320	16 5"PMTs, n=1.06
AC2	$135^{\mathrm{W}}\times40^{\mathrm{H}}\times25^{\mathrm{T}}$	345	16 5"PMTs, n=1.06
LC	$135^{\mathrm{W}}\times40^{\mathrm{H}}\times4^{\mathrm{T}}$	369	9 cm × 18-segments, n=1.5
TOF2X	$130^{\mathrm{W}}\times30^{\mathrm{H}}\times2^{\mathrm{T}}$	398	7.5 cm × 17-segments, $\sigma = 80$ ps
TOF2Y	$130^{\mathrm{W}}\times30^{\mathrm{H}}\times1^{\mathrm{T}}$	403	4 cm × 8-segments
GC	$200^{\mathrm{W}}\times40^{\mathrm{H}}\times100^{\mathrm{T}}$	461	4 5"PMTs

6.1 Drift chambers

We plan to adopt the cell structure of the SOS drift chamber, 5 mm drift space. Thus we expect to obtain the position resolution at least $\sigma \sim 200$ μm, which was assumed in the GEANT simulation.
As seen in the table, the singles rate of pions per plane will be as high as several MHz and the electronics should be able to handle the rate. However, it is expected the present LeCroy 2735 type front end card and the fast bus TDC system can handle the rate.

6.2 Time-of-flight walls

Unlike the SOS, the height of the TOF scintillator will be much shorter and is 30 cm. Since the time resolution of the TOF walls is important to distinguish kaons from large background of pions, we intend to realize as good time resolution as possible, around $\sigma \sim 80$ ps. We plan to use the high resolution tube of Hamamatsu H1949 for the TOF scintillators. The length of the TOF scintillator will be much shorter than those of SOS and will help us achieve the better time resolution. We may also consider thicker scintillator for further better time resolution, if necessary.
Horizontal TOF scintillator hodoscope will be installed only for one of the TOF scintillator walls and will be used for calibrating the timing of vertical hodoscopes.

6.3 Aerogel Cerenkov counter

Two layers of aerogel Cerenkov counters will be installed between the first and the second TOF walls. Assuming we will have 5 MHz pions and 98 % efficiency for each aerogel Cerenkov counter for pions, we expect to obtain the pion rejection rate 4×10^{-4}, resulting in 200 pion events in the trigger. It is absolutely necessary to employ the two layers of the Aerogel Cerenkov walls in contrast to SOS.
The aerogel radiator will have refractive index of 1.06 instead of 1.034 used in SOS since the maximum momentum of HKS will be less than 1.4 GeV/c(See Fig. 6-1). We will have more Cerenkov photons by using the higher index radiator and still we can discriminate pions clearly from kaons.
The aerogel radiator will by purchased from Matsushita Electric Works. Their Aerogel has high resistance against water and moisture and the maintenance of the Cerenkov counter should be easier.

6.4 Lucite Cerenkov counter

Lucite Cerenkov counter wall will be prepared in order to reject proton events in the trigger. Since HKS has a large angular acceptance and the particles enter the Cerenkov counter with large angular spread, we will use Lucite which contains 5 ppm(in weight) wave-length shifter which is available from Bicron. Such Lucite Cerenkov counter was used for the PIK and SKS spectrometers at KEK 12 GeV PS. As very good time resolution is not required for the Lucite Cerenkov counter, ordinary 2" PMTs(Hamamatsu H7195) will be used.

6.5 Gas Cerenkov counter

The Gas Cerenkov counter should be installed downstream end of the HKS counter system in order to reject positron events. Although the spectrometer will be positioned at the angle where dominant part of the forward positrons do not enter, the gas Cerenkov counter should be powerful to discriminate background positron events. Since the aerogel Cerenkov counters already distinguish both positrons and pions from kaons, kaon events may be identified without the Gas Cerenkov counter. However, the Gas Cerenkov counter is necessary for positron identification which is required for some calibration runs. It is also used for pion identification when positron singles rate is not negligible.

6.6 Other trigger counters

Although a shower counter array is installed in SOS and is efficient to tag positron events, at present we have not considered the use of the shower counter. It may be necessary to explore such possibility later if it is needed.

7 ENGE spectrometer and the focal plane detectors

Since we plan to employ the tilt method, the rate of scattered electrons at the focal plane will be less than 10 MHz, much less than that of the 0 degree tagging method, 200 MHz.
However, as shown in Fig. 7-1, measurement of the incident angle to the focal plane is required to achieve the energy resolution better than 200 keV. Thus we need two layers of tracking detectors. We propose to prepare two identical drift chambers, although there is an option to use the existing SSD array for the second plane and the MWDC for the first plane. The distance between the two chambers will be about 20 cm. Angular resolution of a few mrad, which is good enough for the above requirement, will be obtained with this setup.
The HNSS scintillator hodoscope will be modified as a new hodoscope array.
The whole detector package should be supported from the Enge magnet yoke.

8 Specification of the kaon spectrometer magnets

The present design of the spectrometer magnets are summarized in Fig. 8-1 and the result of the 2D field calculation is also shown in Fig. 8-2,3,4 for each magnet.
The first quadrupole, Q1, will have special shape and narrow width so that it does not bump to the Enge spectrometer yoke. The second quadrupole have large horizontal aperture in order to match the dipole gap. It is planned to shim the dipole pole in order to obtain better field uniformity in the radial direction. The basic parameters of the three magnets are listed in Table 8

Table 6: Magnet specification for the QQD high resolution kaon spectrometer

Dipole magnet		
	Outer radius	4 m
	Inner radius	1 m
	Mean radius	2.5 m
	Height	2.3 m
	Gap	0.2 m
	Pole width	1.2 m
	Expected weight	$\sim$ 160 ton
	Maximum field	1.65 T
Q1 magnet		
	Length	0.7 m
	Bore diameter	0.24 m
	Horizontal spread	0.5 m
		(Larger than the bore)
	Vertical spread	0.2 m
		(smaller than the bore)
	Maximum field at pole	1.6 T
	Expected weight	7 ton
Q2 magnet		
	Length	0.5 m
	Bore diameter	0.32 m
	Horizontal spread	0.8 m
		(Larger than the bore)
	Vertical spread	0.2 m
		(smaller than the bore)
	Maximum field at the pole	1.6 T
	Expected weight	10 ton

All the three magnets will be connected by vacuum pipes. A sieve slit box similar to the one used in SOS and the vacuum gate valve will be installed between the splitter and the Q1. The vacuum pump system should be also prepared.

9 Expected Jlab Infrastructures

9.1 Magnet power supply and cooling water

The present spectrometer system requires 5 DC power supplies to excite the splitter magnet, the Enge split-pole dipole, Q1, Q2 and the dipole magnets of the kaon spectrometer. They are all

normal-conductor magnets. Table 7 shows the list of the magnets and required power for each of them. We assume at present that the splitter magnet, ENGE split-pole magnet, Q1 and Q2 magnets of the HKS can be powered by the existing hall C power supply. For the HKS dipole magnet which requires a large-capacity power supply, we will prepare a new one. The power supply need be installed in low-radiation area in the hall where the power supplies are safely located. The power supply for the HKS dipole should be equipped with an interface standard at Jlab control system.
When we install the spectrometer system used in Hall A, the 4 power supplies except for the NKS dipole power supply are additionally required.
The magnets also need cooling water. The required flow rates will be later specified when the magnet and power supply designs are fixed. We will also design them to meet the pressure of the cooling water.

Table 7: Required power supplies for the new hypernuclear spectrometer system

1.	160V1000A	Q1	Currently used for SOS Q
2.	250V1000A	Q2	Currently used for SOS D1
3.	160V1000A	spare	Currently used for SOS D2
4.	150V1500A	Enge	Currently shared by Moller and Enge
5.	150V1000A	Splitter	Currently used for splitter
6.	500kW	New dipole	New Specification to be matched with the new dipole max. current 10% higher than that for 1.65 T

9.2 Spectrometer support structure

It is our present intension to construct Q1, Q2 and Dipole magnets for HKS in Japan as well as the dipole magnet power supply.
In order that we can install the spectrometer system both to Hall A and Hall C, we need design the spectrometer support system compatible for the two halls. Major difference between the two halls is the beam height, about 2 m in Hall A and about 5 m in Hall C. Therefore, the basic support structure will be designed so that the height of the spectrometer mid-plane is less than 2 m. When the spectrometer is installed in Hall C, the spectrometer system should be lifted by 3 m with some additional support structure. This part has to be discussed as the design of the magnets proceeds.
As discussed in the section of the spectrometer configuration, the spectrometer will be installed with the prefixed geometry. Therefore, it is not planned to mount the spectrometer on the rotating platform as far as the hypernuclear spectroscopy experiments are concerned. However, it is vitally important to carry out some calibration experiments and obtain information on the optical properties of the high resolution kaon spectrometer, such as deriving coefficients for momentum reconstruction, prior to the (e,e'K^+) experiments. It will be, therefore, necessary to install the kaon spectrometer not only at very forward angles around 5 degrees but also at larger angles. Then it is possible to measure elastic scattering of electrons with a heavy target for the spectrometer calibration. This should be kept in mind when the HKS support system is designed.

9.3 Vacuum window and the safety issue

As described in section 5, the window thickness of the vacuum chamber contribute to the momentum resolution of the kaon spectrometer. The size of the exit window will be about 30 cm

high and 80 cm wide and should be equipped with a thin window material. We would like to use the thin Kevlar(0.008" Kevlar29 style 713) with Mylar sheets on both side instead of the one used for the SOS window(0.015" Kevlar). Safety test may be required and we ask for assistance by the Jlab and Hampton staffs.

9.4 Hall arrangement and requirement for the beam line

Possible configuration of the new hypernuclear spectrometer system in Hall C is shown in Fig. 9-1. The target pivot will be moved downstream of the present Hall C pivot. As seen in the figure, the whole system will fit the space between the Hall C pivot and the G0 detector package. Since the present system assumes an intense beam almost 100 times than the Hall C HNSS case, it is necessary to steer the beam back to the 0 degree beam line after the target and splitter, and put into the Hall C beam dump. Therefore, it is required to install steering magnets much powerful than the ones used in the previous HNSS experiments.

10 Budget

As mentioned in the introduction, we have allocated about 3 M$ for the construction of the spectrometer system, including both magnets and the detectors. Although the cost of the spectrometer magnets and power supply is yet to be determined after negotiation with companies, Table 8 explains our preliminary plan for the budget break up. It is very much dependent on the cost of the magnets but also on to what extent additional contribution can be obtained for detectors and associated items from the collaborators.

Table 8: Preliminary budget allocation

Magnets etc.	2 M$	Q1, Q2, Dipole, vacuum chambers, transportation, field mapping
Kaon arm detectors	0.9 M$	Drift chambers(DC1, DC2), TOF1,2, Lucite Cerenkov, Aerogel radiator, 2" PMTs, 5" PMTs
Electron arm detectors	0.1 M$	2 MWDC, hodoscope

Those which are not included in the present budget plan are listed in Table 9 to clarify what else we need consider as extra. Some of the item may be transfered from HNSS if it is agreed or can be prepared by the collaborators. Others may be covered by the present budget later when the spectrometer design is fixed and budget become available.

11 Expected time line

The Monbusho "specially promoted research program" is subject to every-year review and also is required to complete its goal with physics output within the proposed period, that is 4 years this case. To meet the requirement, we hope to conduct the first experiment with HKS in an early part of 2003 and analyze the data by the beginning of 2004, though it should be subject to PAC and Jlab decision. Our planned schedule for the spectrometer construction is summarized in Table 10.

Table 9: Missing items from the present preliminary budget allocation

General		
	Modification of the splitter magnet	
	Target chamber	
HKS		
	Magnet support from the Hall floor	
	Power supply and water connection	
	Vacuum window material that satisfies the Jlab safety standard	
	Vacuum pump of HKS	
	Sieve slit box, gate valve	
	Detector support structure	
	Detector hut	
	Readout electronics including front-end electronics	
	Gas Cerenkov counter	
	Cables between the detector hut and the counting house	
ENGE		
	Hodoscope PMT & scintillator	from HNSS
	Shielding structure	One similar to HNSS
	Drift chamber and hodoscope support	
	Modification of the splitter pole gap	
	Vacuum connection between HKS and the target chamber	
	Safety consideration	

Table 10: Present expected time line of the project

April, 2000 - March, 2001	
	Design of the spectrometer system
	Contract with a magnet manufacture
	Construction of Q1 and Q1
	Design of detectors
	Physics proposal preparation
April, 2001 - March, 2002	
	Construction of the dipole magnet
	R&D test of detectors(TOF, AC etc.)
	Design and construction of the drift chambers
	Design and construction of TOF, LC
April, 2002 - March, 2003	
	Field mapping of the dipole magnet
	Transportation of the dipole to Jlab
	Assembly and test of the spectrometer magnet at Jlab
	Completion of the detector fabrication
	Assembly of the detector system at Jlab
	Installation of the spectrometer system in the Hall
April 2003 - March, 2004	
	Test experiments for HKS calibration
	Hypernuclear spectroscopy experiments
	Data analysis

12 Collaboration

The collaboration will be established after the first meeting on September 15, 2000 by whoever has interest in the hypernuclear physics program at Jlab and also those who may work together for the HKS and the new hypernuclear spectrometer system.

13 Summary

A budget proposal to Monbusho has been approved recently, which allows us to construct high-resolution high-efficiency spectrometer for hypernuclear spectroscopy by the (e,e'$^{+}$) reaction at Jlab. The design of the spectrometer system and the plan for the construction has been described together with the optics study. It is a 4 year program and is supposed to be completed by the end of March, 2004. 3 M$ is allocated to the construction of the magnets and detector packages. Necessary infrastructures at Jlab and support are identified. Whoever have interest in hypernuclear physics program or in using the kaon spectrometer are welcome to join the collaboration and work together. Strong support by the Jlab staffs and close collaboration are needed for the success of the program.

Figures

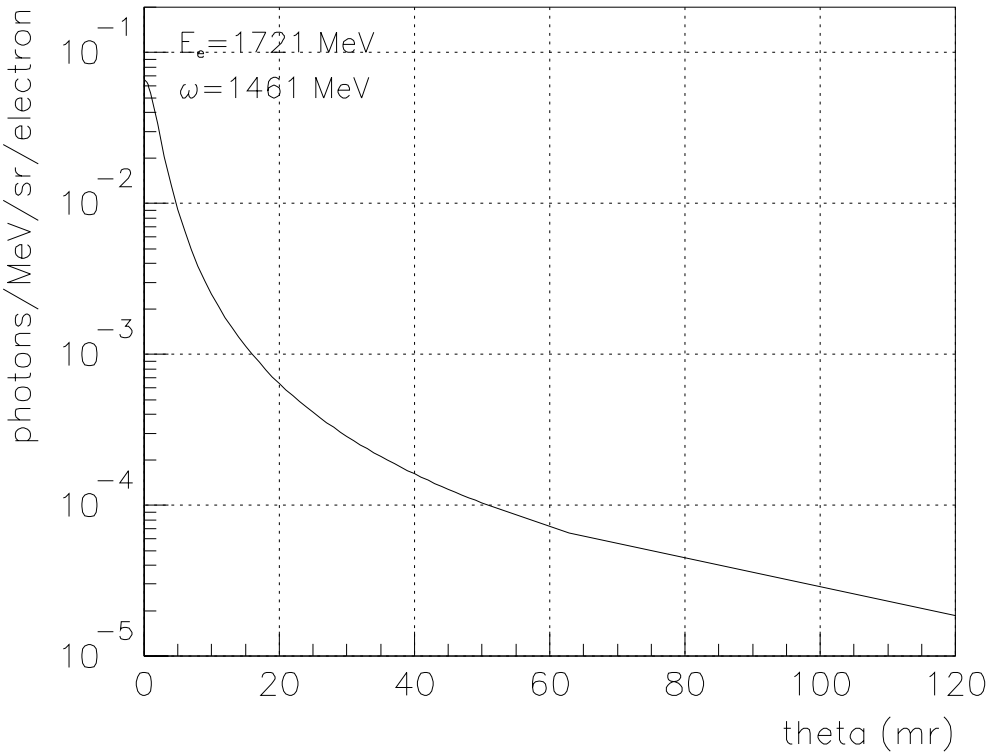

Figure 2–1: Angular distribution of virtual photon flux calculated with Eq. (A-10) of Ref. [1].

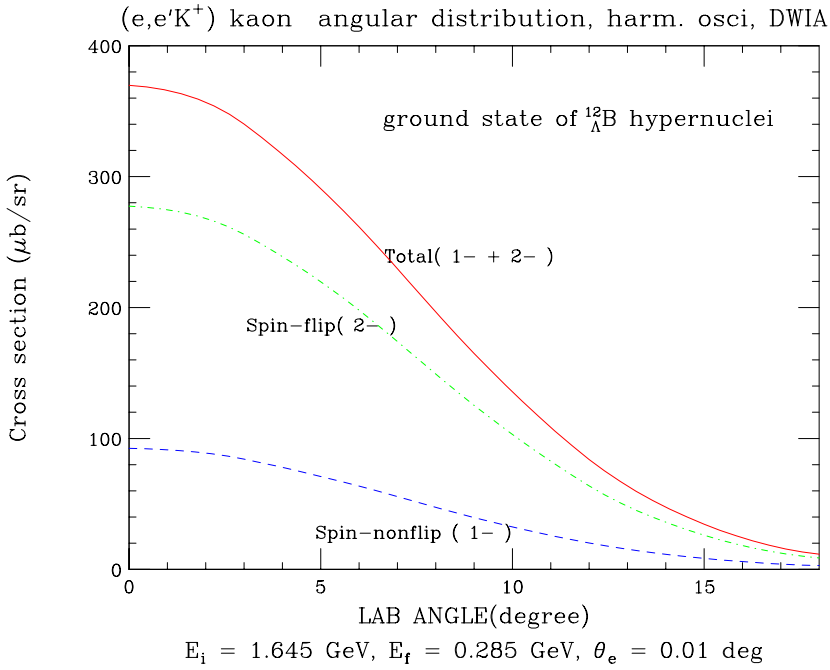

Figure 2–2: Angular distribution of K^+ from ^{12}C (e,e'K^+) $^{12}_{\Lambda}B$ reaction was calculated by DWIA with the harmonic oscillator potential. Spin flip and non-flip cross section and their sum are plotted.

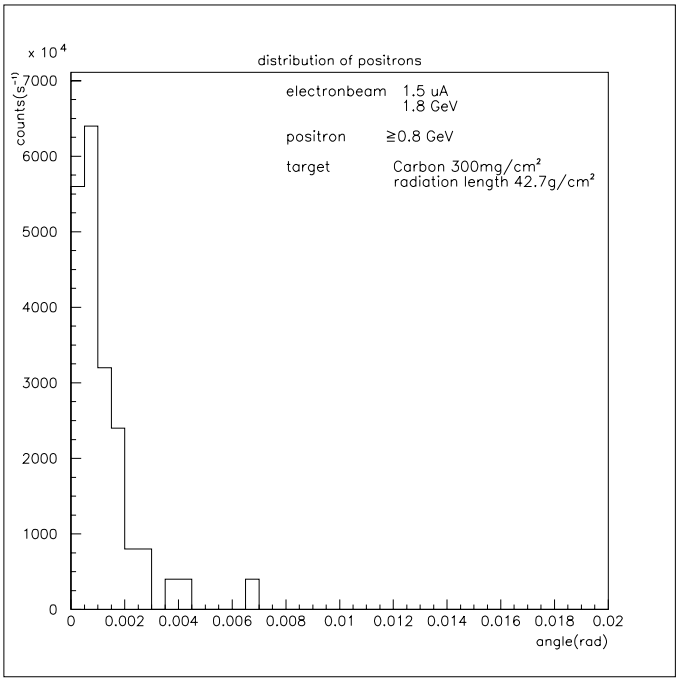

Figure 2–3: Angular distribution of positrons from pair creation.

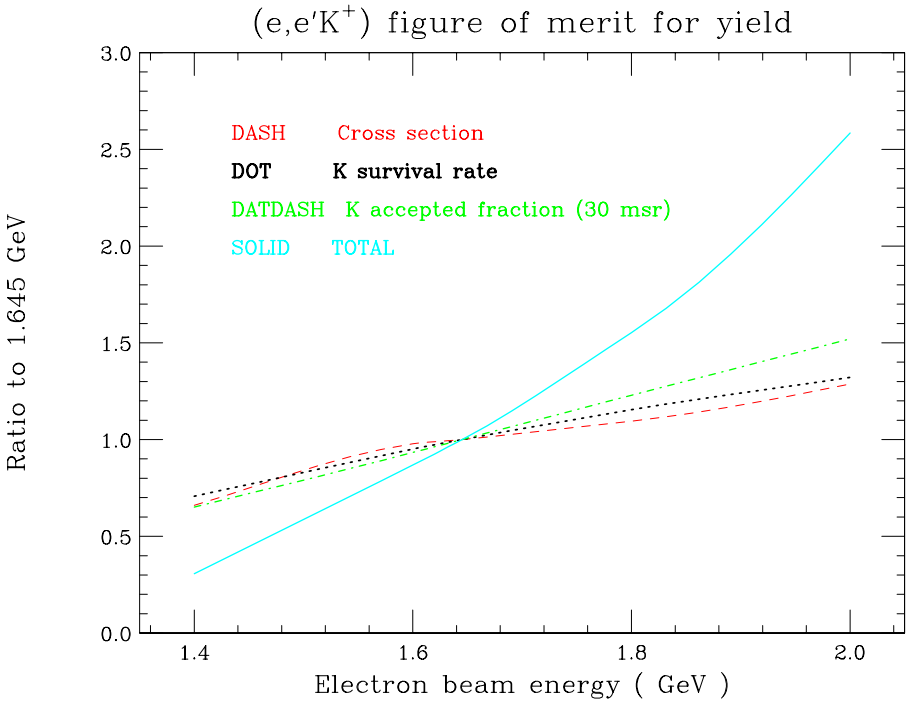

Figure 2–4: The beam energy dependence of the figure of merit comparing with 1.645 GeV. The dashed, dotted and dot-dashed lines show respectively the cross section, kaon survival rate and the kaon accepted fraction. The solid line shows the result with all above effects.

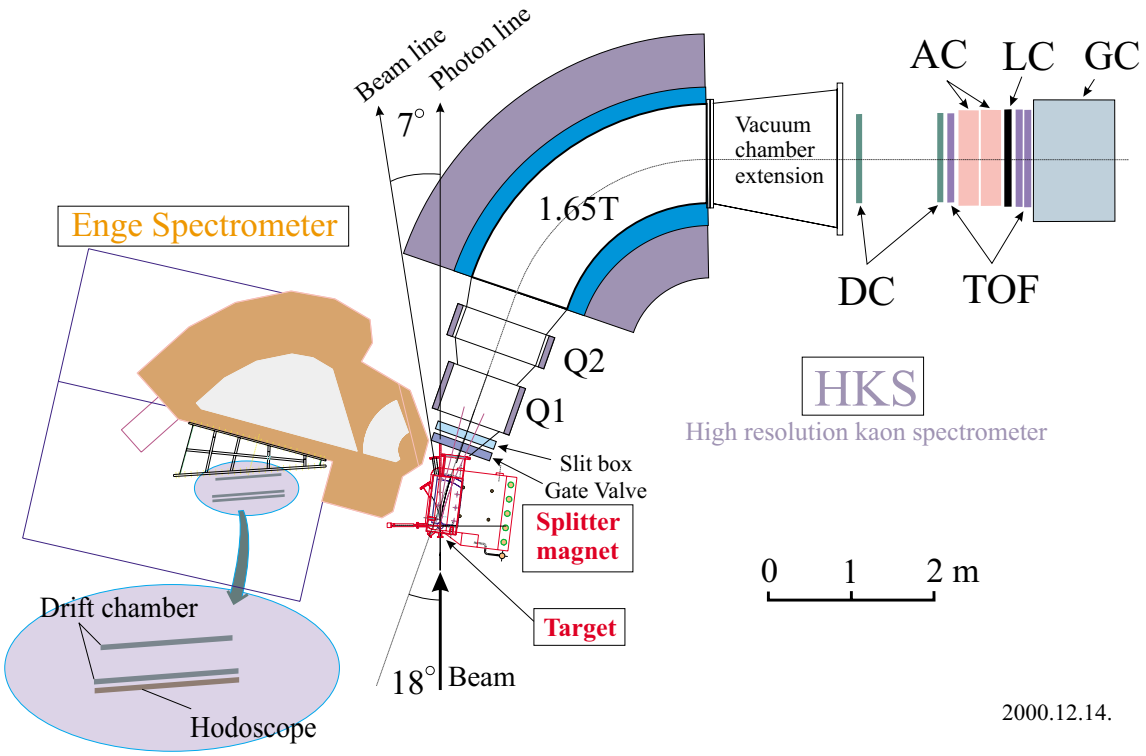

Figure 4–1: The HKS general configuration with detectors.

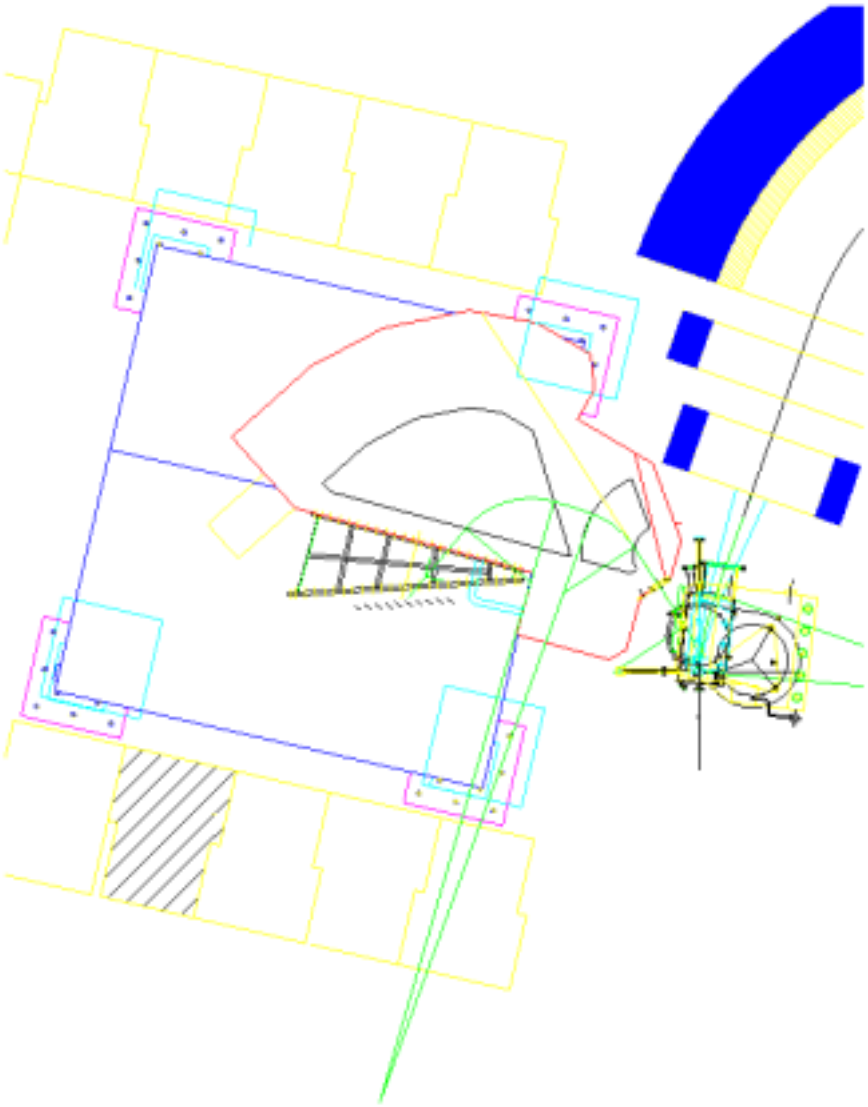

Figure 4–2: Closer view of the Enge magnet part. In order to measure the direction of electrons, two wire chambers will be placed at the exit of Enge.

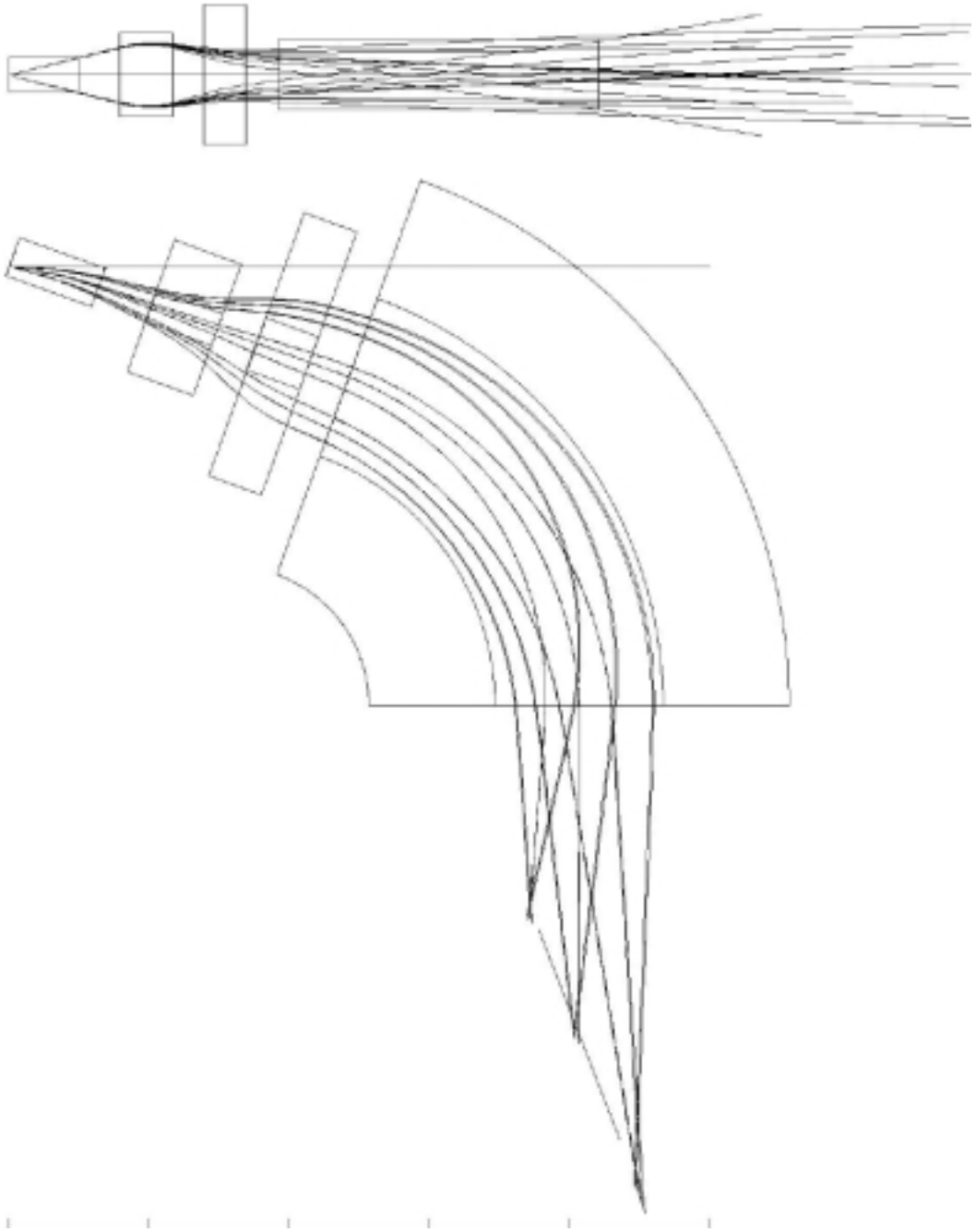

Figure 5–1: HKS trajectories. Each ray corresponds to: 0, +100, and −100 mr in horizontal, 0,+75, and −75 mr in vertical, 1.2 GeV/c, +10%, and −10% in momentum.

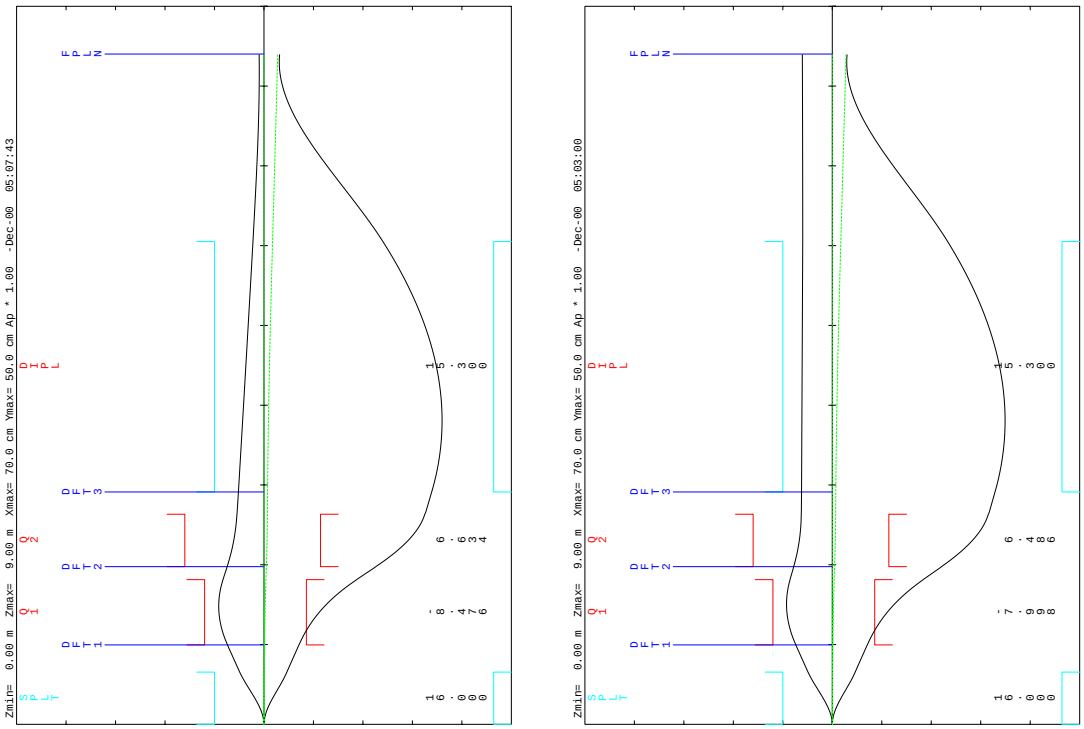

Figure 5–2: The beam envelopes calculated with TRANSPORT. Left figure is for $R_{12} = R_{34} = 0$ and right one for $R_{12} = R_{34} = 0$. See appendix 14.1.

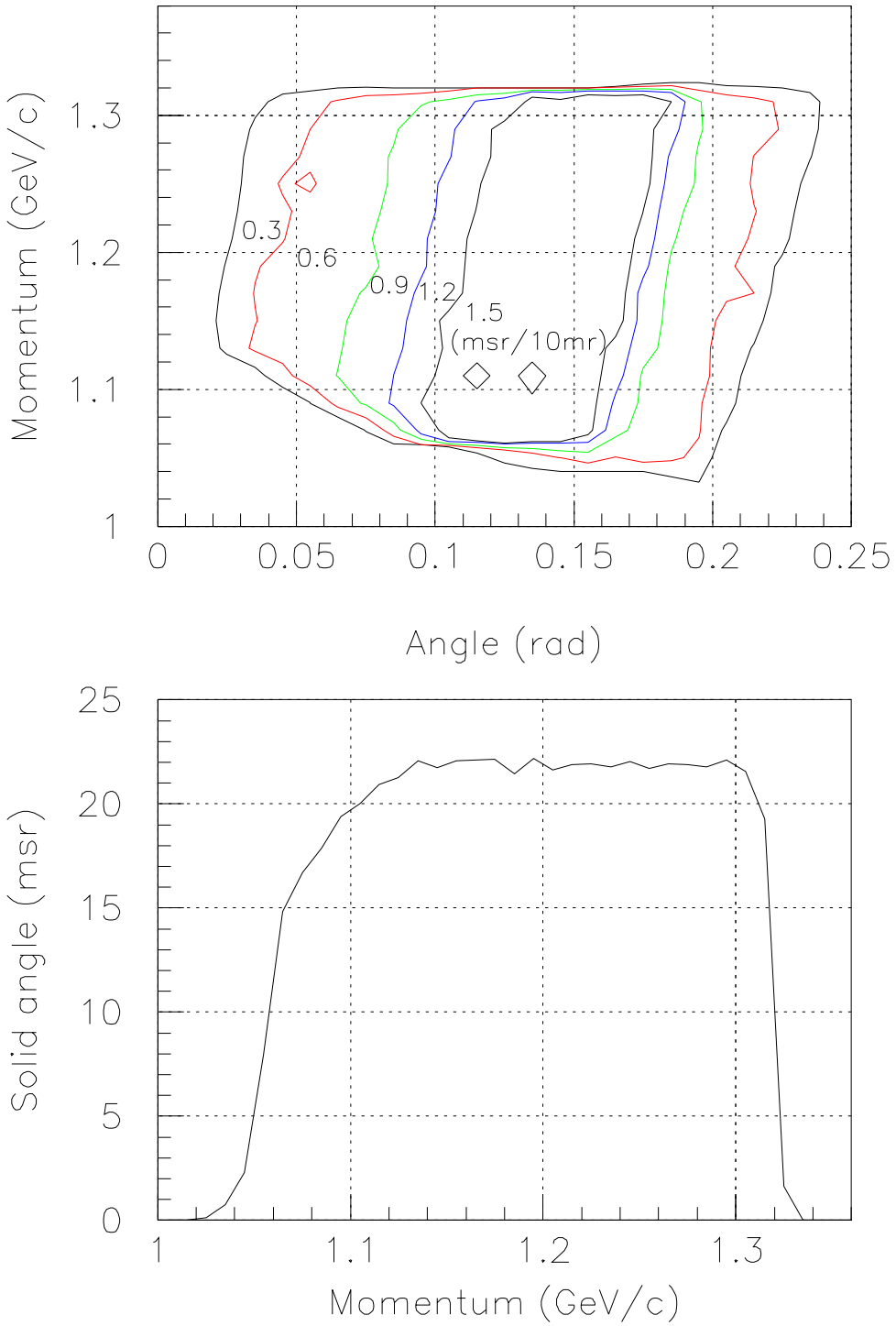

Figure 5–3: Angular and momentum dependence of solid angle of HKS. The top panel shows the angular and momentum dependence of solid angle. The bottom panel shows the+ momentum dependence of total solid angle; projection onto y axis of the top panel.

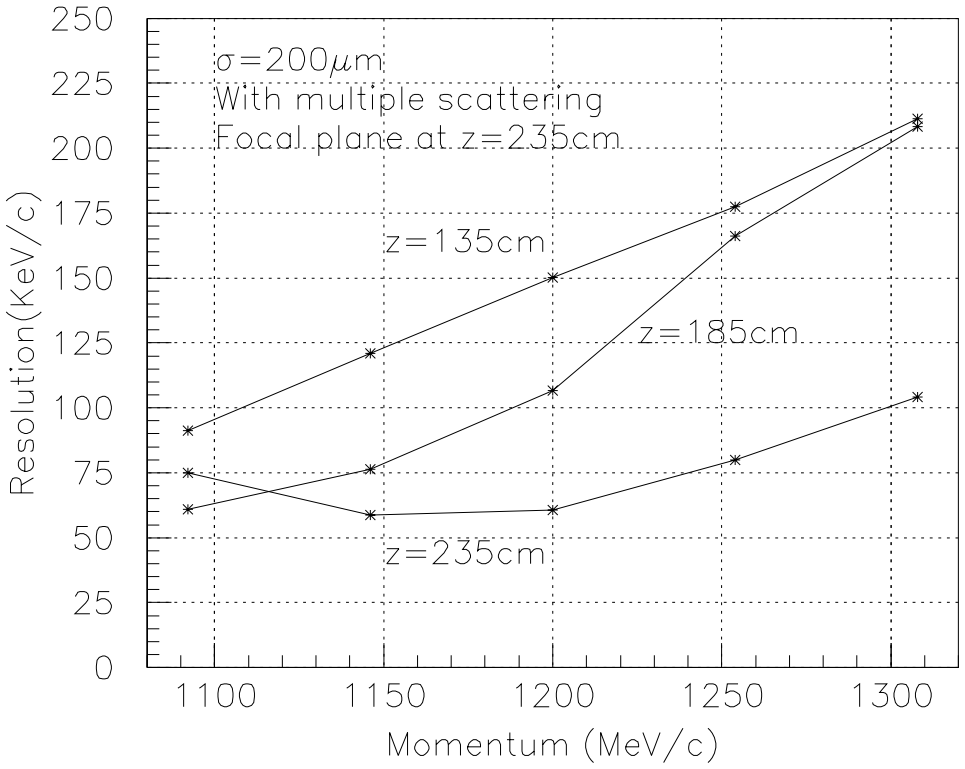

Figure 5–4: Chamber z position dependence of momentum resolution as a function of particle momentum obtained with a Monte Carlo simulation code. Two chambers are placed at $z \pm 50$ cm.

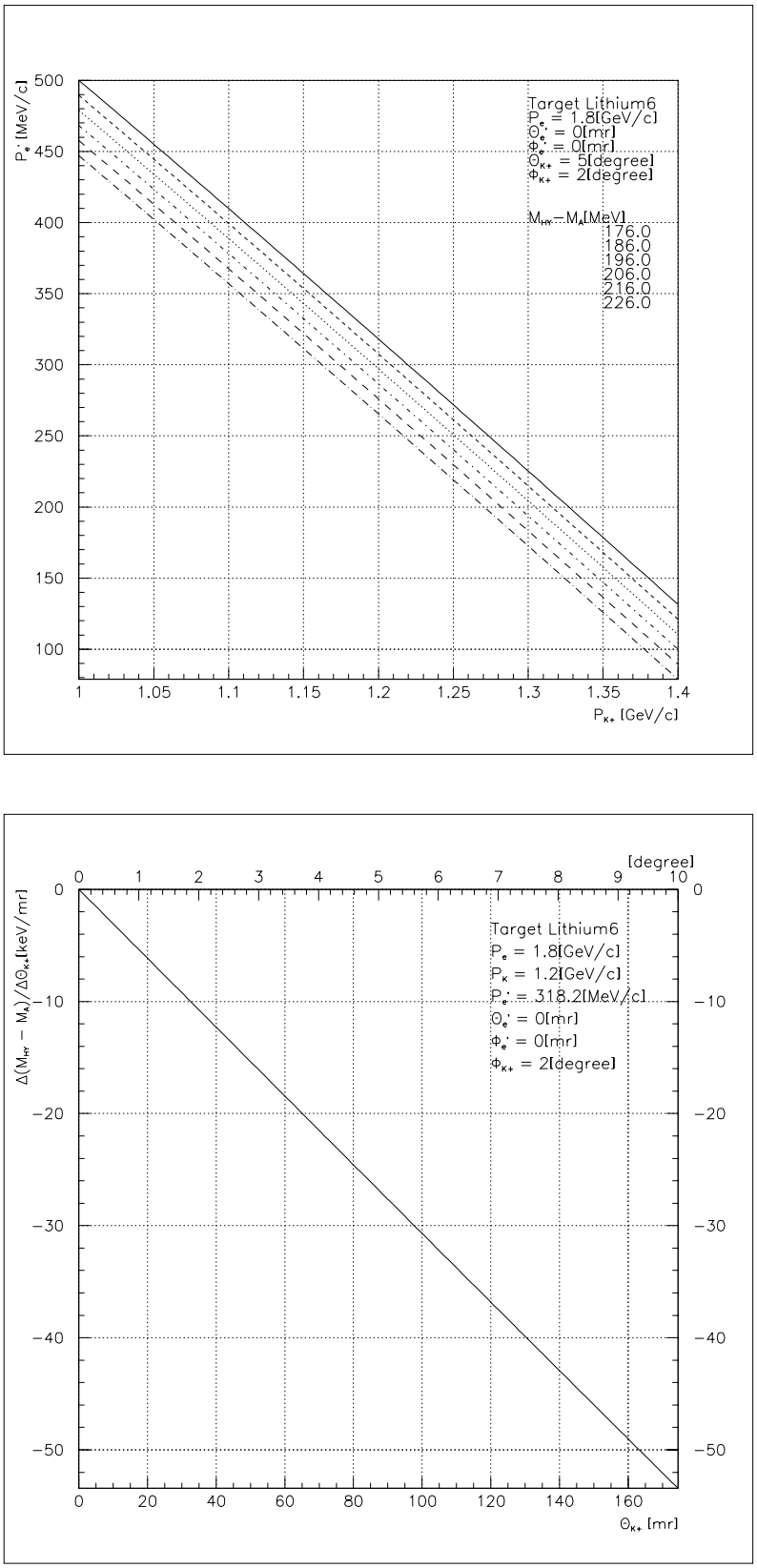

Figure 5–5: The kinematical broadening estimation for ^{6}Li (e,e'K^{+})$^{6}_{\Lambda}$He reaction. Top figure shows the correlation between momenta of the kaon and outgoing electron for various M_{HY}-M_A. The bottom one shows the θ_K dependence of $(\Delta M_{HY}\text{-}M_A)/(\Delta\theta_K)$. At $\theta_K = 87$ mrad (5°), uncertainty of 1 mrad in θ_K will cause 30 keV ambiguity in the energy spectrum.

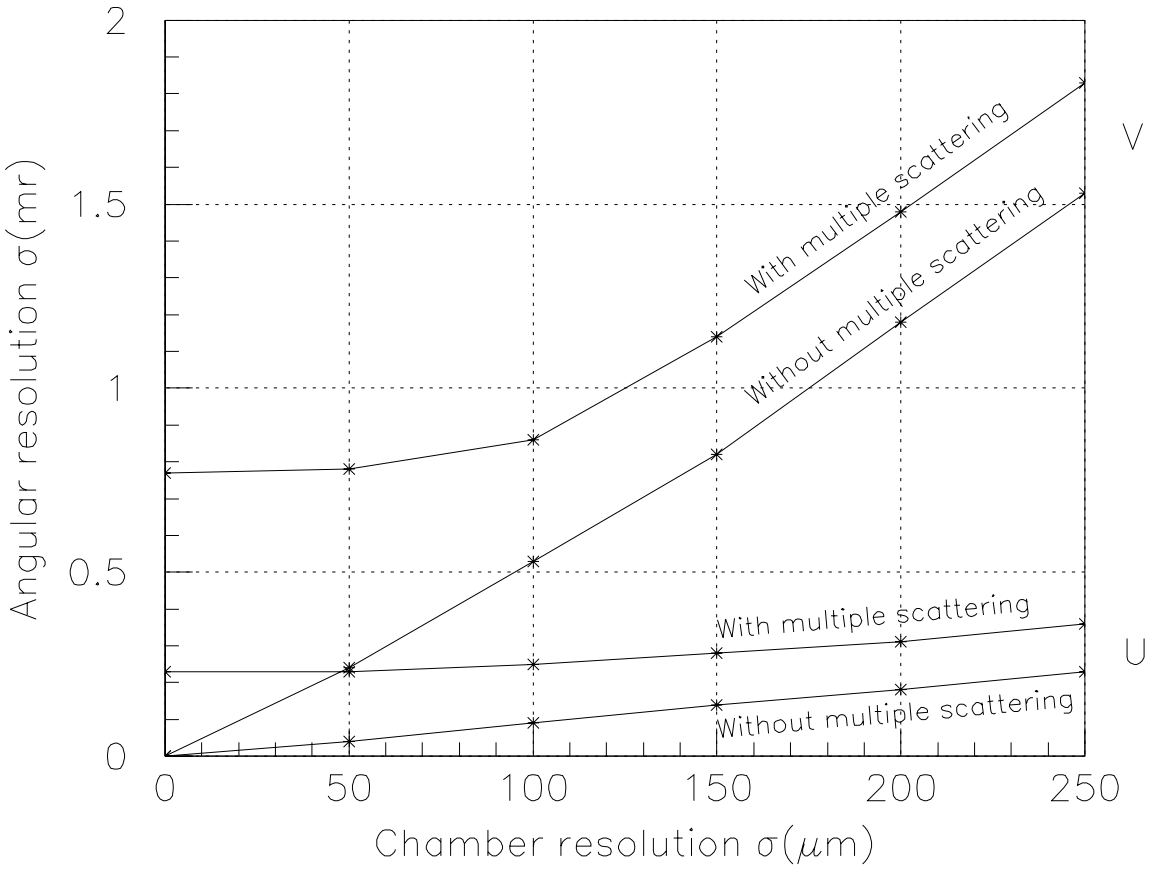

Figure 5–6: Angular resolution as a function of chamber resolution with and without multiple scattering obtained with a Monte Carlo simulation code

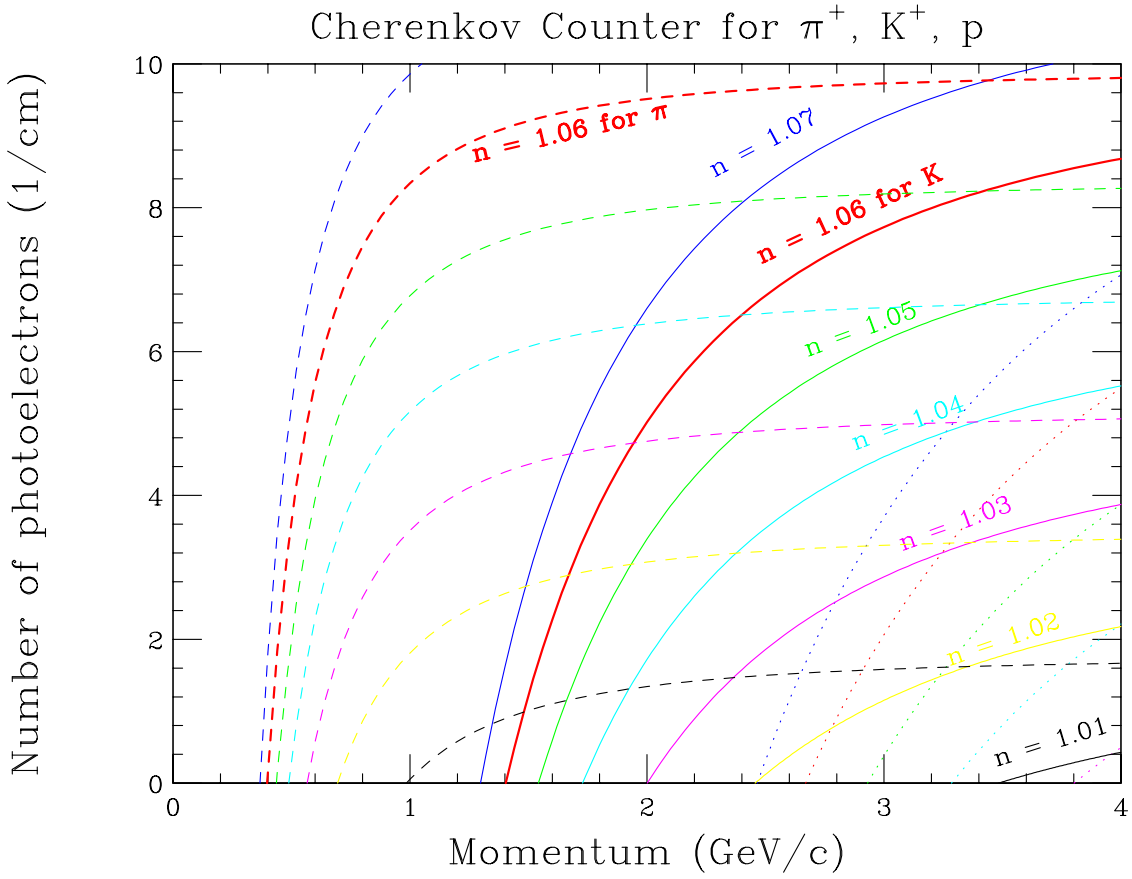

Figure 6–1: The refraction index dependence of the number of photo electrons from the Čerenkov counter. The number of photo electrons per path length in the radiator is calculated assuming; the efficiency of the light correction and quantum efficiency of PMT are 90% and 27%, respectively. The calculation was carried out for π^+, K^+ and p. For our energy region of interest, $n = 1.06$ gives good result.

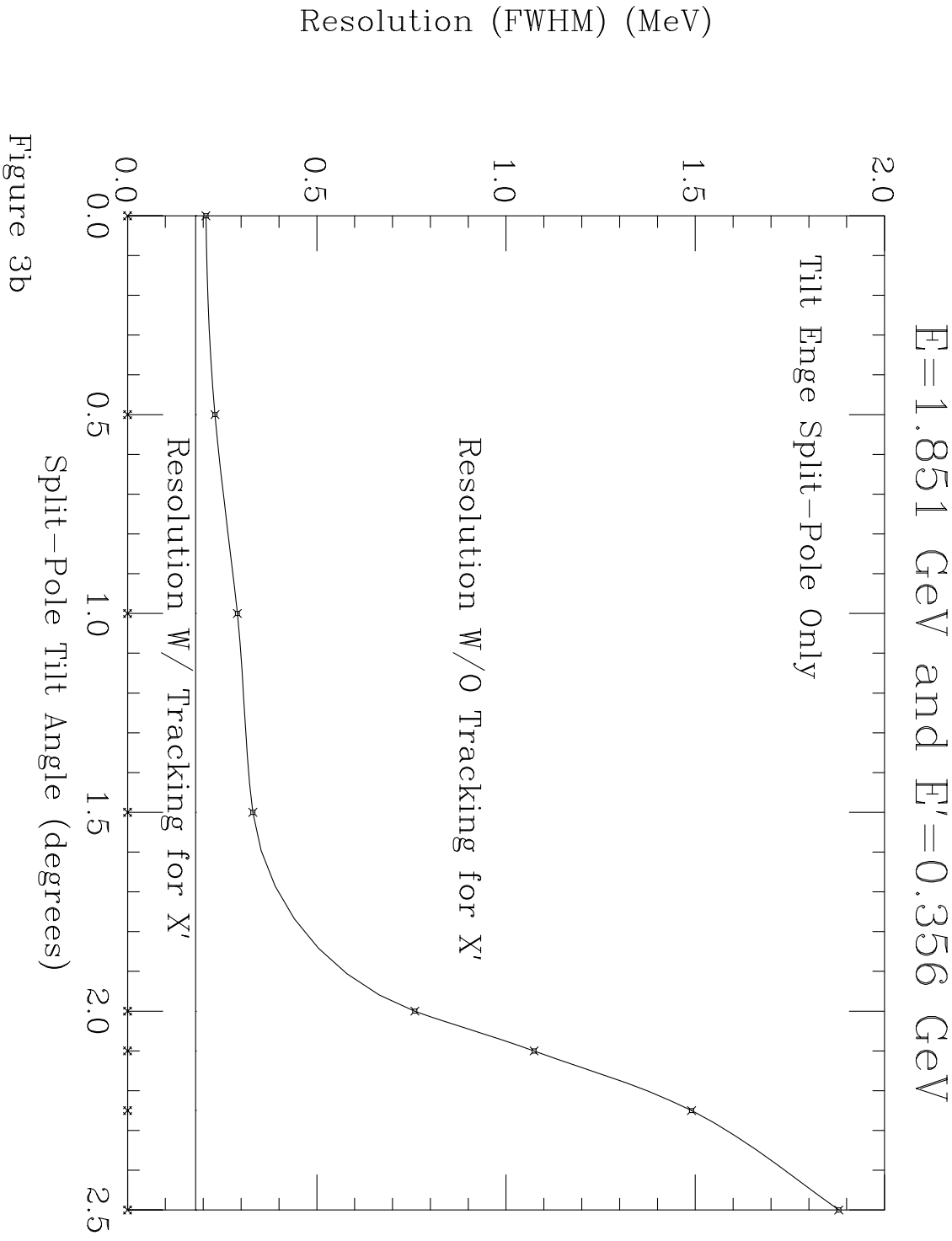

Figure 3b

Figure 7–1: The split-pole tilt angle dependence of the Enge resolution. Without tracking for x dispersion (x'), the resulution deteriorates for larger tilting angle. With tracking, we can give correction with x' information, and thus it is important to measure not only x but also x' at the exit of the Enge magnet.

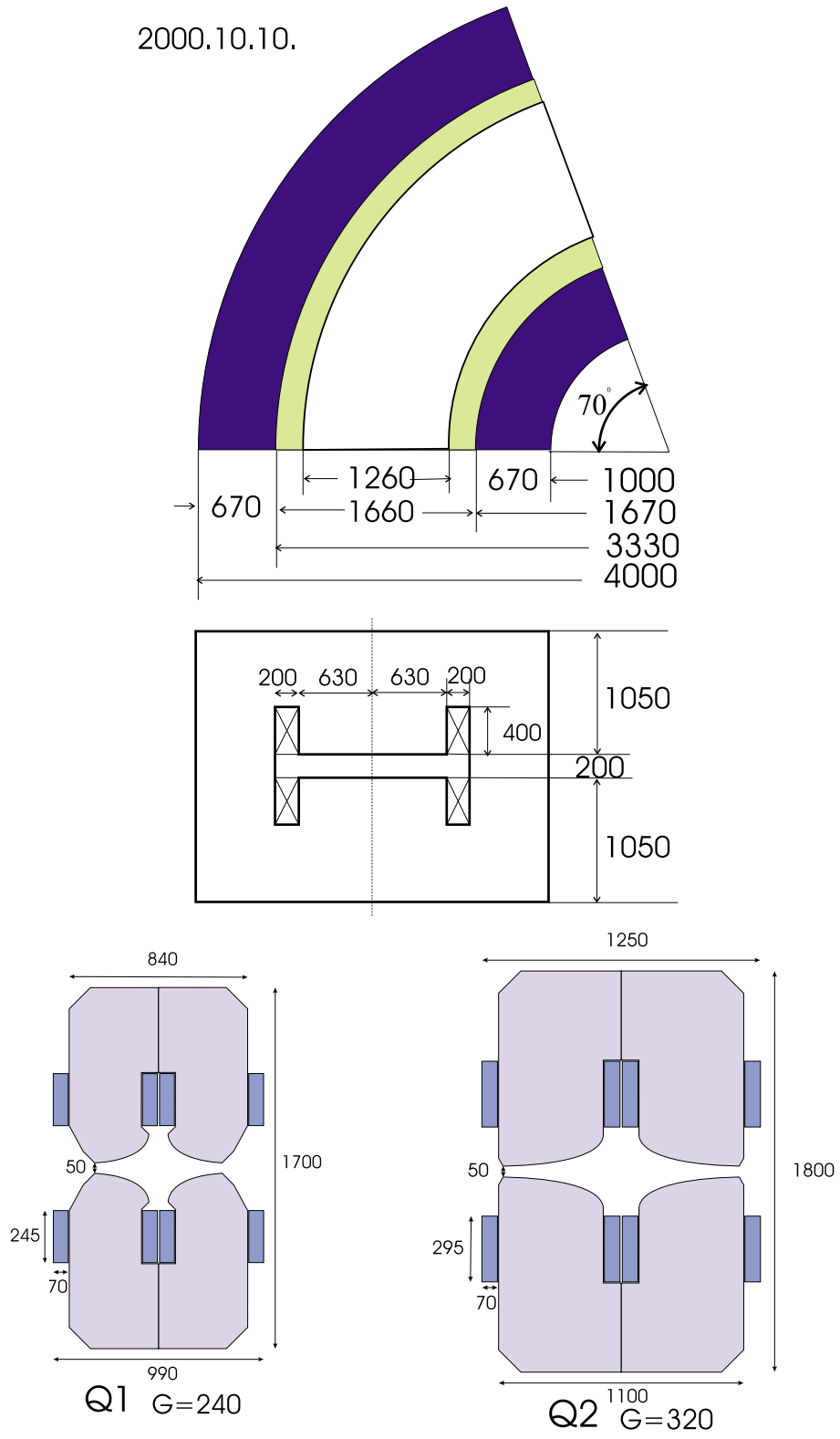

Figure 8–1: The geometrical sizes of the HKS components. The HKS consists of two quadrupole magnets (Q1 and Q2) and one dipole magnet.

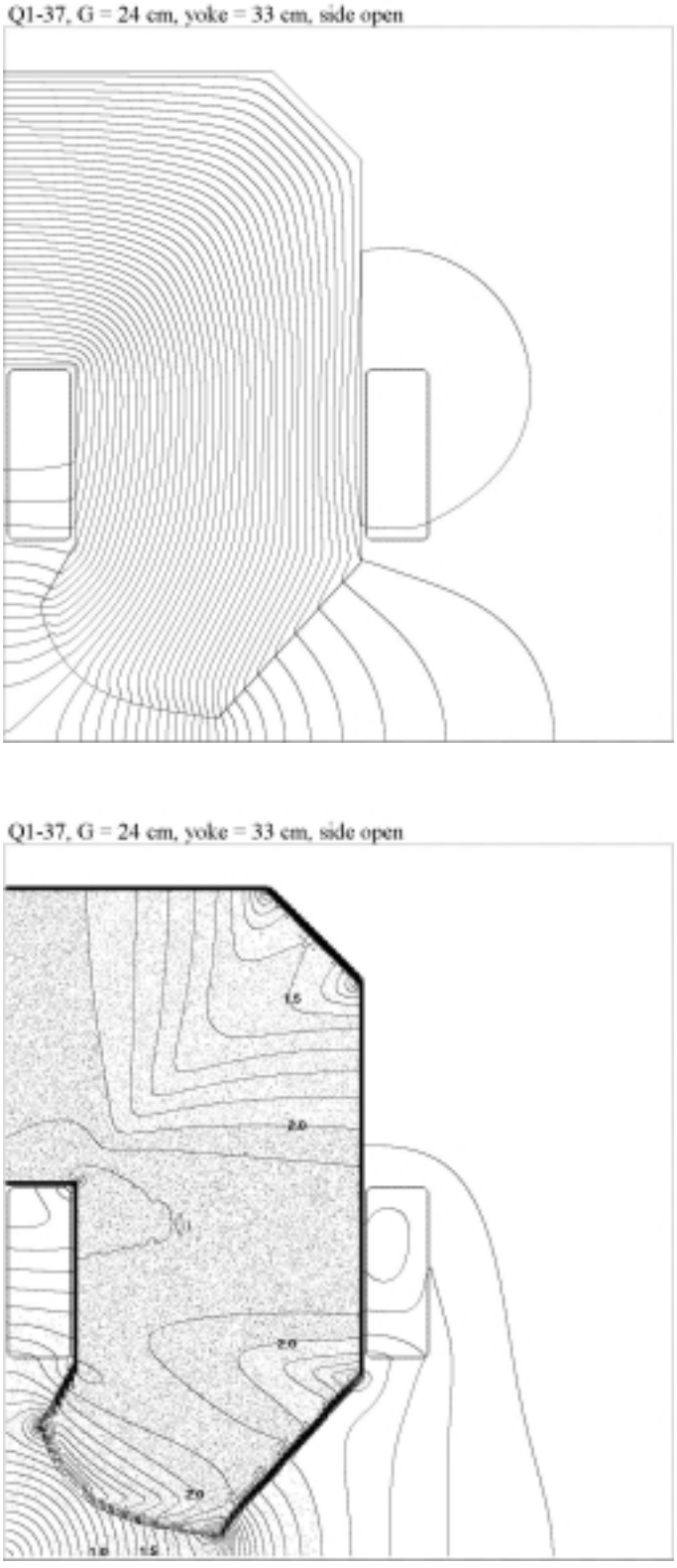

Figure 8–2: The result of the 2 dimensional field calculation for the Q1 magnet. The field gradient and the field contour plots are given.

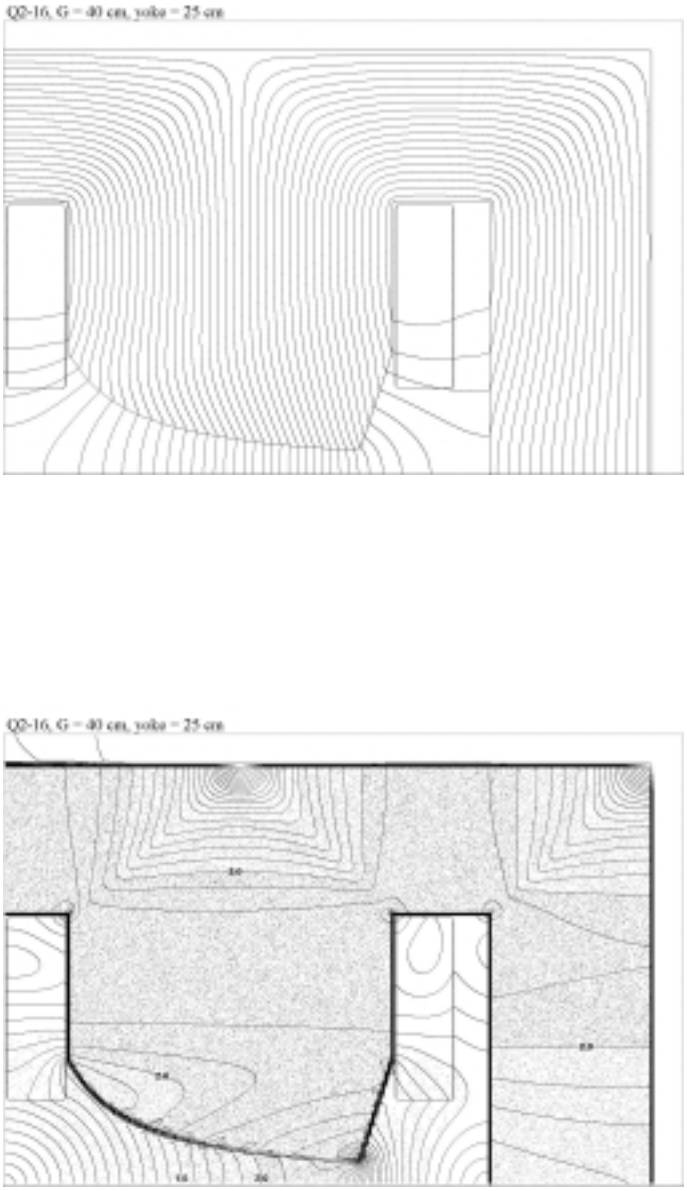

Figure 8–3: The result of the 2 dimensional field calculation for the Q2 magnet. The field gradient and the field contour plots are given.

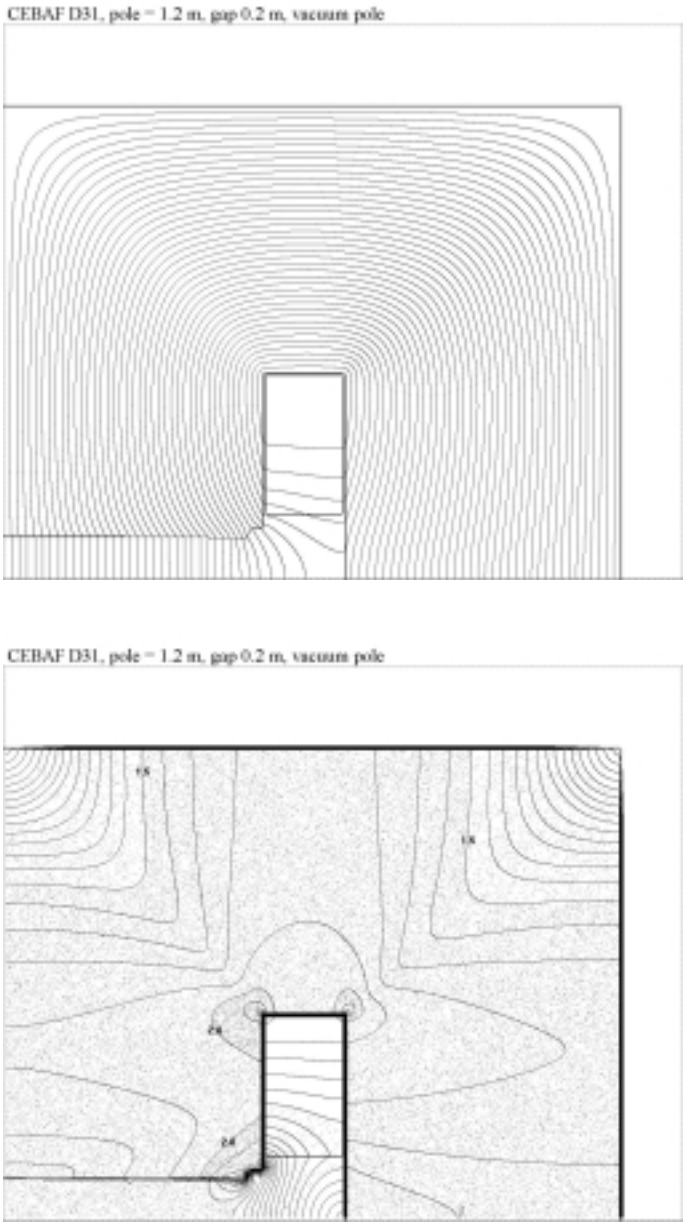

Figure 8–4: The result of the 2 dimensional field calculation for the dipole magnet. The field gradient and the field contour plots are given.

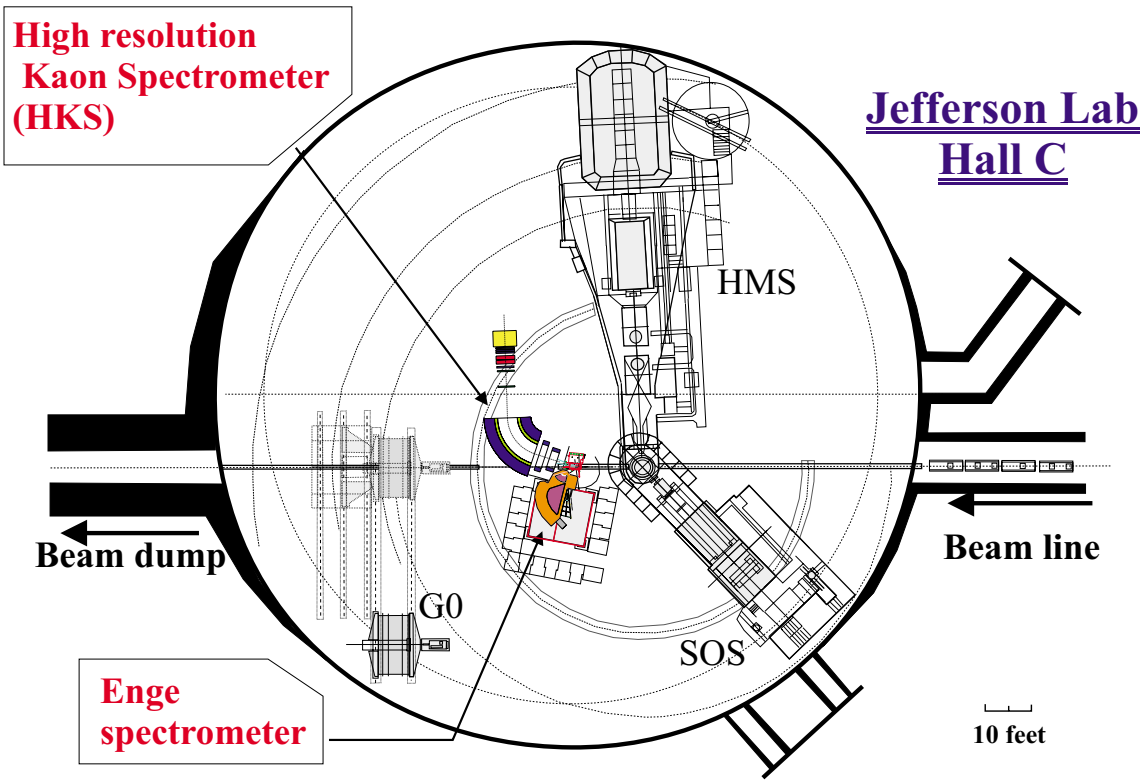

Figure 9–1: General setup for the case that the HKS is placed in Hall C.

References

[1] C. Hyde-Wright *et al.*, Proc. of the 1985 CEBAF Workshop.

14 Appendix

14.1 Design principle of the kaon spectrometer

Why QQD spectrometer? — a design principle —

The basic idea of a quadrupole-quadrupole-dipole (QQD) spectrometer can be seen from a quadrupole doublet of a beam transport system. Let the sign of the first quadrupole magnet be vertically focusing and horizontally defocusing and that of the second magnet opposite to the first. By adjusting the field strengths of the two magnets, we can easily achieve the horizontal and vertical focusing simultaneously for almost any free space lengths before and behind the doublet because there are two degrees of freedom. Even if a horizontally bending dipole magnet is added after the doublet, we will still be able to retain the focusing property. Because a dipole magnet brings about a focusing effect in the bending plane, the strength of the second quadrupole magnet can be decreased as we increase the bending angle. If the rotation angles of iron boundary at the entrance and exit are zero, the strength of the second quadrupole magnet vanishes for the bending angle of about 130 degrees. By removing the second quadrupole, we obtain a quadrupole-dipole (QD) spectrometer.

If we change the bending angle of a QD spectrometer according to the required resolution, we will have to tune the rotation angles at the entrance and exit of the dipole magnet so as to compensate the change of the horizontal focusing strength of the dipole magnet. These angles and focal length will no longer be adjustable once the spectrometer is designed. If there is a need to correct the discrepancy between the designed and the constructed spectrometer, we have to tune the strength of the quadruple magnet so as to move the measured focal point to the designed position. By saving a quadrupole magnet, we will lose the flexibility. Because the vertical focusing strength of the quadrupole magnet of a QD spectrometer is smaller than that of a QQD one, the achievable solid angle of the former is smaller than that of the latter.

The experimental design of the hypernuclear physics experiment by the (e,e'K) reaction require the kaon spectrometer to detect kaons which emerge at 4 degrees from the beam direction and are bent 15 degrees by the splitter magnet. The horizontal spreading due to the finite momentum bite of the kaons will cause a serious difficulty to the spectrometer. The horizontal spread of kaons in the dipole magnet becomes very large unless we bend back the spread. A QD spectrometer will suffer from the necessity of a huge pole width of the dipole magnet because a QD spectrometer cannot bend the kaons back to the direction without the splitter. On the other hand, a QQD spectrometer can bend the kaons so that they enter the dipole magnet parallel to the central ray utilizing the additional degree of freedom.

The first quadrupole magnet focuses vertically and defocuses horizontally. The vertical focusing is so strong that it has to be compensated by the second quadrupole magnet. After bent back parallel to the median plane of the dipole magnet, particles can enter a relatively small gap of the dipole magnet. The strong vertical focusing plays an important role in gaining a large vertical acceptance. Since the first quadrupole magnet defocus the rays horizontally, the horizontal focal point is moved downstream, increasing the dispersion. Thus, the strong vertical focusing an the horizontal defocusing at the first quadrupole magnet is essential for large solid angle and high resolution.

The advantage of a QQD spectrometer over a QD one can be summarized as

1. larger solid angle
2. smaller loss of the momentum bite and solid angle by the insertion of the splitter
3. no need of rotation angles at the entrance and the exit of the dipole magnet
4. adjustable focal length

14.2 Optics study

In this appendix, the optics study of the HKS will be explained.

14.2.1 TRANSPORT

The TRANSPORT calculation was performed to optimize magnetic field for the proposed configuration of the HKS magnets. The calculation took into account the second order effect and the fringe field effect with the Graphical Transport which was modified at PSI.

The fringing field of the quadrupole is given by Kato as follows:

$$B_x = B \times [yh - \frac{y^3 + 3x^2 y}{12G^2}\frac{d^2h}{ds^2}], \quad (1)$$

$$B_y = B \times [xh - \frac{x^3 + 3xy^2}{12G^2}\frac{d^2h}{ds^2}], \quad (2)$$

$$B_z = \frac{Bxy}{G}\frac{dh}{ds}, \quad (3)$$

$$h(s) = 1/(1 + \exp C_0 + C_1 s + C_2 s^2 + C_3 s^3), \quad (4)$$

where s = z/G, and C_{0-3} = -0.9842, 6.3375, -3.5134, 0.9895.

The PSI TRANSPORT requires following three parameters to calculate Q-fringing field:

$$I_1 = k_0^{-1} \int_{z_a}^{z_b} \int_{z_a}^{z} k(z) dz dz - \frac{1}{2} z_b^2, \quad (5)$$

$$I_2 = k_0^{-1} \int_{z_a}^{z_b} z[\int_{z_a}^{z} k(z) dz] dz - \frac{1}{3} z_b^3, \quad (6)$$

$$I_3 = k_0^{-2} \int_{z_a}^{z_b} [\int_{z_a}^{z} k(z) dz]^2 dz - \frac{1}{3} z_b^3. \quad (7)$$

Comparing the paper [1] and Kato's equations (Eq. 1-4), we have:

$$k(z - z^*) = B \cdot h(-s), \quad (8)$$

$$k_0(z_b - z^*) = \int_{z_a}^{z} k(z) dz, \quad (9)$$

$$k_0 = B. \quad (10)$$

Unit of the length was taken as the gap distance (G). The parameter z^* is so called the ideal field boundary and it was defined $z^* = 0$ in z coordinate. The region of the integral was set as $z_a = -2, z_b = +2$ to cover completely from the field free region to the main field. The shape of the fringe field is shown in figure 14–1.

The result was:

$$I1 = 0.0902, \quad (11)$$

$$I2 = -0.00765, \quad (12)$$

$$I3 = 0.0256. \quad (13)$$

They are little different from the PSI default values. The optimization of the magnets were carried out by two ways ; 1) minimize R_{12} and R_{34} and 2) minimize R_{12} and R_{44}. The first condition tries to focus vertically as well as horizontally, and the second one does to make vertically parallel beam.

Geometrical position of the magnets were already shown in previous section. The distance between Q1 and the splitter magnet was set to be 40 cm and the focal plane was placed 200 cm

after the dipole magnet. Incoming beam was p =1.2 GeV kaon with a momentum bite of $\Delta p/p$ = 0.1 and horizontal and vertical dispersions were respectively $X' \leq 100$ and $Y' \leq 75$ mrad. The envelopes of the transported beam through HKS were shown in figure 14–2,14–3. The results of the transport calculation is summarized in table 14–1

Table 14–1: Summary of the HKS TRANSPORT calculation

minimized term	Q1 (kG)	Q2 (kG)	R16	R22	R44
R12, R34	-8.48	6.63	3.88	-1.45	-0.124
R12, R44	-8.00	6.49	3.88	-1.41	0

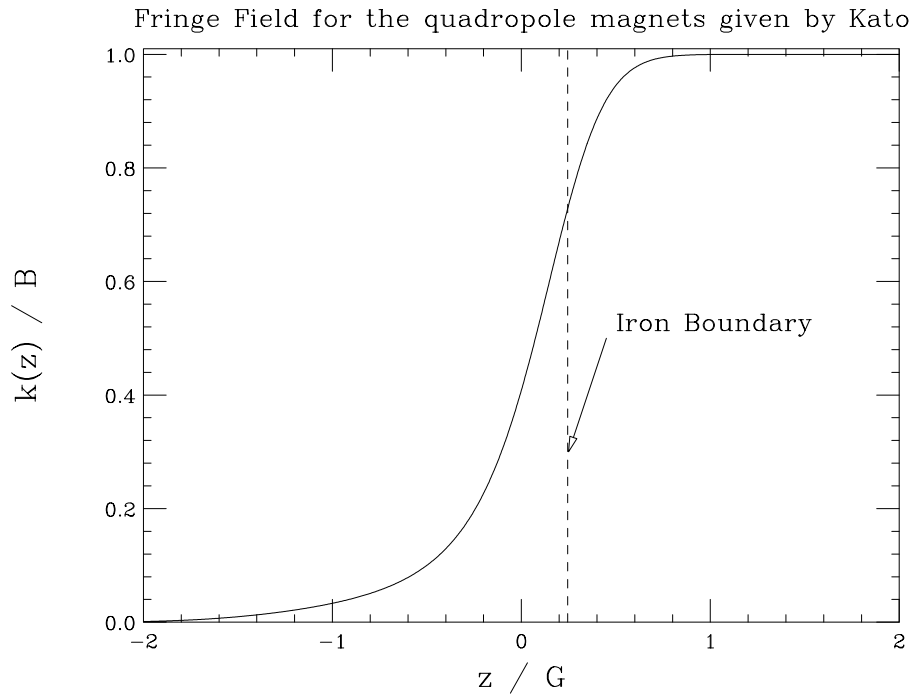

Figure 14–1: Quadrupole fringe field given by Kato. The field strength and unit of the length are normalized to be dimension less values. The ideal field boundary (z^*) was set to be zero.

14.2.2 TURTLE

Results of the TRANSPORT calculation were fed to TURTLE (also with the PSI patch). The input file for the TURTLE calculation was given in list 1. The beam profiles (x-y image, x-x', and y-y') were checked after passing each magnet. The beam images at the entrance of the magnet were also monitored for the kaons stopped in the magnet to know which part of the beam hit the magnet.

The result shows that 43% of incoming non-decay kaons passed through HKS for the minimized $R_{12} = R_{34} = 0$ condition. For $R_{12} = R_{44} = 0$ condition, 44% of kaons passed. These numbers correspond to HKS acceptance of 23.5 and 24.1 msr. Taking kaon decay into account, the survival rates of kaon for $R_{12} = R_{34} = 0$ and $R_{12} = R_{44} = 0$ conditions at 9.73 m from the target (entrance to GC) were 0.146 and 0.151. The survival rate of 15% is consistent with 44% times $\exp(-9.7/\gamma\beta c\tau)$ for 1.2 GeV kaon ($c\tau = 3.713m, \gamma = 2.63$). Results are summarized in table 14–2 and beam profiles with kaon decay are shown in figures 14–4-14–13.

Table 14–2: Summary of HKS turtle calculation

minimized term	stopped in Q1	stopped in Q2	stopped in Dipole	Survive (w/o decay)	Survive (w/ decay)
R12, R34	0.480	0.093	0.000	0.426	0.146
R12, R44	0.472	0.091	0.001	0.436	0.151

In order to know the correlation between the initial beam dispersion and the accepted beam momentum, figures 14–14 and 14–15 are prepared. Top figures shows the initial x'-p and y'-p correlation for non-decay kaons which stopped somewhere in HKS and bottom ones are for survived kaons. Initial momentum bite was enlarged to 25% in the calculation to see the correlation in wider momentum region.

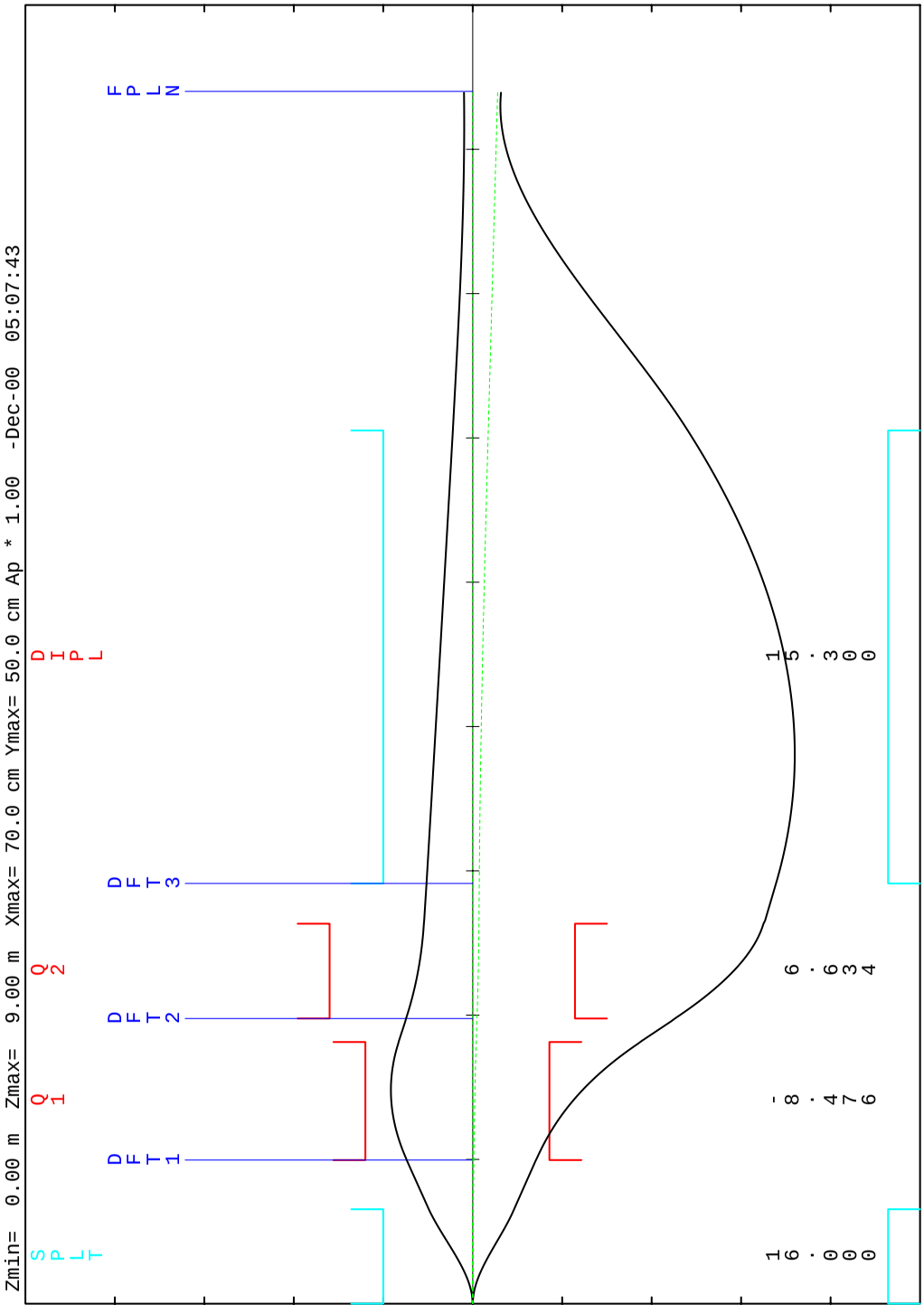

Figure 14–2: The beam envelope for $R_{12} = R_{34} = 0$ fit. Both of x and y dispersions were tried to be minimized on the focal plane.

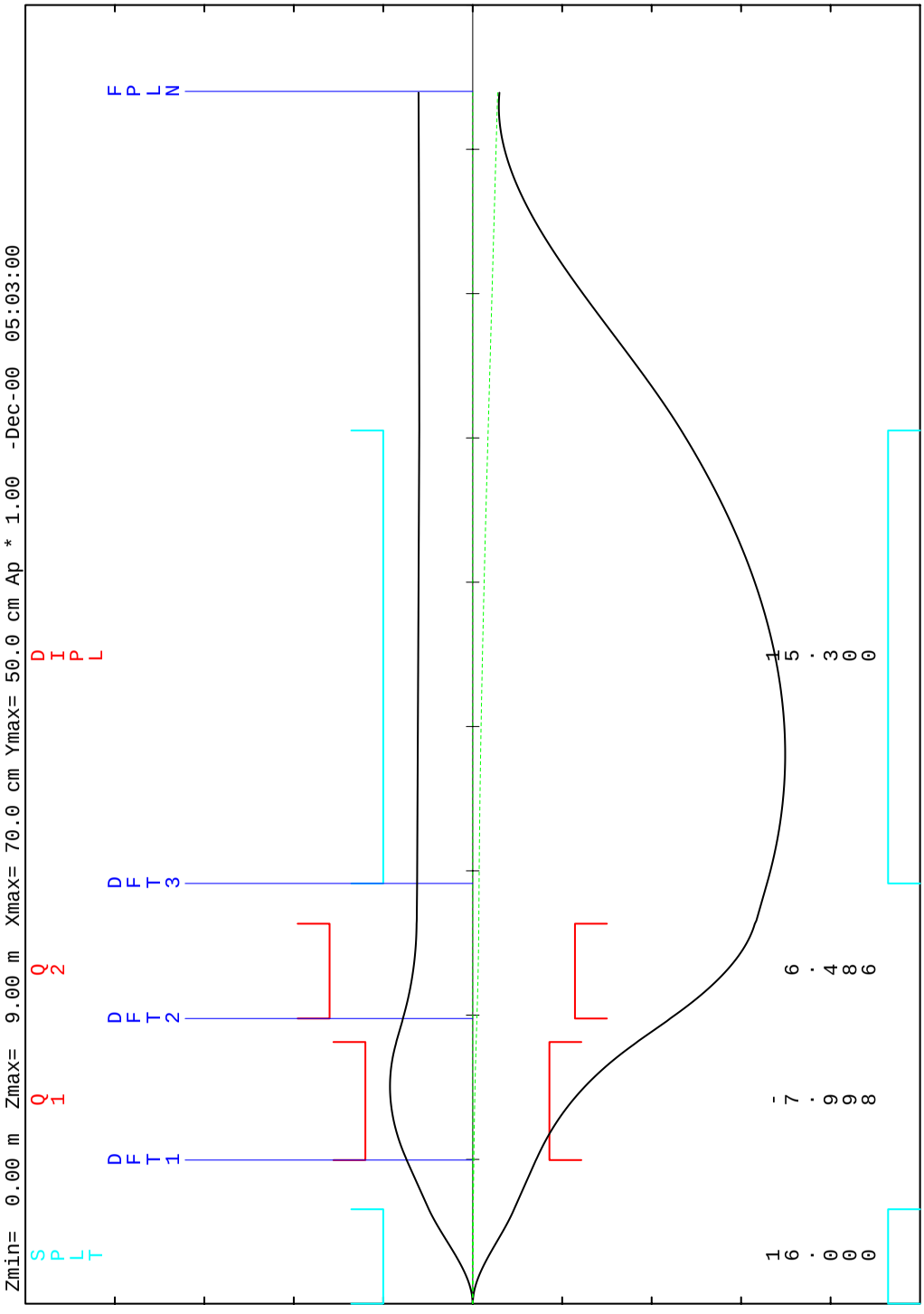

Figure 14–3: The beam envelope for $R_{12} = R_{44} = 0$ fit. X dispersion was tried to be minimized. For y direction, magnets were tuned to make parallel beam.

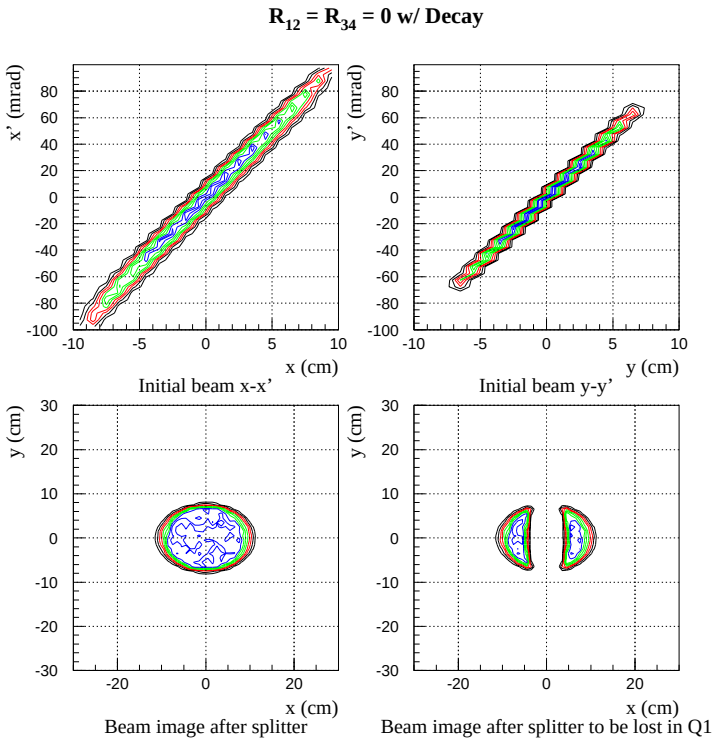

Figure 14–4: The beam profile of the initial beam for $R_{12} = R_{44} = 0$. Left bottom figure shows the beam image after the splitter magnet and right bottom one shows the image of the particles after the splitter which will be lost in the Q1.

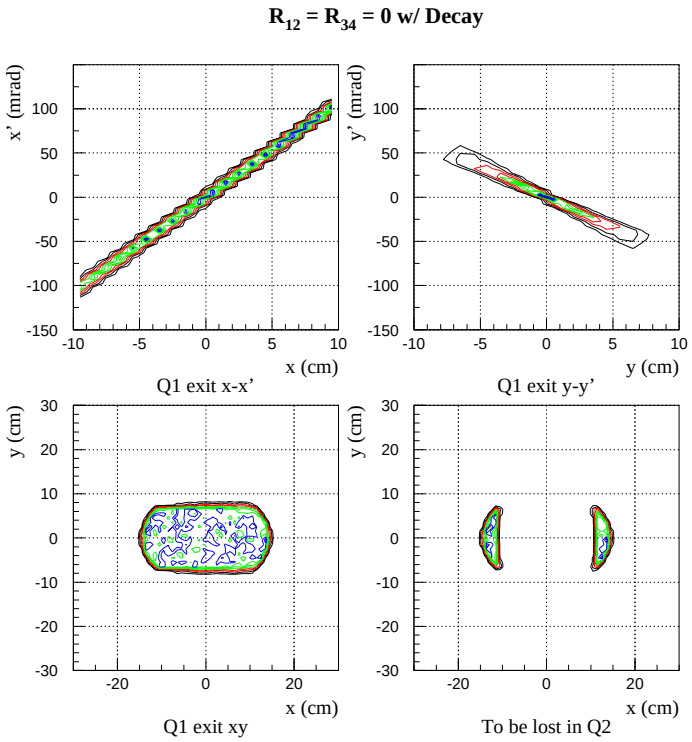

Figure 14–5: The beam profile at the exit of the Q1 magnet for $R_{12} = R_{34} = 0$. Right bottom one shows the image of the particles after Q1 which will be lost in Q2. Unit for x and y is cm and it for x' and y' is mrad.

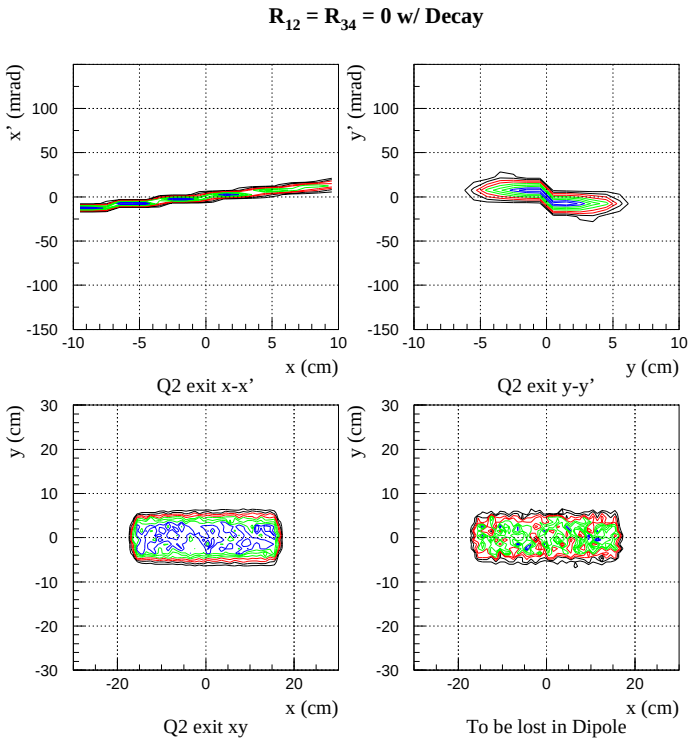

Figure 14–6: The beam profile at the exit of the Q2 magnet for $R_{12} = R_{34} = 0$.

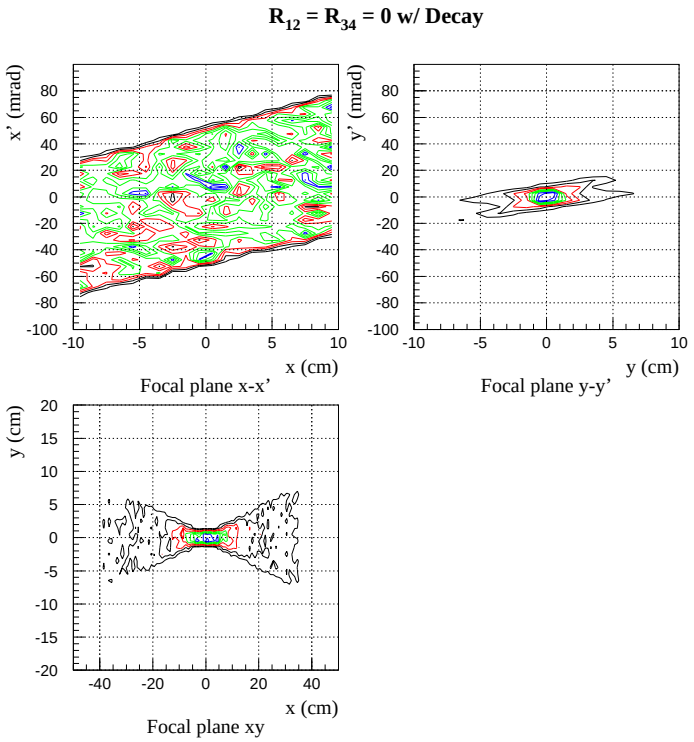

Figure 14–7: The beam profile on the focal plane for $R_{12} = R_{34} = 0$.

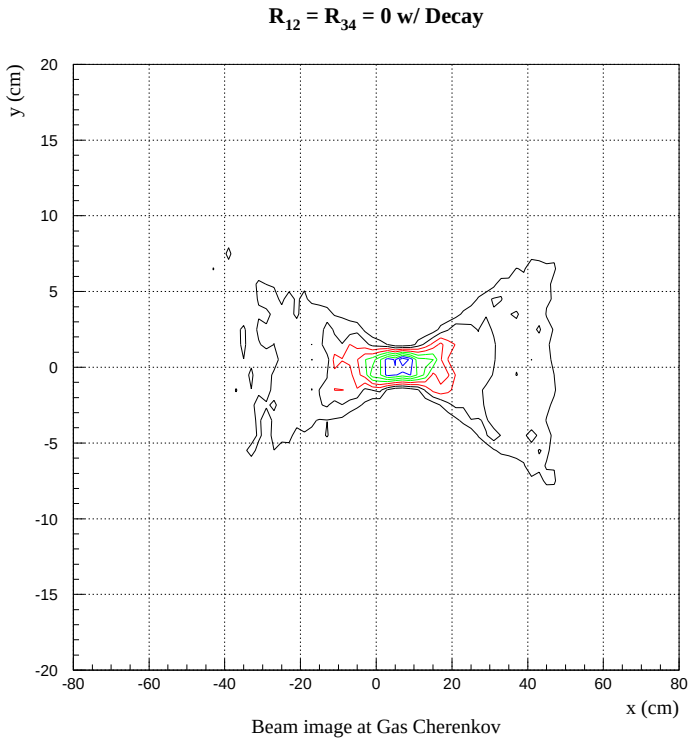

Figure 14–8: The beam profile just before Gas Čerenkov for $R_{12} = R_{34} = 0$.

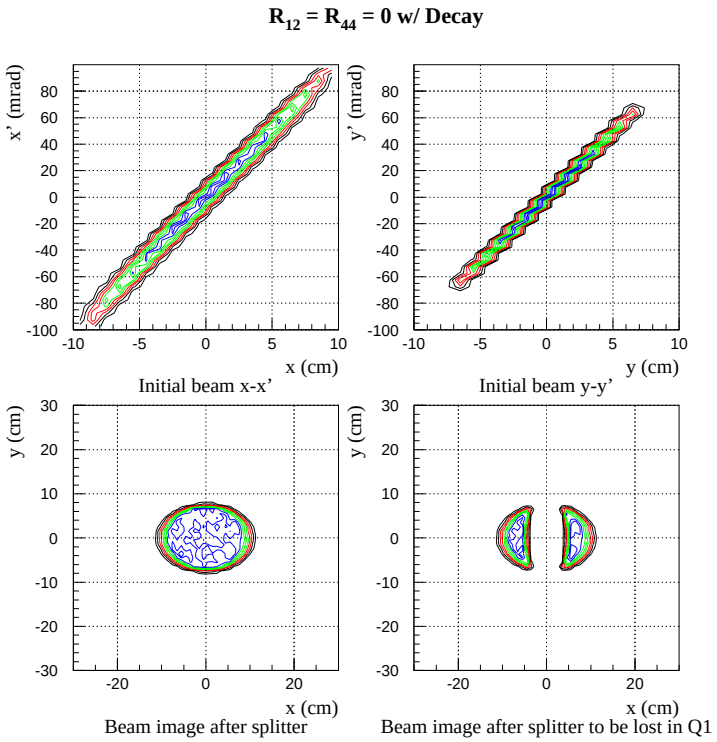

Figure 14–9: The beam profile of the initial beam for $R_{12} = R_{44} = 0$. Left bottom figure shows the beam image after the splitter magnet and right bottom one shows the image of the particles after the splitter which will be lost in the Q1.

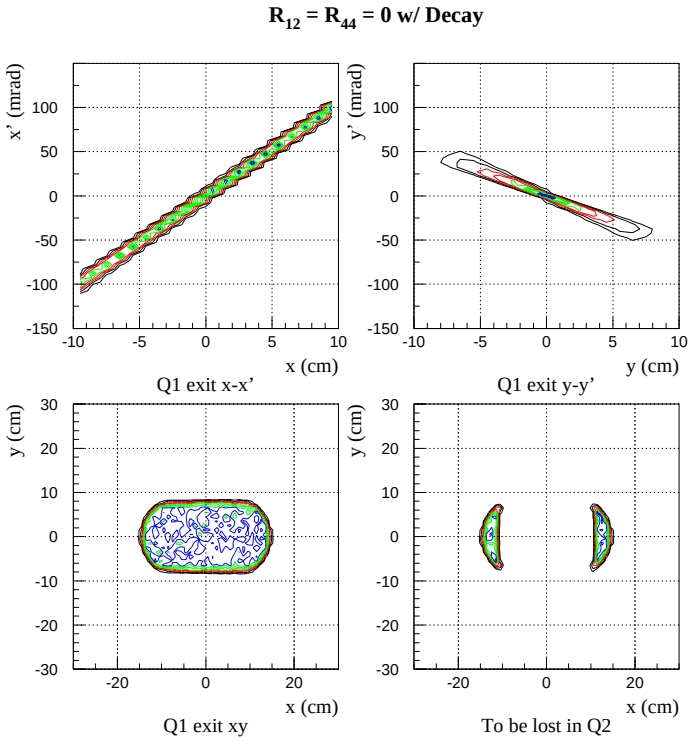

Figure 14–10: The beam profile at the exit of the Q1 magnet for $R_{12} = R_{44} = 0$. Right bottom one shows the image of the particles after Q1 which will be lost in Q2.

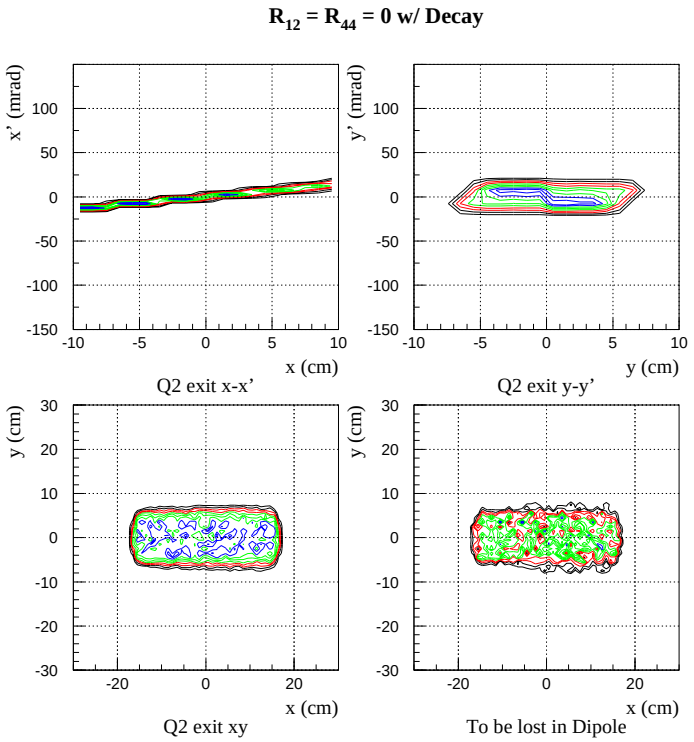

Figure 14–11: The beam profile at the exit of the Q2 magnet for $R_{12} = R_{44} = 0$.

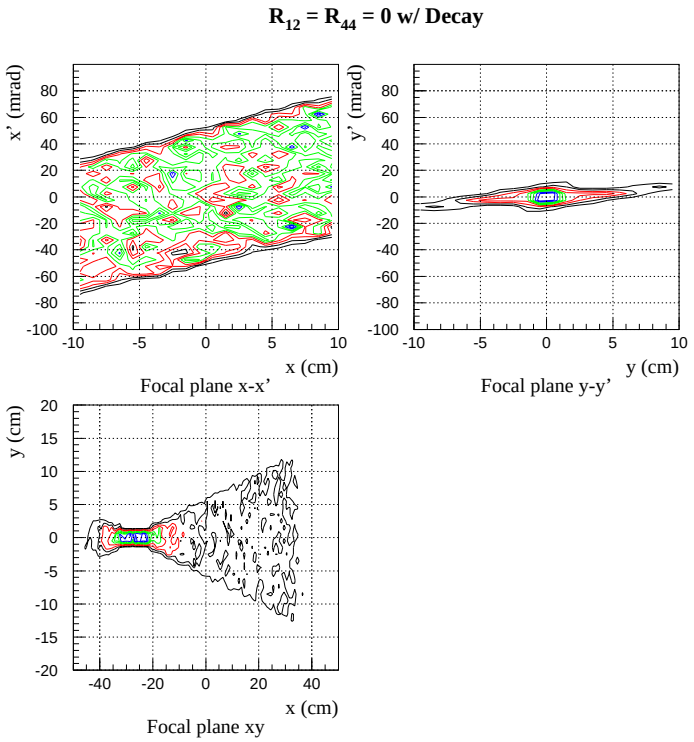

Figure 14–12: The beam profile on the focal plane for $R_{12} = R_{44} = 0$.

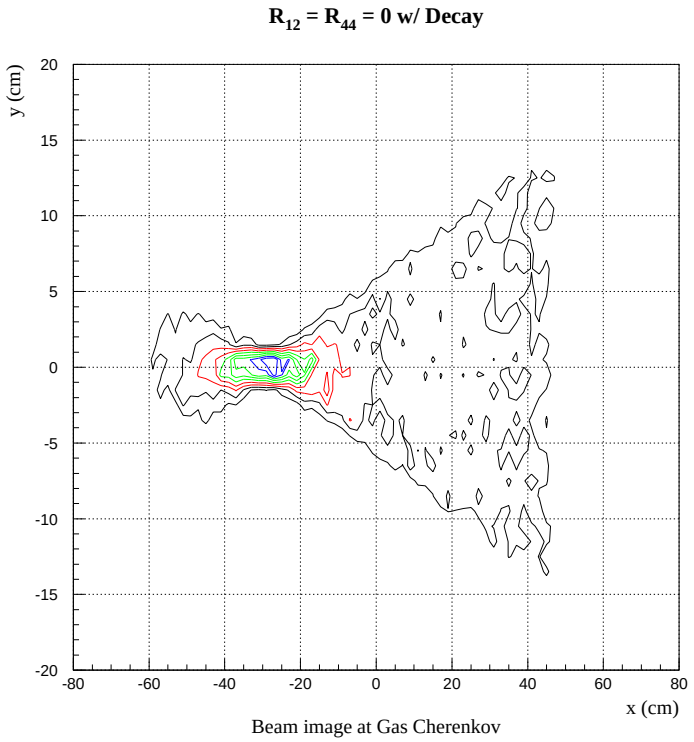

Figure 14–13: The beam profile just before the Gas Čerenkov for $R_{12} = R_{44} = 0$.

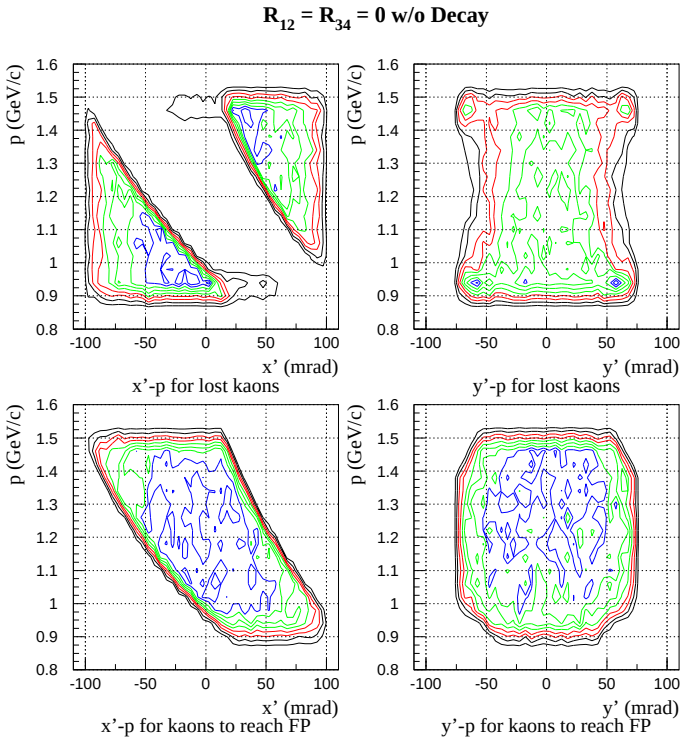

Figure 14–14: The correlation between the initial beam dispersion and momentum for lost and survived kaons in the case of $R_{12} = R_{34} = 0$.

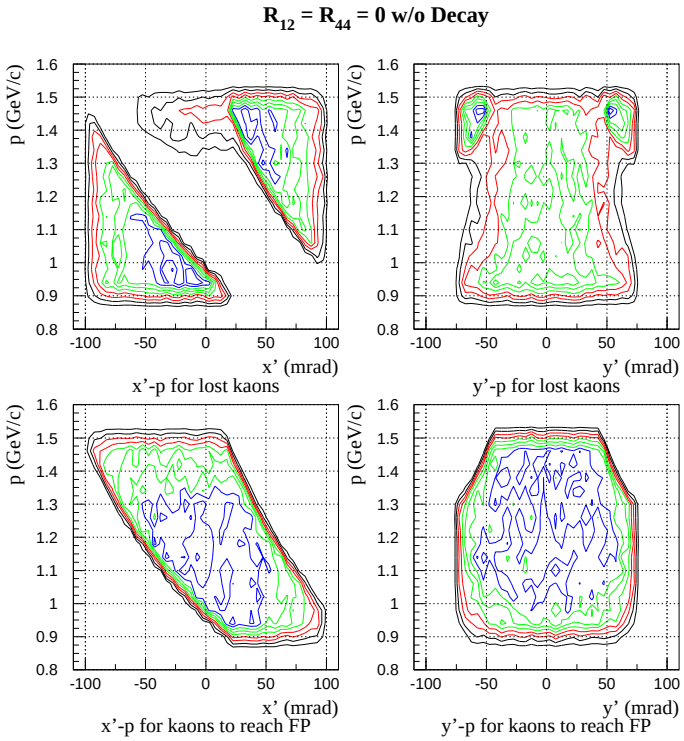

Figure 14–15: The correlation between the initial beam dispersion and momentum for lost and survived kaons in the case of $R_{12} = R_{44} = 0$.

List 1 Turtle input file for $R_{12} = R_{34} = 0$

```
/HKS 8 Dec 2000, R12=R34=0/
100000
16. 190. 2. 100. /FILE/ ;
16. 20. 0. /Flat BEAM/ ;
1. 0.01 100. 0.01 75. 0. 10.0 1.2 /KAON/ ;
13.0 10.0;
17. 'SEC' ;
16. 3.0 966.0998 /MASS of KAON/;
60.0 0.49367 0.10566 0.0 12.386 /DCAY/ ;

16. 7. 0.167 /K1 Linear/ ;
16. 8. 3.8 /K2 Linear/ ;

51. 1. -30. 30. 1.;
52.-4 3. -30. 30. 1. /!SP/;
51. 2.0 -110.0 110.0 5.0 ;
52.-5 11.0 0.8 1.6 0.04 /xp/ ;
51. 4.0 -110.0 110.0 5.0 ;
52.-5 11.0 0.8 1.6 0.04 /yp/ ;
51. 2.0 -110.0 110.0 5.0 ;
52.5 11.0 0.8 1.6 0.04 /xpok/ ;
51. 4.0 -110.0 110.0 5.0 ;
52.5 11.0 0.8 1.6 0.04 /ypok/ ;

16.0 4.0 20. /W/ ;
16.0 5.0 10. /G/;
2.0 0.0 /ROT1/ ;
4. 0.6545 16.0 0.0 /SPLT/ ;
2. 8.0 /ROT2/ ;
3. 0.341 'DFT1' ;

51. 1.0 -10. 10. 1. ;
52.4 2.0 -100. 100. 5. /SPX/;
51. 3. -10. 10. 1. ;
52.4 4. -100. 100. 5. /SPY/;
51. 1. -30. 30. 1. ;
52.4 3. -30. 30. 1. /SPXY/;
53.4;

51. 1. -30. 30. 1. ;
52.-3 3. -30. 30. 1. /!Q1/;

16. 25. 0.0902 /I1/ ;
16. 26. -0.0765 /I2/ ;
16. 27. 0.0256 /I3/ ;
2. 1000. /PSI Special Q fringe/ ;
5.01 0.818 -8.476 12. /Q1/ ;
2. 1000. /Q fringe/ ;
3. 0.163 'DFT2' ;

51. 1.0 -10. 10. 1. ;
52.3 2.0 -150. 150. 5. /Q1X/;
51. 3. -10. 10. 1. ;
52.3 4. -150. 150. 5. /Q1Y/;
51. 1. -30. 30. 1. ;
52.3 3. -30. 30. 1. /Q1XY/;
53.3;
51. 1. -30. 30. 1. ;
52.-2 3. -30. 30. 1. /!Q2/;

2. 1000. /Q Fringe/ ;
5.01 0.657 6.634 16.0 /Q2/ ;
2. 1000. /Q fringe/ ;
3. 0.279 'DFT3' ;
51. 1.0 -10. 10. 1.;
52.2 2.0 -150. 150. 5. /Q2X/;
51. 3. -10. 10. 1. ;
52.2 4. -150. 150. 15. /Q2Y/;
51. 1. -30. 30. 1. ;
52.2 3. -30. 30. 1. /Q2XY/;

53.2;

51. 1. -30. 30. 1. ;
52.-1 3. -30 30. 1. /!FC/;

16.0 5.0 10. 'G' ;
16.0 4.0 60. 'W' ;
16. 7. 0.45 /K1/ ;
16. 8. 2.8 /K2/ ;
2. 0.0 'ROT3' ;
4. 3.139 15.3 0.0 /DIPL/ ;
2. 0.0 'ROT4' ;
-4. 3.0543 16.0 0.0 /DIPL/ ;
-4. 3.4906 16.0 0.0 /DIPL/ ;
-4. 3.927 16.0 0.0 /DIPL/ ;
3. 2.307 'FPLN' ;
51. 1. -10.0 10.0 1.0 ;
52.1 2. -100. 100. 5.  /FCX/;
51. 3. -10. 10.0 1. ;
52.1 4. -100. 100. 5. /FCY/;
51. 1. -50. 50. 1. ;
52.1 3. -20. 20. 1. /FCXY/;

53.1;

3. 1.37 /D/ ;

51. 1. -80. 80. 2.0 ;
52.5 3. -20. 20. 1. /GCXY/ ;
53.5 ;

SENTINEL
SENTINEL
```

References

[1] H. Matsuda and H. Wollnik, *Nucl. Inst. and Meth.* **103** (1972) 117.

14.3 Monte-Carlo simulation

Momentum/Angular resolution and solid angle of HKS are estimated with a Monte-Carlo simulation code. Magnet configurations and field settings are from Kato's design. In the simulation, chamber configuration is similar to SOS ones ($xx'uu'vv'$, $\pm 60°$). Figure 14–16 shows particle trajectories in the horizontal plane (θ = 0, $\pm$75 mr, p = 1.08, 1.20, 1.32 GeV/c). In this figure two chambers (first two detectors after dipole) are placed at $z = 235 \pm 50$cm; z is measured from dipole exit.

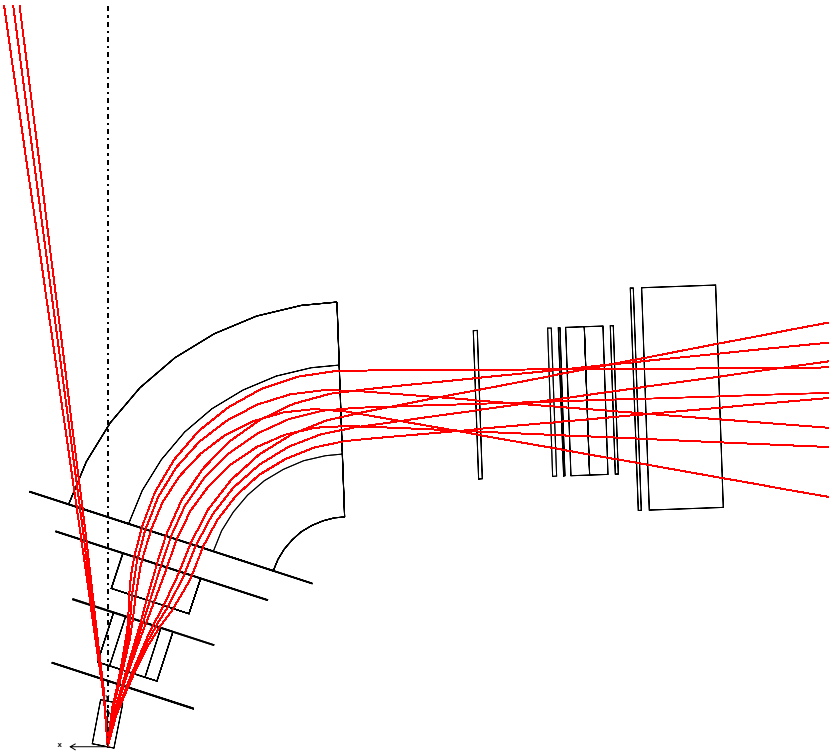

Figure 14–16: Particle trajectories in the horizontal plane (θ = 0, $\pm$75 mr, p = 1.08, 1.20, 1.32 GeV/c). The dotted line shows the photon line, and solid lines show deflected beam (E=1.845 GeV, $\pm$10%)

14.3.1 Chamber position

Spacing between two chambers (L) is determined by balancing two factors, chamber resolution and multiple scattering. Angular resolution ($\Delta\theta$) due to chamber position resolution (σ) is

$$\Delta\theta \sim \sqrt{2}\sigma/L.$$

Particle deflection angle due to multiple scattering is,

$$\Delta\theta = \frac{13.6\text{MeV}}{\beta cp} z\sqrt{x/X_0}\,[1 + 0.038\ln(x/X_0)]\,.$$

Assuming σ = 200 μm and $x/X_0 \sim 1\times10^{-3}$, Optimum value for L is $\sim$1 m.

14.3.2 Detector size

Active area of the detectors, listed in Table 5, are determined to make them cover all the particle passed through dipole. Events are generated uniformly within 1.2 GeV/$c \pm 10\%$ and 200 mr(U) $\times$ 150 mr(V). Figure 14–17 shows beam profile at each detector. The square shows the required active area of detectors to cover 1.2 GeV/$c \pm 10\%$.

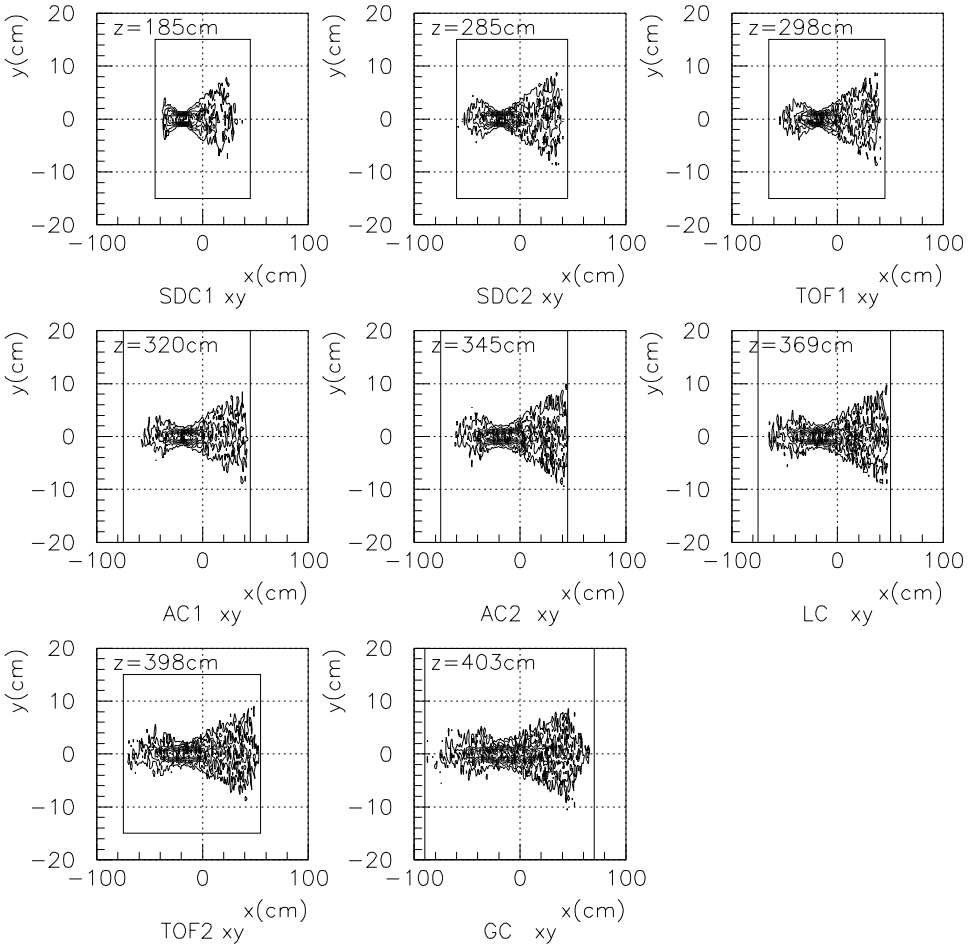

Figure 14–17: Beam profile at each detector.

Table 14–3: Material list and properties included in the simulation

Item	t (cm)	ρ (g/cm^3)	X_0 (g/cm^2)	r.l.
Dipole Exit Window				
Kevlar($C_{14}N_2O_2H_{10}$)	0.02	0.74	55.2	2.68×10^{-4}
Mylar($C_{10}O_4H_8$)	0.01+0.0025	1.39	39.95	4.35×10^{-4}
SDC1				
Mylar	0.012	1.39	39.95	4.18×10^{-4}
Ar gas	5.08	1.78×10^{-3}	19.55	4.63×10^{-4}
SDC1-SDC2 gap				
He gas	100	1.79×10^{-4}	94.32	1.68×10^{-4}
SDC2				
Mylar	0.012	1.39	39.95	4.18×10^{-4}
Ar gas	5.08	1.78×10^{-3}	19.55	4.63×10^{-4}

14.3.3 Momentum and angular resolution

Rays are generated uniformly within 200 mr(U) × 150 mr(V) and 1.2GeV/c ± 10%. Table 14–3 shows materials assumed in the simulation. From target to dipole exit (just before the first chamber) is vacuum. Table 14–4 shows momentum and angular resolution obtained with the simulation.

Even for modest position resolution of 250 μm gives better than momentum resolution of 2×10^{-4} FWHM (σ = 100 keV/c) and angular resolution of 2 mr.

Rough estimation of dP, dU and dV for σ=200 keV are,

$$dP = p \cdot \frac{\sigma}{D} = 1.2\mathrm{GeV}/c \cdot \frac{200\mu\mathrm{m}}{3.6\mathrm{cm}/\%} = 67\mathrm{keV}/c,$$

$$dU = \frac{1}{< u'|u >} \cdot \frac{\sqrt{2}\sigma}{L} = \frac{1}{1.4} \cdot \frac{\sqrt{2} \cdot 200\mu\mathrm{m}}{1\mathrm{m}} = 0.20\mathrm{mr},$$

$$dV = \frac{1}{< v'|v >} \cdot \frac{\sqrt{2}\sigma}{L} = \frac{1}{0.2} \cdot \frac{\sqrt{2} \cdot 200\mu\mathrm{m}}{1\mathrm{m}} = 1.4\mathrm{mr}.$$

These are consistent with the result of the simulation code.

Table 14–4: Momentum and Angular resolution

Description	dP(keV/c)	dU(mr)	dV(mr)
50μm only	20	0.04	0.24
100μm only	33	0.09	0.53
150μm only	46	0.14	0.82
200μm only	59	0.18	1.18
250μm only	72	0.23	1.53
He 1m only	13	0.05	0.18
(Air 1m only)	(48)	(0.21)	(0.72)
DC Ar only	36	0.15	0.52
DC window only	23	0.08	0.30
Dipole window only	33	0.13	0.44
Mul. total	47	0.23	0.77
Mul. + 50μm	50	0.23	0.78
Mul. + 100μm	59	0.25	0.86
Mul. + 150μm	71	0.28	1.14
Mul. + 200μm	83	0.31	1.48
Mul. + 250μm	97	0.36	1.83

14.3.4 Solid angle

HKS is placed at 7° with respect to the 1.2GeV/c 0° ray (18° with respect to the beam line). Rays are generated uniformly within 0° to 15° and from 1.00 GeV/c to 1.35 GeV/c. 14 cm × 14 cm collimator is placed between splitter and Q1. Aperture of Q1 and Q2 is 50 cm × 20 cm and 110 cm × 20 cm, respectively. No decay factor is included in the solid angle.

Figure 14–18 shows beam profile at collimator, Q1 exit, Q2 exit, and dipole entrance. It is clearly seen that the solid angle is limited by mostly Q1 pole. Figure 14–19 shows two dimensional plot for angular acceptance of HKS for each momentum.

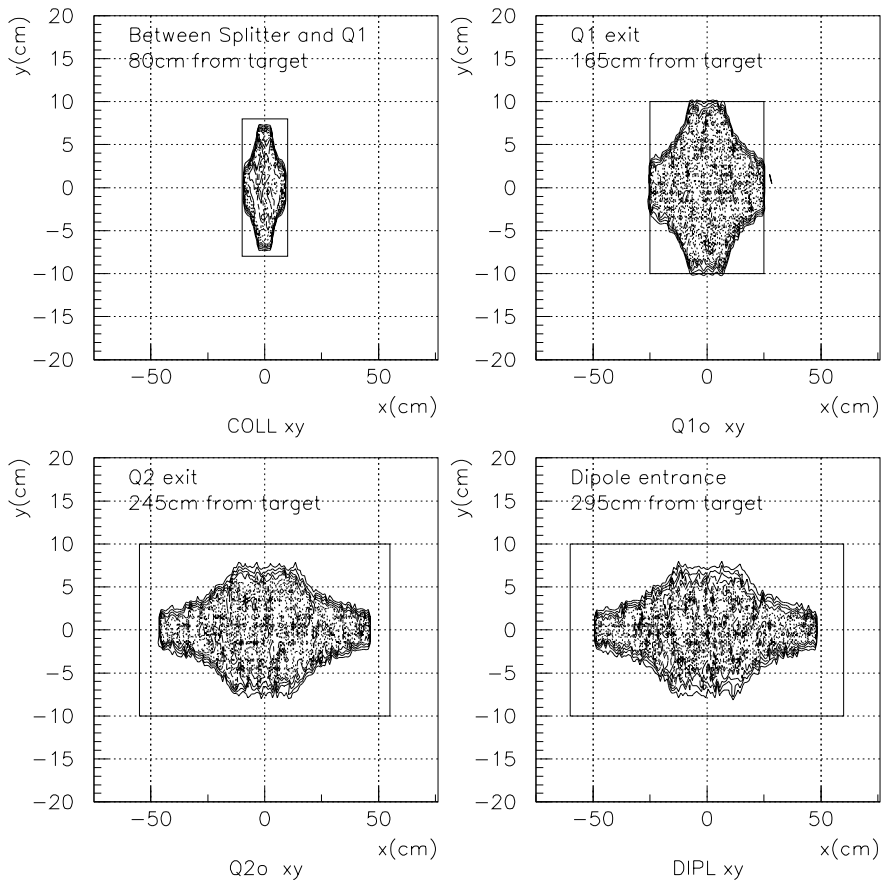

Figure 14–18: Beam profile at collimator, Q1 exit, Q2 exit, and dipole entrance.

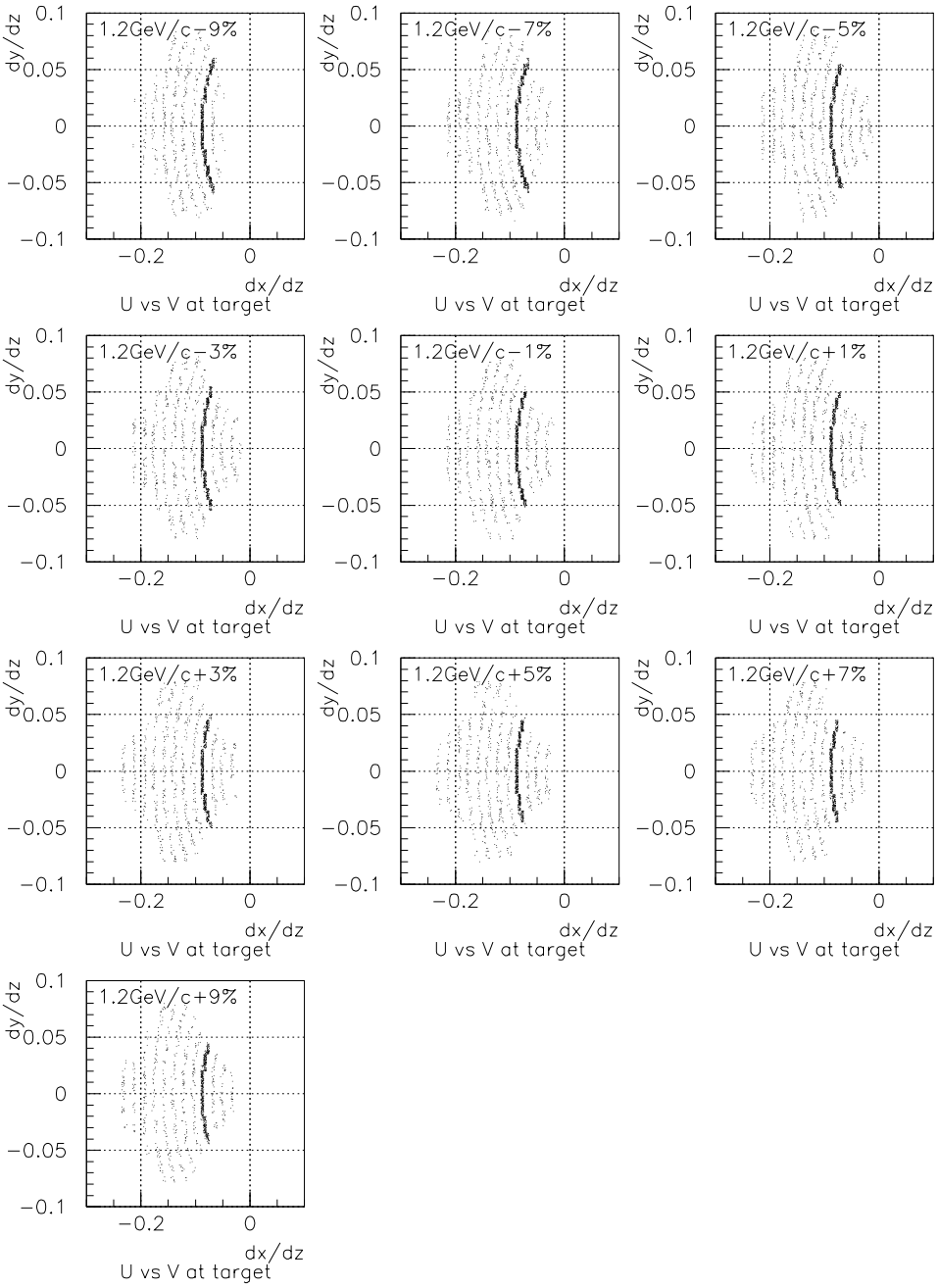

Figure 14–19: Two dimensional plot for angular acceptance of HKS for each momentum. The thick ring corresponds to 5°, and others corresponds to 4°, 6° and so on.

14.4 Singles rates for SOS and ENGE

Table 14–5 shows rough estimation of singles rates for SOS from trigger rate study. Values listed in the table are calculated as follows.

R(e^+)=(4/4),
R(π^+)=(4/4)(!GC)−(4/4)(!GC)(!AC),
R(p)=(4/4)(!GC)(!AC)−(4/4)(!GC)(!AC)(LC).

Followings are raw data of the study.

```
Trigger rate study raw data, triggers/10sec

           |  Target    6Li            7Li     10B    11B     C       Si
Trigger    |  Current   1.13uA         0.79uA  1.3uA  0.75uA  0.5uA   1.0uA
-------------------------------------------------------------------------
(4/4)                   1727k          1081k   1480k  1090k   1073k   1100k
(4/4)(!GC)              31.2k          18.6k   27.0k  19.4k   18.7k   17.5k
(4/4)(!AC)              58.5k          32.1k   49.5k  34.6k   33.3k   30.8k
(4/4)(!GC)(!AC)         7.15k          4.16k   6.3k   4.5k    3.9k    3.13k
(4/4)(!GC)(!AC)(LC)     3.95k(1.15uA)  2.42k   3.6k   2.8k    2.4k    2.13k
(4/4)(!GC)(!AC)(!SHhi)  7.04k          4.12k   6.0k   4.6k    -       2.98k
-------------------------------------------------------------------------
```

Figure 14–20 shows measured singles rate for ENGE hodoscope #38 (1.1 cm wide, at the middle of the focal plane). Solid lines show the calculated rates using Eq. (3.84) of Tsai. For details see hclog(http://www.jlab.org/~cdaq/hclog/html/) 25449-25463.

Table 14–5: SOS singles rate for each target estimated from trigger study The rates are normalized to the currents in the table, which give the electron singles rate of 2 MHz to a ENGE scintillator (1.1 cm wide) at the middle of the focal plane. Singles rate in the parenthesis for C is obtained from offline analysis and is more reliable; less positron contamination in the pion rate and less LC inefficiency effect to the proton rate.

Nucleus	Thickness (mg/cm^2)	Current (μA)	e^+ Hz	π^+ Hz	p Hz
^{6}Li	16.1	0.74	110k	1.6k	210
^{7}Li	19.0	0.85	120k	1.6k	190
^{10}B	16.3	1.67	91k	1.3k	170
^{11}B	20.8	0.80	97k	1.3k	130
C	22	0.47	100k	1.4k(0.75k)	140(180)
Si	5.2	1.11	120k	1.4k	110

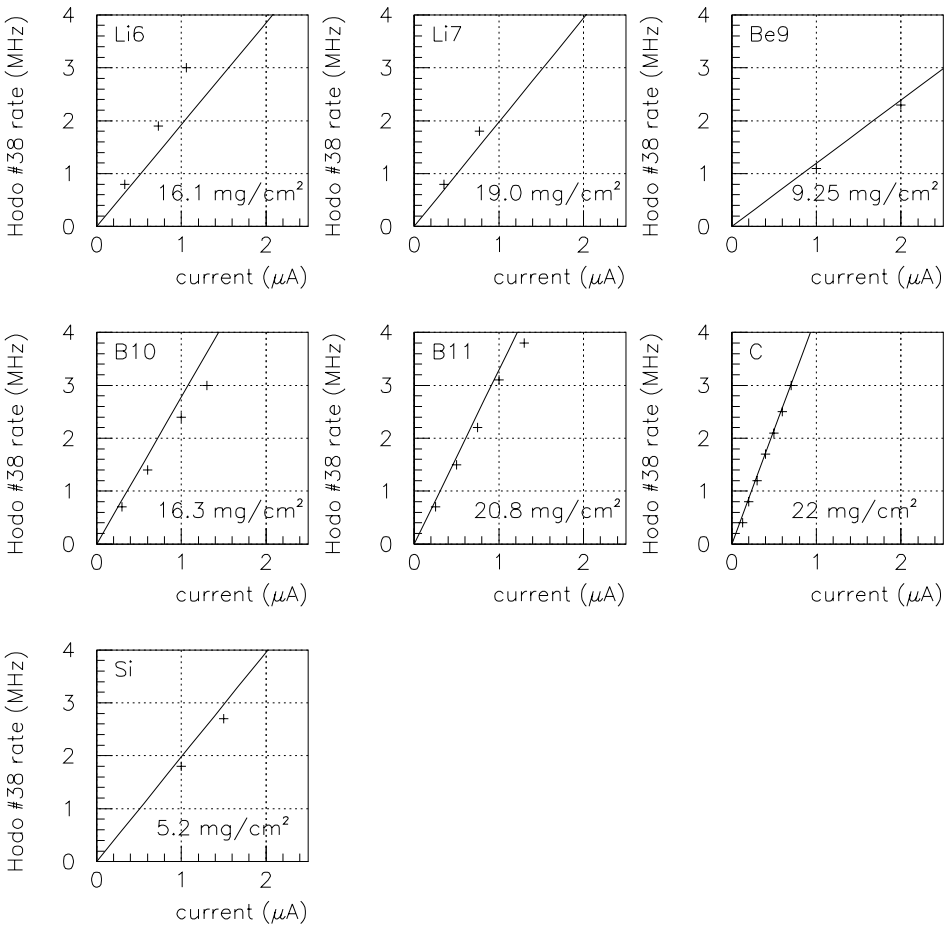

Figure 14–20: Measured singles rate for ENGE hodoscope #38 (1.1 cm wide, at the middle of the focal plane). Solid lines show the calculated rates using Eq. (3.84) of Tsai.